

ROBUST ESTIMATION OF FRACTURE PARAMETERS

CENTRE FOR NEWFOUNDLAND STUDIES

**TOTAL OF 10 PAGES ONLY
MAY BE XEROXED**

(Without Author's Permission)

SHAOJUN WU



**ROBUST ESTIMATION OF FRACTURE
PARAMETERS**

By

Shaojun Wu

A DISSERTATION
SUBMITTED TO THE SCHOOL OF GRADUATE STUDIES
IN PARTIAL FULFILLMENT OF THE REQUIREMENTS
FOR THE DEGREE OF
DOCTOR OF PHILOSOPHY

FACULTY OF ENGINEERING AND APPLIED SCIENCE
MEMORIAL UNIVERSITY OF NEWFOUNDLAND

St. John's, Newfoundland, Canada

June 1996

©Copyright: Shaojun Wu 1996

Abstract

Fracture mechanics is mainly concerned with the analysis of fracture-dominant failure. Various methods of analyses for cracks are used in the determination of fracture characterizing parameters, which in turn can be used to predict loads and crack sizes at which failure would occur.

In engineering practice, robust methods for estimating fracture parameters are useful, given the lack of details of material data, geometric configuration and computational sophistication in an operational industrial plant. This thesis focuses on the approximate methods for the determination of (1) crack tip plastic zone size, (2) the J of circular-ended notches and (3) the J for three-dimensional pressure vessels and piping components. Furthermore, this thesis focuses on design perspectives based on robust methods.

The assessment of the integrity of structures and components with defects has been shown to be possible using the robust methods developed in this thesis. The robust method for estimating the elastic-plastic energy release rate has been presented which is suitable for the purpose of design. In order to estimate the effect of out-of-plane loading which is parallel to the crack front, the so-called “ $2\frac{1}{2}$ -D” model is proposed in this thesis. This model has been developed to evaluate J for three-dimensional pressure vessels and piping components with defects such as pressure vessels and piping with a circumferential flaw or a longitudinal flaw.

Acknowledgment

The author wishes to acknowledge his supervisor, Dr. R. Seshadri, for his support and guidance, and for the many challenging technical discussions in the course of his doctoral program. The financial support provided by Memorial University of Newfoundland, Faculty of Engineering and Applied Science, and Dr. Seshadri's research grant is gratefully acknowledged. Appreciation is also directed to fellow graduate student Mr. S. P. Mangalaramanan.

The author would also like to acknowledge the role played by his parents, Mr. Zhaojiong Wu and Mrs. Qinglan Qi.

Dedication

To my wife, **Suqin Ma** and my daughter, **Jane Yajie Wu** with their patience, understanding and love.

Contents

| | |
|--|-------------|
| Abstract | i |
| Acknowledgment | ii |
| Dedication | iii |
| Table of Contents | iv |
| List of Figures | viii |
| List of Tables | xi |
| List of Symbols | xii |
| 1 Introduction | 1 |
| 1.1 Objectives | 1 |
| 1.2 Fracture Parameters | 2 |
| 1.3 Organization of the Thesis and Major Contributions of the Research | 3 |
| 2 Literature Review | 5 |
| 2.1 Approximate Methods for Notch Root Strain Concentration | 5 |
| 2.2 Approximate Methods for Inelastic Fracture Parameters | 8 |

| | | |
|----------|---|-----------|
| 2.3 | Fracture Design Methods | 14 |
| 2.4 | Three-Dimensional Consideration for Fracture Parameters | 17 |
| 3 | Theoretical Analysis of J-Integral | 20 |
| 3.1 | Analysis of Two-Dimensional J -Integral | 20 |
| 3.1.1 | Rice's Original Analysis | 20 |
| 3.1.2 | Generalized Two-Dimensional J -Integral | 28 |
| 3.2 | Analysis of Three-Dimensional J -Integral | 33 |
| 3.2.1 | First Conservation Law | 33 |
| 3.2.2 | Application to Three-Dimensional Cracked Bodies | 36 |
| 3.2.3 | Energy Release Rate in Three-Dimensional Field | 41 |
| 4 | Estimation of Mode I Crack Tip Plastic Zone Size | 45 |
| 4.1 | Introduction | 45 |
| 4.2 | GLOSS Analysis | 46 |
| 4.3 | Multiaxial Constraint | 49 |
| 4.4 | Normalized Constraint Parameter $\bar{\lambda}$ | 49 |
| 4.5 | Approximate Method for Determining Crack-Tip Plastic Zone Size . | 50 |
| 4.6 | Remarks | 54 |
| 5 | J-Estimation of Circular-Ended Notches | 55 |
| 5.1 | Introduction | 55 |
| 5.2 | Notch Root Stress and Strain | 56 |
| 5.3 | J -Integral for Smooth-Ended Notches | 57 |
| 5.4 | J -Estimation Methods | 61 |
| 5.5 | Remarks | 68 |

| | | |
|----------|---|-----------|
| 6 | A Simplified Three-Dimensional Model for Analyzing Pressure Vessels and Piping Components with Defects | 69 |
| 6.1 | Introduction | 69 |
| 6.2 | Crack Tip Constraint Parameter for $2\frac{1}{2}$ -D Specimens | 70 |
| 6.3 | J -Estimation of $2\frac{1}{2}$ -D Specimens for Linear Elastic Materials | 74 |
| 6.4 | Size Requirement For Plane Strain Fracture Toughness Testing | 82 |
| 6.5 | Numerical Examples | 86 |
| 6.5.1 | Analysis of Practical Pressure Vessels and Piping Components with Defects | 86 |
| 6.5.2 | Circumferential Flaw in a Pressure Vessel | 87 |
| 6.5.3 | Longitudinal Flaw in a Pressure Vessel | 90 |
| 6.6 | Remarks | 93 |
| 7 | Robust J Estimation - Design Perspectives | 96 |
| 7.1 | Introduction | 96 |
| 7.2 | Redistribution Nodes (R-Nodes) | 97 |
| 7.3 | Robust Determination of J | 100 |
| 7.4 | Estimation of J and C^* for Design Purposes | 111 |
| 7.5 | Numerical Examples | 115 |
| 7.5.1 | Single-Edge Crack Specimen | 115 |
| 7.5.2 | Compact Tension Specimen | 119 |
| 7.5.3 | Single Edge Notched Bend Specimen | 120 |
| 7.6 | Consideration of the Effect of Strain-hardening | 120 |
| 7.7 | Remarks | 126 |

| | | |
|----------|---|------------|
| 8 | Conclusions | 127 |
| 8.1 | Contributions of the Thesis | 127 |
| 8.2 | Future Research | 130 |
| | References | 131 |
| | Appendices | 138 |
| A | Implementation of GLOSS Analysis | 138 |
| A.1 | GLOSS Method | 138 |
| A.1.1 | 3-D Mode I Single Edge Through-Cracked Specimen | 139 |
| A.1.2 | 2-D Single-Edge Circular Notch Specimen | 154 |
| A.1.3 | 2 $\frac{1}{2}$ -D Specimen | 158 |
| A.2 | GLOSS R-Node Method | 166 |
| A.2.1 | Single-Edge Crack Specimen (SEC) | 167 |
| A.2.2 | Compact Tension Specimen (CT) | 173 |
| A.2.3 | Single Edge Notched Bend Specimen (SENB) | 177 |
| B | ANSYS Input Files for Inelastic Analysis | 180 |
| B.1 | Elasto-Plastic Analysis for Cracked Specimens | 180 |
| B.1.1 | Single-Edge Crack Specimen | 183 |
| B.1.2 | Compact Tension Specimen | 191 |
| B.1.3 | Single Edge Notched Bend Specimen | 195 |
| B.1.4 | Circumferential Flaw in a Pressure Vessel | 198 |
| B.1.5 | Longitudinal Flaw in a Pressure Vessel | 201 |
| B.2 | Elasto-Plastic Analysis for Notched Specimen | 205 |

| | | |
|----------|---|------------|
| C | Derivation of Equivalent Reference Stress | 209 |
| C.1 | A Cylindrical Pressure Vessel with Circumferential Flaw | 209 |
| C.2 | A Cylindrical Pressure Vessel with Longitudinal Flaw | 213 |

List of Figures

| | | |
|-----|---|----|
| 2.1 | Arbitrary Contour around the Tip of a Crack | 9 |
| 2.2 | Turner's Engineering- J Design Curve (Turner, 1981) | 13 |
| 2.3 | EPRI Method (Turner, 1984a) | 18 |
| 3.1 | Two Cracked Specimens with Neighboring Crack Sizes | 23 |
| 3.2 | Closed Contour, Γ^* , in a 2-D Solid | 24 |
| 3.3 | Two Arbitrary Contour, Γ_1 and Γ_2 around a crack tip | 26 |
| 3.4 | Crack Meandering and Branching | 30 |
| 3.5 | General Crack Extension in 2-D | 31 |
| 3.6 | Translation of Subregion Ω with Respect to a Body R | 34 |
| 3.7 | Typical Subregion in Relation to a Defect with an Associated Bound- ary Sets | 37 |
| 3.8 | Subregion of Infinitesimal Thickness with a Smoothly Notched Defect | 39 |
| 3.9 | Schematic Representation for 3-D Crack Front | 43 |
| 4.1 | GLOSS Diagram - Local System Response in a Crack | 47 |
| 4.2 | 3-D Finite Element Model | 51 |
| 4.3 | Normalized Constraint Parameter ($\bar{\lambda}$) vs. Geometry (B/a) | 52 |
| 5.1 | Typical Flat-surfaced Notch in a Two-dimensional Deformation Field | 59 |

| | | |
|------|--|-----|
| 5.2 | Notch Root Stress-Strain Curve | 62 |
| 5.3 | J vs. Load P for Single-Edge Circular Notch Specimen | 66 |
| 5.4 | J vs. ρ/a for Single-Edge Circular Notch Specimen | 67 |
| 6.1 | $2\frac{1}{2}$ -D Model | 71 |
| 6.2 | $\bar{\lambda}$ vs. B/a and $\bar{\sigma}_3^R$ | 73 |
| 6.3 | Consideration of Crack Tip Singularity | 80 |
| 6.4 | Cylinder or Pipe with a Circumferential Flaw Subjected to Internal Pressure - $J/(a\sigma_y)$ vs. p_a/σ_y | 91 |
| 6.5 | Cylinder or Pipe with a Longitudinal Flaw Subjected to Internal Pressure - $J/(a\sigma_y)$ vs. σ_θ/σ_y | 94 |
| 7.1 | Energy Release Rate (J) vs. R-Node Strain (ϵ_{r-n}) | 102 |
| 7.2 | Typical Load-Displacement ($P - \delta$) Record | 105 |
| 7.3 | Constraint Parameter (λ) vs. load point displacement (δ) | 107 |
| 7.4 | Constraint Parameter (λ) vs. Normalized Load (P/P_L) | 109 |
| 7.5 | $\Phi(\lambda)$ vs. Normalized Load P/P_L | 110 |
| 7.6 | Robust J Design Curve | 114 |
| 7.7 | Determination of σ_{r-n} for SEC Specimen with $a/W=0.2$ | 116 |
| 7.8 | Determination of σ_{r-n} for SEC Specimen with $a/W=0.4$ | 117 |
| 7.9 | $J/J_e(\epsilon_y)$ vs. $\epsilon_{r-n}/\epsilon_y$ for SEC Specimen | 118 |
| 7.10 | $J/J_e(\epsilon_y)$ vs. $\epsilon_{r-n}/\epsilon_y$ for CT Specimen | 121 |
| 7.11 | $J/J_e(\epsilon_y)$ vs. $\epsilon_{r-n}/\epsilon_y$ for SENB Specimen | 122 |
| 7.12 | Equivalent Elastic Perfectly-Plastic Curve to Strain-hardening . . . | 124 |
| 7.13 | Determination of P_5 for Strain-hardening Behaviors | 125 |

C.1 Collapse Curve for a Rectangular Beam 211

C.2 Cylindrical Pressure Vessel with Circumferential Flaw 212

C.3 Cylindrical Pressure Vessel with Longitudinal Flaw 215

List of Tables

6.1 Constraint Parameter λ of $2\frac{1}{2}$ -D Specimens 95

Nomenclature

| | |
|-------------|--|
| a | crack or notch length |
| B | thickness of cracked or notched specimen |
| C^* | creep fracture parameter |
| E_o | original elastic modulus |
| E_r | relaxation modulus |
| \bar{E}_r | normalized relaxation modulus |
| E_s | secant modulus |
| E' | plane strain corrected modulus ($=E_o/(1-\nu^2)$) |
| G | linear elastic energy release rate |
| J | inelastic energy release rate |
| J_e | J on a linear elastic basis |
| J_{e-p} | J on an elastic perfectly-plastic basis |
| $J_{e/p}$ | elastic-plastic value of J |
| J_p | J on a rigid plastic basis |
| K_I | Mode I linear elastic stress intensity factor |
| K_I^* | simplified-3D linear elastic stress intensity factor |
| K_{Ic} | plane strain fracture toughness |
| K_r, S_r | parameters in the Failure Assessment Diagram |
| n | strain-hardening exponent |
| p_i | internal pressure of a vessel |
| P | externally applied load |
| P_L | limit load |
| R | defect-size parameter |

| | |
|--------------------------------------|--|
| R_i | inner radius of a cylinder |
| R_o | outer radius of a cylinder |
| W | strain energy density or width of cracked and notched specimen |
| β | geometric factor in fracture |
| δ | load-point displacement |
| $\bar{\delta}$ | normalized load-point displacement |
| ϵ_e | equivalent strain |
| ϵ_r | notch root strain |
| ϵ_{r-n} | r-node strain |
| ϵ_y | yield strain |
| λ | constraint parameter |
| $\bar{\lambda}$ | normalized constraint parameter |
| ν | Poisson's ratio |
| ρ | radius of curvature of notch root |
| σ_e | equivalent stress |
| σ_{ei} | notch root equivalent stress in the first linear elastic FEA |
| σ_r | notch root stress |
| σ_{r-n} | r-node stress |
| σ_y | yield stress |
| σ_1^R | remote stress in X_2 (Y) direction |
| σ_2^R | remote stress in X_1 (X) direction |
| σ_3^R | remote stress in X_3 (Z) direction |
| $\bar{\sigma}_1^R, \bar{\sigma}_3^R$ | normalized remote stresses ($=\sigma_1^R/\sigma_y, \sigma_3^R/\sigma_y$) |

Chapter 1

Introduction

1.1 Objectives

The primary set of objectives of this thesis is to develop robust assessment methods for evaluating the integrity of structures and components with defects, and to characterize fracture behavior of cracked components under three-dimensional loadings.

The current fracture assessment procedures rely on analytical methods which are subjected to limitations in terms of material specification, loading and geometric configuration. For more complex situations, numerical methods such as the finite element or the boundary element methods are routinely used. Inelastic finite element analysis, although accurate, can often be quite elaborate, time-consuming and possibly expensive. Furthermore, the need for detailed numerical analysis has to be judged on account of the presence of scatter in material data and the difficulty in obtaining a suitable constitutive relationship. Therefore, any effort directed towards developing approximate methods that are simple, direct and yet reasonably accurate would be of importance from a design standpoint. Such methods are designated as robust methods.

In the purview of this thesis, the term “robustness” implies the ability to provide acceptable results based on less than reliable input, together with conceptual insight and economy of computational effort (Marriott, 1992). Robust methods are appropriate for the following situations:

- (i) initial scoping and feasibility studies, based on preliminary information;
- (ii) screening of critical situations in large complex systems for further detailed analyses; and
- (iii) “sanity” checks or benchmarking of results obtained by detailed nonlinear analysis.

1.2 Fracture Parameters

Strength failures of load-carrying structures can be due to either dominant yielding or dominant fracture. For failures that are fracture-dominant, i.e., where fracture precedes net-section yielding, the defects are essentially macroscopic, and only the local stress-strain fields that are associated with the defects are involved.

Fracture mechanics is concerned almost entirely with fracture-dominant failures. Based on the dominant behaviors, fracture mechanics is classified as: (1) linear elastic fracture mechanics (LEFM), (2) elastic-plastic fracture mechanics (EPFM), and (3) dynamic and time-dependent fracture mechanics. Usually, G (linear elastic energy release rate) and K (stress intensity factor) are considered as fracture characterizing parameters in LEFM, while J -integral (inelastic energy release rate) and COD (crack opening displacement) for EPFM. The C^* -integral has found use in estimating steady-state creep crack growth. Fracture mechanics

essentially predicts the condition under which a load-carrying structure can fail in a load-controlled manner due to the enlargement of a dominant crack in a given structure or component.

A majority of the literature on fracture mechanics focuses on two-dimensional idealizations that involves approximations such as plane-stress and plane-strain stress states. Real life components or structures, on many occasions, do not lend themselves to such simplifications. Three-dimensional influences can be prevalent in many situations and there is therefore a need to characterize fracture parameters for such configurations and come up with robust assessment methods that can be used by design engineers.

The current literature assumes that the stress system parallel to the crack front does not influence the crack behavior for, say, the mode I specimen. Therefore, the fracture parameter calculations in the neighborhood of the crack are primarily based on a biaxial loading condition with a loading plane perpendicular to the crack face. In order to estimate the effect of out-of-plane loading which is parallel to the crack front, the so-called “ $2\frac{1}{2}$ -Dimensional” model is developed. This model, which essentially incorporates simple distributions of the three-dimensional remote stress field into a two-dimensional geometry, can find widespread use in practice.

1.3 Organization of the Thesis and Major Contributions of the Research

The related literature is reviewed and presented in Chapter 2. A discussion of the theoretical basis of J -integral in two-dimensional and three-dimensional configurations is contained in Chapter 3. An approximate method for the determination of

mode I crack tip plastic zone is introduced in Chapter 4 in conjunction with the use of the Generalized Local Stress and Strain (GLOSS) analysis. Chapter 5 describes J -estimation of circular-ended notches, wherein edge-crack problems are viewed as the limiting case. A simplified three-dimensional model, designated as the $2\frac{1}{2}$ -D model, is proposed in Chapter 6 that is applicable to practical pressure vessels and piping configurations with defects. Robust J design method, which is useful in the integrity assessment of industrial equipment and systems, is presented in Chapter 7. The concluding chapter, Chapter 8, contains the contributions of this thesis and a discussion on future research.

The key aspects of the research in this thesis are:

1. the development of a simplified three-dimensional model for analyzing practical pressure vessels and piping components with defects; and
2. the development of robust methods for the analysis and design of linear elastic, elastic-plastic and perfectly plastic components. The effects of strain-hardening and creep on fracture assessments are also considered.

The significance of the research lies in the recognition that neglecting the “out-of-plane” remote stress can be unconservative and can lead to premature failures and potential loss of human life, human injury, loss of production capability and environmental damage. The development of robust methods should provide the practitioner with an assessment tool that can be used to evaluate the integrity of structures and components with defects.

Chapter 2

Literature Review

2.1 Approximate Methods for Notch Root Strain Concentration

A crack can be considered as a limiting case of a smooth-ended notch in notched components. Approximate analytical methods for determining the notch strain concentration have been discussed by Stowell (1950), Hardrath and Ohman (1953), and Neuber (1961).

The Neuber's formula which is given by

$$K_T^2 = K_\sigma K_\epsilon \quad (2.1)$$

postulates that, during plastic action in the vicinity of the notch, the product of the stress concentration factor (K_σ) and the strain concentration factor (K_ϵ) remains constant, and is equal to the square of elastic stress (or strain) concentration factor (K_T).

The approximate formula proposed by Stowell (1950) for predicting stress concentration factors has been modified by Hardrath and Ohman (1953) as:

$$K_\sigma = 1 + (K_T - 1) \frac{E_s}{E_{ns}}. \quad (2.2)$$

Here, $E_s = \sigma_{max}/\epsilon_{max}$ is the secant modulus at the point of maximum local notch deformation, and $E_{ns} = \sigma_n/\epsilon_n$ is the nominal secant modulus. Both Neuber's and Hardrath and Ohman's formulae are known to consistently overpredict notch root strains.

Based on the energy method, a relationship for determining the elastic-plastic notch root stress and strain has been proposed by Molski and Glinka (1981), of the form

$$W_n K_T^2 = W_a^{max} \quad (2.3)$$

where W_n is the nominal elastic strain energy density, and W_a^{max} is the actual maximum strain energy density at the notch root. Strictly speaking, their method is valid only in the elastic range. Based on the assumption that localized plasticity at notch root does not significantly affect the energy distribution, equation (2.3) can also be used for determining the notch root stress and strain even in the plastic range. As a result, for nominal stress approaching or exceeding the yield stress, equation (2.3) tends to underestimate the notch root strain.

On the basis of the averaged similarity measure of the strain energy density along a smooth notch boundary considered in the path-independent J -integral, Ellyin and Kujawski (1987) have presented an approximate method for a material stress-strain relationship of the form

$$\epsilon = \sigma/E + (\sigma/K')^{1/n'} \quad (2.4)$$

where n' is the cyclic (or monotonic) strain hardening exponent and K' is the strength coefficient such that the notch root stress, σ_{max} , and notch root strain, ϵ_{max} , can be related by the equation

$$K_T^2 \left(\frac{\sigma_n^2}{2E} \right) + \frac{1}{1+n'} \sigma_n \epsilon_n^p = \frac{\sigma_{max}^2}{2E} + \frac{1}{1+n'} \sigma_{max} \epsilon_{max}^p \quad (2.5)$$

where σ_n and ϵ_n are nominal applied stress and strain. In deriving equation (2.5) it is assumed that the relationship between σ_{max} and ϵ_{max} is similar to that of equation (2.4). Equation (2.5) has been shown to be equivalent to Molski and Glinka's method in the elastic range, and equivalent to Neuber's method for high strain hardening materials.

The GLOSS (Generalized Local Stress Strain) analysis (Seshadri and Kizhatil, 1993) is a practical compromise between the elaborate methods (i.e. the inelastic finite element technique) and the approximate analytical techniques. In GLOSS method, described by Seshadri (1991), the mechanical component or structure is divided into the local and remainder region. The local region typically experiences the largest inelastic effect and is often of interest from a design standpoint. The GLOSS theory essentially relates the multiaxial stress distribution in the local region to the uniaxial redistribution process. The varying degree of interaction between the local and remainder regions is characterized by a "constraint parameter" which can be used in conjunction with the uniaxial model to generate inelastic

results.

2.2 Approximate Methods for Inelastic Fracture Parameters

The J -integral procedure is used widely in characterizing inelastic fracture. By idealizing elastic-plastic deformation as nonlinear elastic, Rice (1968a) provides the basis for extending fracture mechanics methodology well beyond the validity of the limits of LEFM.

The J -integral is given by the expression

$$J = \int_{\Gamma} \left(W \, dy - T_i \frac{\partial u_i}{\partial x} \, ds \right) \quad (2.6)$$

where Γ is an arbitrary counter-clockwise path around the tip of a crack as illustrated in Fig. 2.1, W is the strain energy density, T_i are components of the traction vector, u_i are displacement vector components, and ds is a length increment along the contour Γ .

Alternately, the J -integral can be calculated by using the expression (Broek, 1986)

$$J = -\frac{1}{B} \frac{d\Pi}{da} \quad (2.7)$$

where Π is the potential energy in an edge-cracked specimen and B is the thickness of the specimen. Equation (2.7) shows that J -integral is equal to the energy release rate in a nonlinear elastic body that contains a crack and is interpreted as

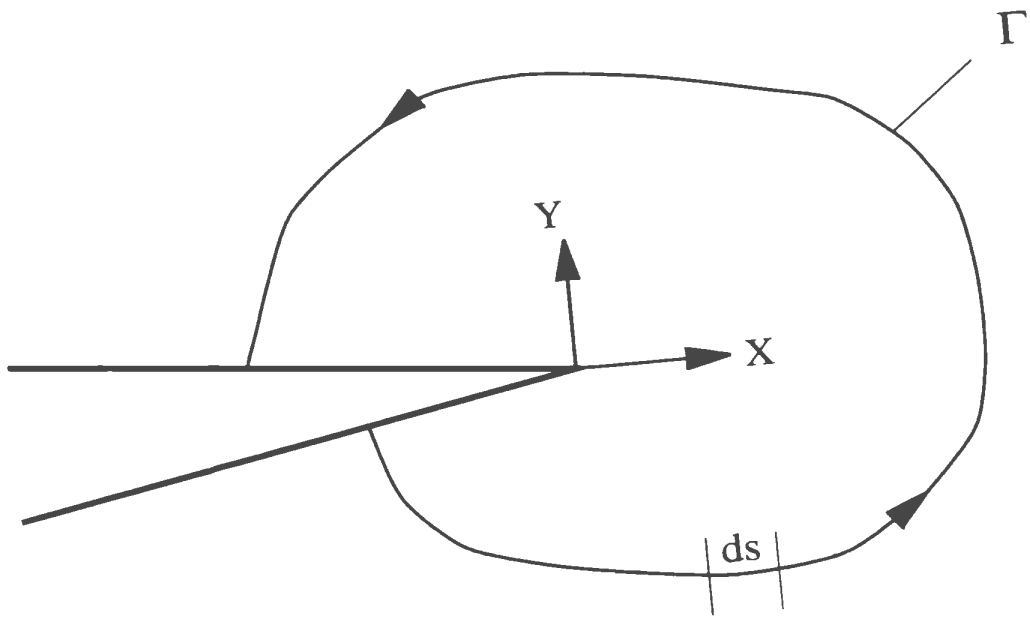


Figure 2.1: Arbitrary Contour around the Tip of a Crack

the potential energy difference for identically loaded elastic-plastic configurations having neighboring crack sizes a and $a + da$.

Bucci et al. (1972) have developed a method to approximately estimate J -integral by making use of plastically adjusted linear elastic J_e , and the perfectly plastic J_p . For the elastic material behavior,

$$J_e = \frac{K^2}{E'} = C_1 \delta^2 \quad (2.8)$$

For the perfectly plastic material idealization,

$$J_p = -\frac{\delta}{B} \frac{\partial P_L}{\partial a} = C_2 \delta \quad (2.9)$$

where a is the crack length, B is the specimen width, K is the stress intensity factor, δ the load line displacement, P_L the limit load, and C_1 and C_2 are constants depending on the geometry of the cracked component and the material behavior. The approximate method is developed on the basis of linear elastic fracture analysis and limit load solutions. The results obtained by Bucci et al. compare well with the experimental test data.

Based on the results by Shih and Hutchinson (1976), Rice et al. (1973) and Bucci et al. (1972), Kumar et al. (1981) have developed an engineering procedure for estimating the elastic-plastic J . The main objective is to obtain elastic-plastic J by simply combining the linear elastic analysis results and fully plastic analysis results. For a material satisfying the Ramberg-Osgood stress-strain law

$$\frac{\epsilon}{\epsilon_o} = \frac{\sigma}{\sigma_o} + \alpha \left(\frac{\sigma}{\sigma_o} \right)^n \quad (2.10)$$

where

$$\frac{\epsilon}{\epsilon_o} = \frac{\sigma}{\sigma_o} \quad \text{for linear elastic case}$$

$$\frac{\epsilon}{\epsilon_o} = \alpha \left(\frac{\sigma}{\sigma_o} \right)^n \quad \text{for fully plastic case,}$$

the $J_{e/p}$ is expressed as:

$$J_{e/p} = \frac{K^2(a_e)}{E'} + \alpha \sigma_o \epsilon_o c h_1(a/w, n) \left(\frac{P}{P_o} \right)^{n+1} \quad (2.11)$$

where a_e is an effective crack length, P is the applied load and P_o is the limit load. For various cracked configurations, the material and the geometry dependent function, $h_1(a/w, n)$, has been tabulated by fully plastic finite element analysis. Based on the reference stress method, Ainsworth (1984) modifies the expression of Kumar et al as follows:

$$J_{e/p} = \frac{K^2(a)}{E'} \left[\frac{K^2(a_e)}{K^2(a)} + \left(\frac{\nu E'}{E} \right) \left(\frac{E \epsilon_{ref}}{\sigma_{ref}} - 1 \right) \right] \quad (2.12)$$

where $\sigma_{ref} = (P/P_o)\sigma_o$ and P_o is a characteristic load that attempts to minimize the dependence of h_1 on n . The following approximation is then proposed:

$$h_1(n) = h_1(1) \quad (2.13)$$

where $h_1(n)$ is the geometry constant for a material with a strain hardening exponent of n , and $h_1(1)$ is the corresponding constant for a linear elastic material. Thus, equation (2.12) is not only simpler than equation (2.11), but also is more widely applicable.

Based on the results of elastic-plastic plane strain finite element analyses of shallow cracks ($a/W \leq 0.1$) in a variety of different geometries and loading configurations, Turner (1981) has described a J design curve. The design curves enable J to be estimated as a function of an effective structural (nominal) strain.

Region I LEFM:

$$J = (e/e_y)^2 G_y, \quad \text{for } e/e_y \leq 0.85 \quad (2.14)$$

Region II NSY (Net Section Yielding):

$$J = 5[(e/e_y) - 0.7]G_y, \quad \text{for } 0.85 \leq e/e_y \leq 1.2 \quad (2.15)$$

Region III GSY (Gross Section Yielding):

$$J = 2.5[(e/e_y) - 0.2]G_y, \quad \text{for } e/e_y > 1.2 \quad (2.16)$$

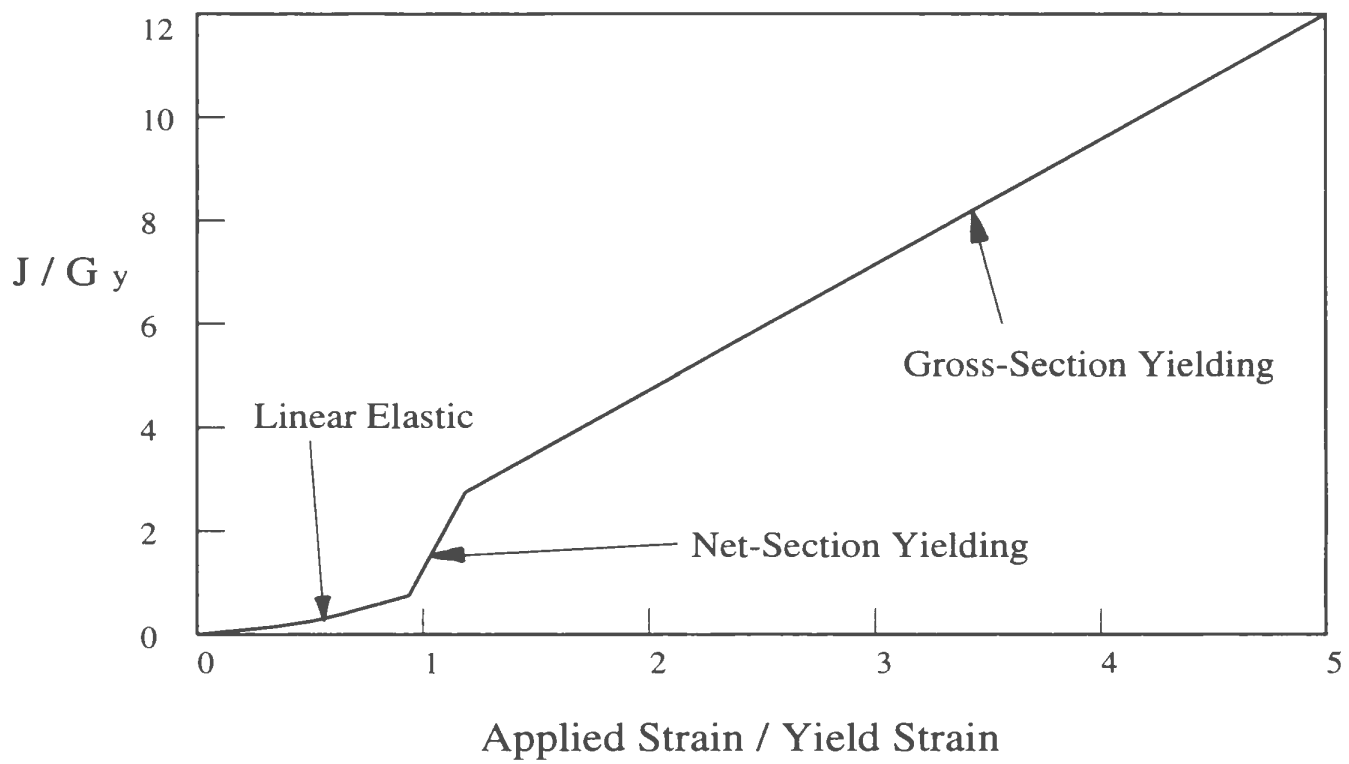


Figure 2.2: Turner's Engineering- J Design Curve (Turner, 1981)

In these equations, e is remote (nominal) strain for the uncracked body, e_y is yield strain, and G_y is the elastic energy release rate at the yielding point. This relation is shown in Fig. 2.2.

2.3 Fracture Design Methods

When designing a structure against fracture, there are three variables that need to be considered: stress, flaw size, and toughness. Fracture mechanics provides a mathematical relationship between these quantities. The fracture design methodology should be selected based on the available data, material properties, environment and loading on a structure. Only quasi-static methodologies are covered in this section. However, such approaches can be extended to rapid loading and crack arrest problems.

A short description of the COD, R-6, EnJ and EPRI methods are presented by Turner (1984a). Unlike the EPRI method, which seeks to provide an estimate of crack tip severity reflecting different material behaviors of various degrees of strain-hardening, the COD, R-6 and EnJ methods attempt to provide a single simple curve of crack tip severity versus the applied load in the component. The crack opening displacement, and not J , forms the basis for the COD method. However, the EPRI and EnJ methods use J , and not the crack opening displacement. Although the evolution of the R-6 method can be attributed to the COD concept, presently it is viewed more in the light of a J -based theory.

The following are the equations for COD (ferritic material) (PD6493, 1980):

$$\Phi = \delta/2\pi e_y \bar{a} = (e/e_y)^2 \quad \text{for } e/e_y \leq 0.5 \quad (2.17)$$

$$\Phi = \delta/2\pi e_y \bar{a} = (e/e_y) - 0.25 \quad \text{for } e/e_y \geq 0.5 \quad (2.18)$$

where $e_y = \sigma_y/E$, $\delta = \text{COD}$, and $\bar{a} = \text{equivalent crack length}$. Equation (2.17), which is derived from LEFM theory, includes a safety factor of 2.0 on the crack size. Equation (2.18) represents an upper envelope of the experimental data. In 1980, the COD design curve approach was incorporated into the British Standards document PD6493.

The equation for R-6 (Dowling and Townley, 1975) can be written as

$$K_r = S_r \left[\frac{8}{\pi^2} \ln \sec\left(\frac{\pi}{2} S_r\right) \right]^{-1/2} \quad (2.19)$$

where $K_r = K_I/K_{IC}$ (or $\sqrt{G/J_{IC}}$), $S_r = S/S_c$ (S is the applied load and S_c the nominal collapse load). The curve essentially represents the locus of predicted failure points. If the toughness is very large, the structure fails by collapse when $S_r = 1.0$. On the other hand, a brittle material will fail when $K_r = 1.0$. In the intermediate cases, collapse and fracture modes interact, and both K_r and S_r are individually less than 1.0 at failure. All points inside the failure assessment diagram are considered safe, and points outside the diagram are considered unsafe.

The following are the equations for EnJ (Turner, 1984b):

$$J/G_Y = (e/e_y)^2[1 + 0.5(e/e_y)^2] \quad \text{for } e/e_y \leq 1.2 \quad (2.20)$$

$$J/G_Y = 2.5[(e/e_y) - 0.2] \quad \text{for } e/e_y \geq 1.2$$

This method results in J -estimation curves which are the revised forms of equations (2.14), (2.15) and (2.16).

The EPRI (Kumar et al., 1981) procedure provides a means for computing the applied J integral under elastic-plastic conditions.

The procedure makes use of the Ramberg-Osgood constitutive relationship [Eq. (2.10)] where α and n are material parameters, specifically n is the strain-hardening index. The elastic and plastic components of J are computed separately and added together in order to obtain the total J , i.e.,

$$J_{tot} = J_{el} + J_{pl}. \quad (2.21)$$

The EPRI estimation, which is given by equation (2.11), can also be expressed in terms of a failure assessment diagram. The J -ratio and the stress-ratio are defined as follows:

$$J_r = \frac{J_{el}(a)}{J_{el}(a_{eff}) + J_{pl}} \quad (2.22)$$

and

$$S_r = P/P_o. \quad (2.23)$$

The equivalent K_r is equal to K_I/K_{Ic} . The shape of EPRI failure assessment diagram depends not only on the geometry of the cracked body, but also on the material behavior (Fig. 2.3).

2.4 Three-Dimensional Consideration for Fracture Parameters

The previous sections are primarily limited to two-dimensional conditions. Only the effects of in-plane dimensions (e.g. crack length, ligament length) and in-plane loadings are considered. However, the dimensions and loadings along the crack front direction can also play a major role while determining fracture parameters. Although three-dimensional geometric effects are investigated, most of the early work on this subject was performed under plane strain, plane stress or antiplane shear assumptions. In the recent years, however, more investigations have been carried out in the area of three-dimensional fracture.

Narasimhan and Rosakis (1988) have performed three-dimensional experimental and numerical investigation on a ductile three-point bend specimen (considering the effect of three-dimensional geometry only). It is found that the average J and COD from the three-dimensional analysis are bounded by those obtained from two-dimensional (plane stress and plane strain) analyses. The three-dimensional numerical results indicate that the plane strain HRR field dominates very near the crack front in the interior of the specimen. On the other hand, the plane stress HRR field agrees well with the three-dimensional numerical results obtained on the

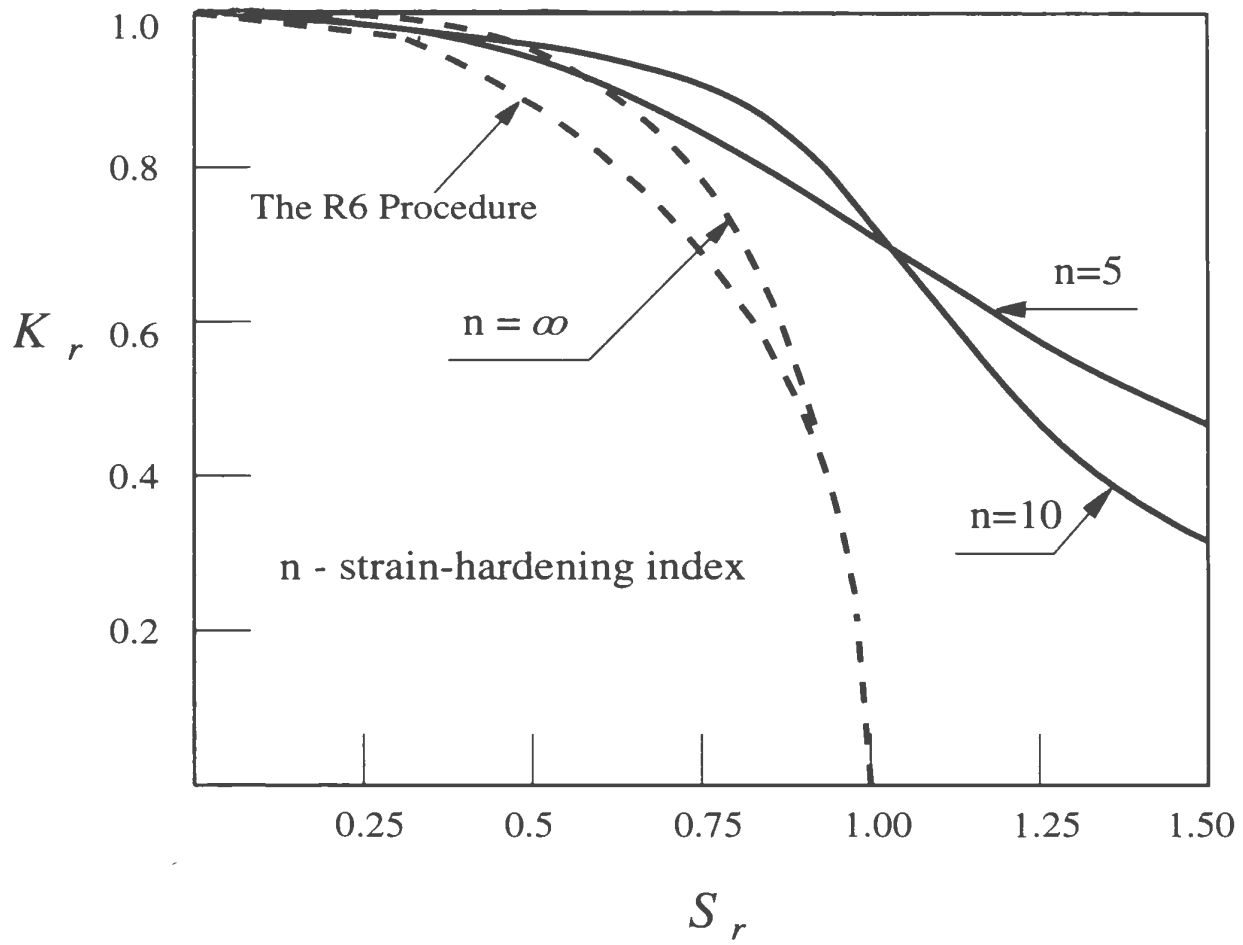


Figure 2.3: EPRI Method (Turner, 1984a)

surface layer of elements.

Dai (1989) has worked on fracture assessment of mechanical components under multiaxial loading. An approximate three-dimensional theory for expressing the crack-tip triaxiality in terms of the component dimensions and the multiaxial remote-field loadings was established.

Newman et al. (1993) have studied the stresses and deformations around a straight-through crack in finite-thickness plates for an elastic perfectly-plastic material under monotonic and cyclic loading using three-dimensional nonlinear finite element analysis. Constraint variations in cracked bodies have also been investigated.

In order that the physical meaning of potential energy is retained with reference to elastic (linear or nonlinear) bodies, several proposals have been made for three-dimensional integrals (Amestoy et al., 1981; Kishimoto et al., 1980; Kikuchi and Miyamoto, 1982; Bakker, 1984). The components of these three-dimensional contour integrals are written as:

$$J_k = \int_{\Gamma} (W n_k - T_i u_{i,k}) ds + \int_A (W \delta_{k3} - \sigma_{i3} u_{i,k})_{,3} dA \quad (2.24)$$

where $k=1, 2$ or 3 , δ_{k3} stands for the Kronecker delta, s is the path length along Γ , and A is the area within the contour. Based on equation (2.24), Chiarelli and Frediani (1993) have computed the three-dimensional J -integral for linear elastic material using three-dimensional finite element analysis.

Chapter 3

Theoretical Analysis of J -Integral

3.1 Analysis of Two-Dimensional J -Integral

3.1.1 Rice's Original Analysis

Rice (1968a) has presented a path-independent contour integral, equation (2.6), for the analysis of cracks. A homogeneous body of linear or nonlinear elastic material free of body forces is subjected to a two-dimensional deformation field. All stresses σ_{ij} which are dependent on the cartesian coordinates $X_1 (=X)$ and $X_2 (=Y)$ are considered in this section. Let the cartesian displacement vector field, its associated strain tensor field and its equilibrium stress tensor field in the absence of body forces, and for zero initial strains, be represented by the differentiable functions u , ϵ and σ , respectively. The infinitesimal strains imply that:

$$\epsilon_{ij} = \frac{1}{2}(u_{i,j} + u_{j,i}). \quad (3.1)$$

Due to moment equilibrium, the stress tensor is symmetric, i.e.,

$$\sigma_{ij} = \sigma_{ji}. \quad (3.2)$$

The equilibrium equations in the absence of body forces are given by the three equations:

$$\sigma_{ij,j} = 0. \quad (3.3)$$

As well, σ and ϵ are related by an elastic (linear or nonlinear) constitutive law, with the associated energy density W given by:

$$W = \int_0^{\epsilon_{ij}} \sigma_{ij} d\epsilon_{ij}. \quad (3.4)$$

In the absence of initial strains, stresses can be obtained from the expression:

$$\sigma_{ij} = \frac{\partial W}{\partial \epsilon_{ij}} \quad (3.5)$$

since, the existence of an elastic constitutive law implies that W is a function of strains alone. Rice then shows that the J -integral, defined by equation (2.6), is path-independent and is equal to the energy release rate in an elastic body that contains a crack. A somewhat different explanation can be attributed to the concept of energy release rate, while applying J to elastic-plastic materials. When the crack extends or when the specimen is unloaded, much of the strain-energy absorbed by an elastic-plastic material is not recovered. Thus J is viewed as the difference of potential energy between two identical specimens, but with neighboring crack sizes. For the purpose of extending to generalized two-dimensional and three-dimensional situations, Rice's J -integral is discussed in detail.

Rice's analysis considers a crack extension along the crack line (X direction) only. The crack sizes of two specimens considered are l and $l + \Delta l$, respectively, with Δl along the X direction (Fig. 3.1). The crack tip is assumed to move "virtually" from the initial location o to the final location o' , with the distance oo' being infinitesimally small. Here, the coordinate system $o - X - Y$ is the fixed frame and the coordinate system $o' - x - y$ is the moving frame.

The fixed coordinate ($o - X - Y$) is related to the moving coordinate ($o' - x - y$) according to the relations:

$$\begin{aligned} x &= X - \Delta l \\ \text{and} & \\ y &= Y. \end{aligned} \tag{3.6}$$

A mathematical proof for the path independence of the J contour integral has been presented by Rice (1968a). Along a closed contour, Γ^* (Fig. 3.2), J can be expressed as:

$$J^* = \int_{\Gamma^*} \left(W dY - T_i \frac{\partial u_i}{\partial X} ds \right). \tag{3.7}$$

Converting equation (3.7) into an area integral by using the divergence theorem, the following expression can be obtained:

$$J^* = \int_{A^*} \left[\frac{\partial W}{\partial X} - \frac{\partial}{\partial X_j} \left(\sigma_{ij} \frac{\partial u_i}{\partial X} \right) \right] dA \tag{3.8}$$

where A^* is the area enclosed by Γ^* . Using equations (3.1) through (3.5), the first

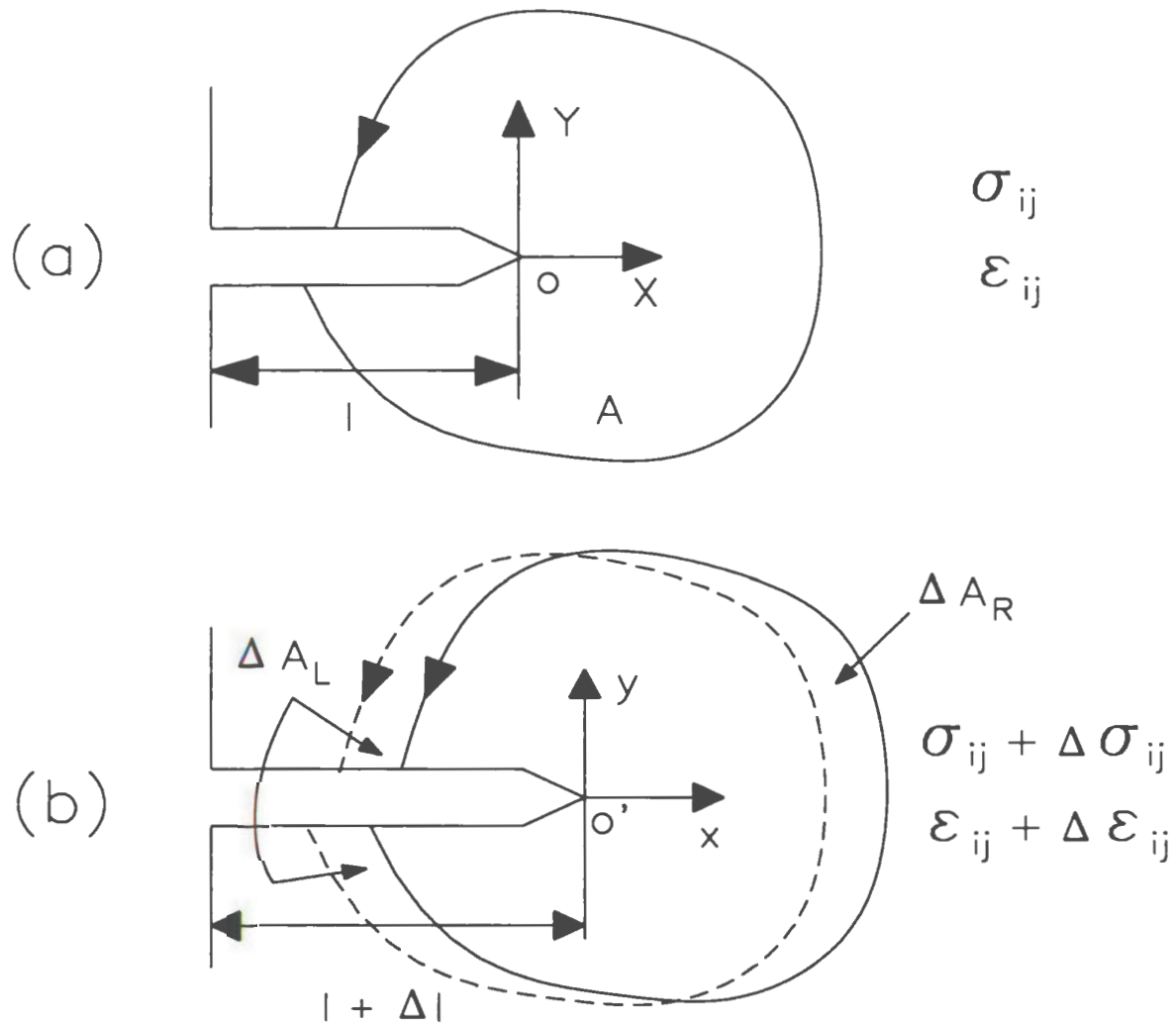


Figure 3.1: Two Cracked Specimens with Neighboring Crack Sizes

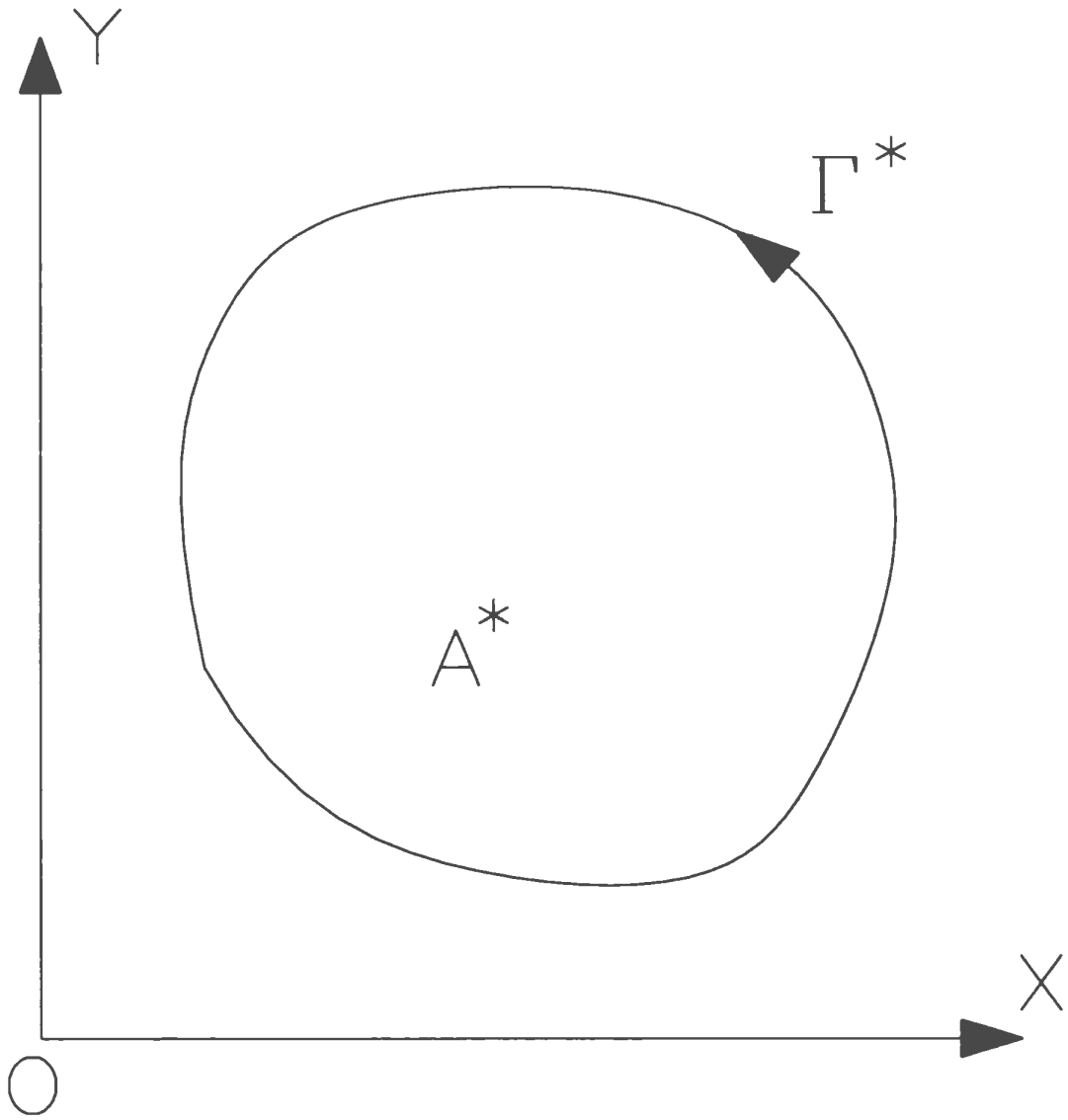


Figure 3.2: Closed Contour, Γ^* , in a 2-D Solid

term is equal to the second term in equation (3.8) and thus $J = 0$ for any closed contour and therefore,

$$J^* = 0. \quad (3.9)$$

Two arbitrary contours, Γ_1 and Γ_2 around a crack tip are considered, as illustrated in Fig. 3.3. If Γ_1 and Γ_2 are connected by segments along the crack face (Γ_3 and Γ_4), a closed contour is formed. On the crack face, $T_i = 0$ and $dY = 0$, thus, $J_{\Gamma_3} = 0$ and $J_{\Gamma_4} = 0$.

From equation (3.9), we have

$$J_{\Gamma_1} = -J_{\Gamma_2}. \quad (3.10)$$

Any arbitrary (counter-clockwise) path around a crack tip will yield the same value, and therefore J is path-independent.

Two bodies of elastic material (linear or nonlinear), each containing a crack (Fig. 3.1), are considered. The same systems of loads, consisting of tractions and/or displacements are prescribed on both the bodies. Except for the crack size, both the bodies are identical in composition, overall geometrical shape, and in every other aspect (Rice, 1968b). Under quasistatic conditions, and in the absence of body forces, the potential energy is given by

$$\begin{aligned} \Pi &= U - F \\ &= \int_A W \, dA - \int_{\Gamma_T} T_i u_i \, ds \end{aligned} \quad (3.11)$$

where Γ_T is the portion of the contour on which tractions are defined.

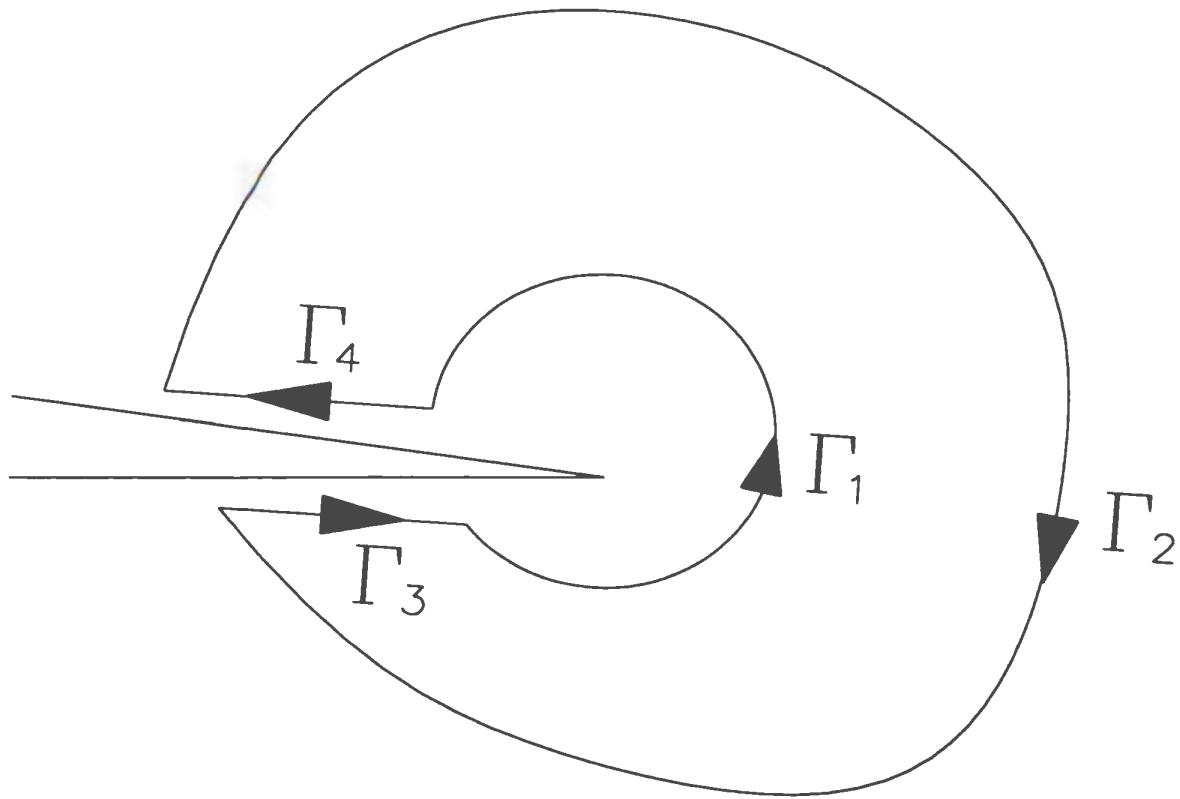


Figure 3.3: Two Arbitrary Contour, Γ_1 and Γ_2 around a crack tip

From equation (3.11), the potential energy of the two bodies in Fig. 3.1 can be expressed as:

$$\Pi(l) = \int_A W(\epsilon_{ij}) dA - \int_{\Gamma_T} T_i u_i ds \quad (3.12)$$

$$\Pi(l + \Delta l) = \int_{A+\Delta A_L-\Delta A_R} W(\epsilon_{ij} + \Delta\epsilon_{ij}) dA - \int_{\Gamma_T} T_i(u_i + \Delta u_i) ds.$$

Therefore, the difference of potential energy is :

$$\begin{aligned} \Delta\Pi &= \int_A [W(\epsilon_{ij} + \Delta\epsilon_{ij}) - W(\epsilon_{ij})] dA - \int_{\Delta A_R - \Delta A_L} W dA - \int_{\Gamma_T} T_i \Delta u_i ds \\ &= \int_A [W(\epsilon_{ij} + \Delta\epsilon_{ij}) - W(\epsilon_{ij})] dA - \Delta l \int_{\Gamma} W dy - \int_{\Gamma} T_i \Delta u_i ds \end{aligned} \quad (3.13)$$

where the third integration can be performed over the entire contour, Γ , because $\Delta u_i = 0$ over the region where the displacements are specified. The energy release rate can now be obtained as:

$$\begin{aligned} -\frac{d\Pi}{d(\Delta l)} &= -\lim_{\Delta l \rightarrow 0} \frac{\Delta\Pi}{\Delta l} \\ &= -\int_A \frac{\partial W}{\partial(\Delta l)} dA + \int_{\Gamma} W dy + \int_{\Gamma} T_i \frac{du_i}{d(\Delta l)} ds \end{aligned} \quad (3.14)$$

Considering equation (3.6), it can be seen that:

$$\frac{du_i}{d(\Delta l)} = \frac{\partial u_i}{\partial(\Delta l)} - \frac{\partial u_i}{\partial x}. \quad (3.15)$$

By using the divergence theorem, in conjunction with equations (3.1) through (3.5), the energy release rate can be obtained as:

$$-\frac{d\Pi}{d(\Delta l)} = \int_{\Gamma} W \, dy - \int_{\Gamma} T_i \frac{\partial u_i}{\partial x} \, ds. \quad (3.16)$$

From equation (3.6), the relationship can be expressed as:

$$\begin{aligned} dy &= dY \\ \text{and} & \\ \frac{\partial u_i}{\partial x} &= \frac{\partial u_i}{\partial X}. \end{aligned} \quad (3.17)$$

Furthermore,

$$-\frac{d\Pi}{d(\Delta l)} = \int_{\Gamma} [W \, dY - T_i \frac{\partial u_i}{\partial X} \, ds] = J. \quad (3.18)$$

Therefore, the J contour integral is equal to the energy release rate for a linear or nonlinear elastic material under quasistatic conditions.

3.1.2 Generalized Two-Dimensional J -Integral

Rice's J -integral formula supposes that the virtual crack extension is along the crack line in two-dimensional deformation fields. Considering the defect of materials and

manufacturing processes, crack propagation may not be exactly along the crack line. For example, a brittle material with a crack meandering and branching (Anderson, 1991) is shown in Fig. 3.4. In this sense, Rice's idealization of propagation of the crack along the crack line is just an assumption.

Similar to the analysis of Kishimoto et al. (1980), we next consider the crack tip virtual translation being along with the line oo' which has an angle θ with the X direction (Fig. 3.5). The initial crack tip o is assumed to move to o' , and the length of oo' is represented by Δl . The dashed curve indicates the virtual translation.

As done for equation (3.6), the fixed coordinate ($o - X - Y$) is related to the moving frame ($o' - x - y$) according to:

$$\begin{aligned} x &= X \cos \theta + Y \sin \theta - \Delta l \\ y &= -X \sin \theta + Y \cos \theta \end{aligned} \quad (3.19)$$

or

$$\begin{aligned} X &= x \cos \theta - y \sin \theta + \Delta l \cos \theta \\ Y &= x \sin \theta + y \cos \theta + \Delta l \sin \theta. \end{aligned} \quad (3.20)$$

Making use of the equations (3.11) through (3.16), the relationship from equation (3.19) can be rewritten as

$$dy = -\sin \theta dX + \cos \theta dY \quad (3.21)$$

$$\frac{\partial u_i}{\partial x} = \cos \theta \frac{\partial u_i}{\partial X} + \sin \theta \frac{\partial u_i}{\partial Y} .$$

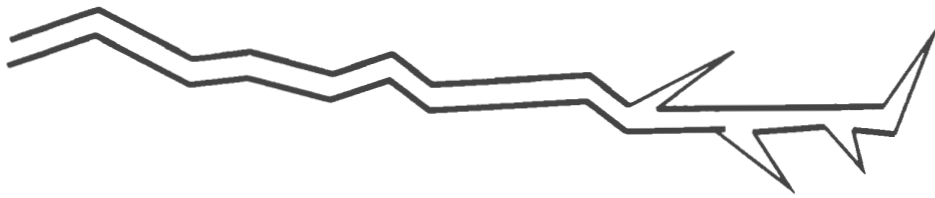


Figure 3.4: Crack Meandering and Branching

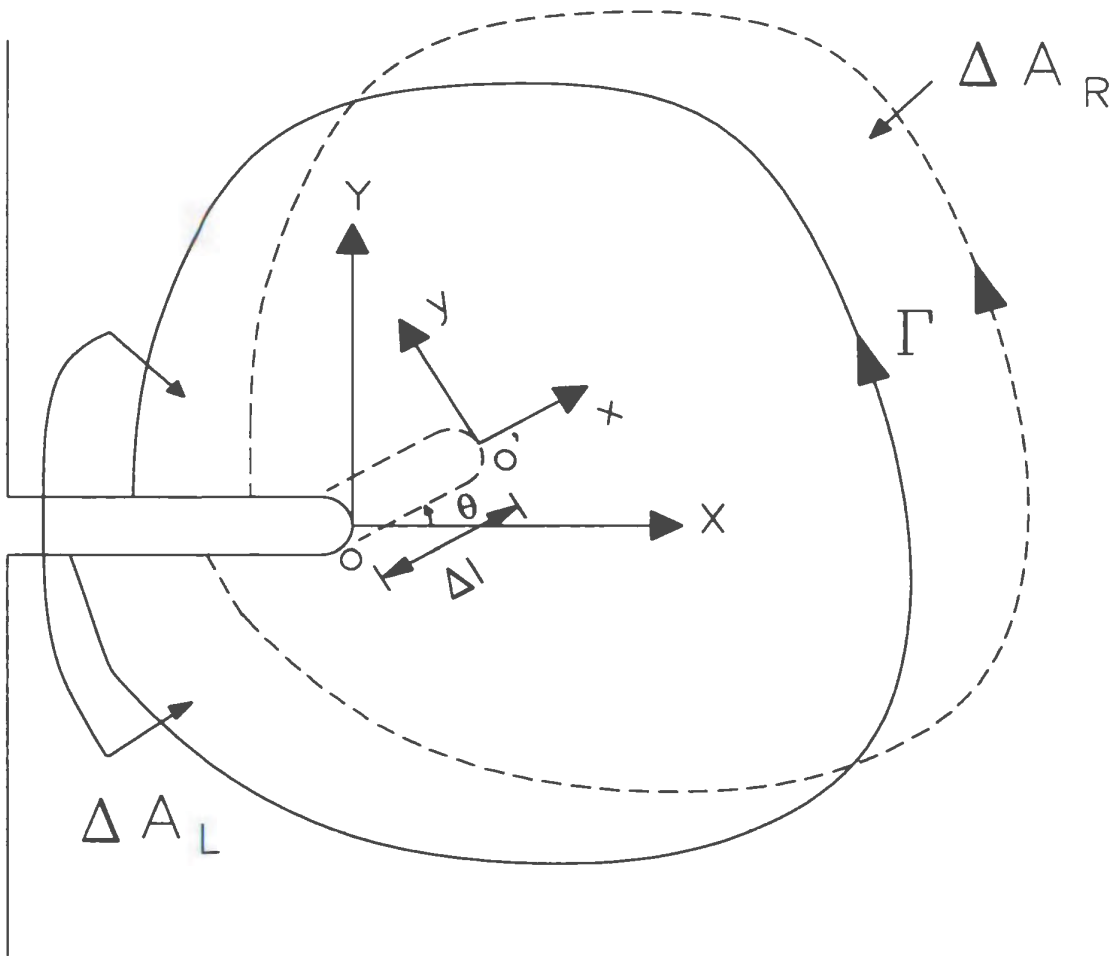


Figure 3.5: General Crack Extension in 2-D

By comparing equation (3.21) with (3.17), the energy release rate can be obtained as

$$-\frac{d\Pi}{d(\Delta l)} = J_1 \cos \theta + J_2 \sin \theta \quad (3.22)$$

where

$$J_1 = \int_{\Gamma} [W dY - T_i \frac{\partial u_i}{\partial X} ds] \quad (3.23)$$

and

$$J_2 = \int_{\Gamma} [-W dX - T_i \frac{\partial u_i}{\partial Y} ds]. \quad (3.24)$$

The above may also be written as

$$J_k = \int_{\Gamma} [W n_k - T_i \frac{\partial u_i}{\partial X_k}] ds \quad k = 1, 2 \quad (3.25)$$

where J_k ($k=1, 2$) are termed as generalized two-dimensional J -integrals. J_1 corresponds to the energy release rate due to a virtual translation in the X direction, and J_2 in the Y direction.

Similar to equation (3.9), the following integrands over a closed contour, Γ^* , are obtained as $(J_1)^* = 0$ and $(J_2)^* = 0$. From Fig. 3.3, dX is not equal to zero on Γ_3 and Γ_4 . Therefore, J_1 is path-independent [equation (3.10)], but J_2 is path-dependent. The result here is an extension of Rice's J -integral in the generalized two-dimensional deformation fields.

3.2 Analysis of Three-Dimensional J -Integral

3.2.1 First Conservation Law

The path independent integrals play a significant role in the evaluation of stress and deformation at a discontinuity by way of determining integrals over a path, away from the discontinuity and nonlinearity. In essence, J integral is a specialization of Knowles and Sternberg's (1972) first conservation law for linear and nonlinear elastic media (Bakker (1984)). For a complete surface, Σ , of a cracked body, the conservation law can be expressed as:

$$\int_{\Sigma} (W n_k - T_i u_{i,k}) dA = 0 \quad (k = 1, 2 \text{ or } 3) \quad (3.26)$$

where n stands for the unit outward normal on Σ (therefore $T_i = \sigma_{ij} n_j$). The principle of minimum potential energy and the invariance of strain energy density with regard to some classes of coordinate mappings form the basis of the conservation law as derived by Knowles and Sternberg (1972).

Fig. 3.6 shows a domain, R , in a cartesian space, representing the interior of a solid body. The divergence theorem can be applied to a regular subregion, Ω , of R with a closed piecewise differentiable surface Σ . Under quasistatic conditions, and in the absence of body forces, the potential energy of the subregion Ω can be expressed as:

$$\begin{aligned} \Pi &= U - F \\ &= \int_{\Omega} W dV - \int_{\Sigma} T_i u_i dA. \end{aligned} \quad (3.27)$$

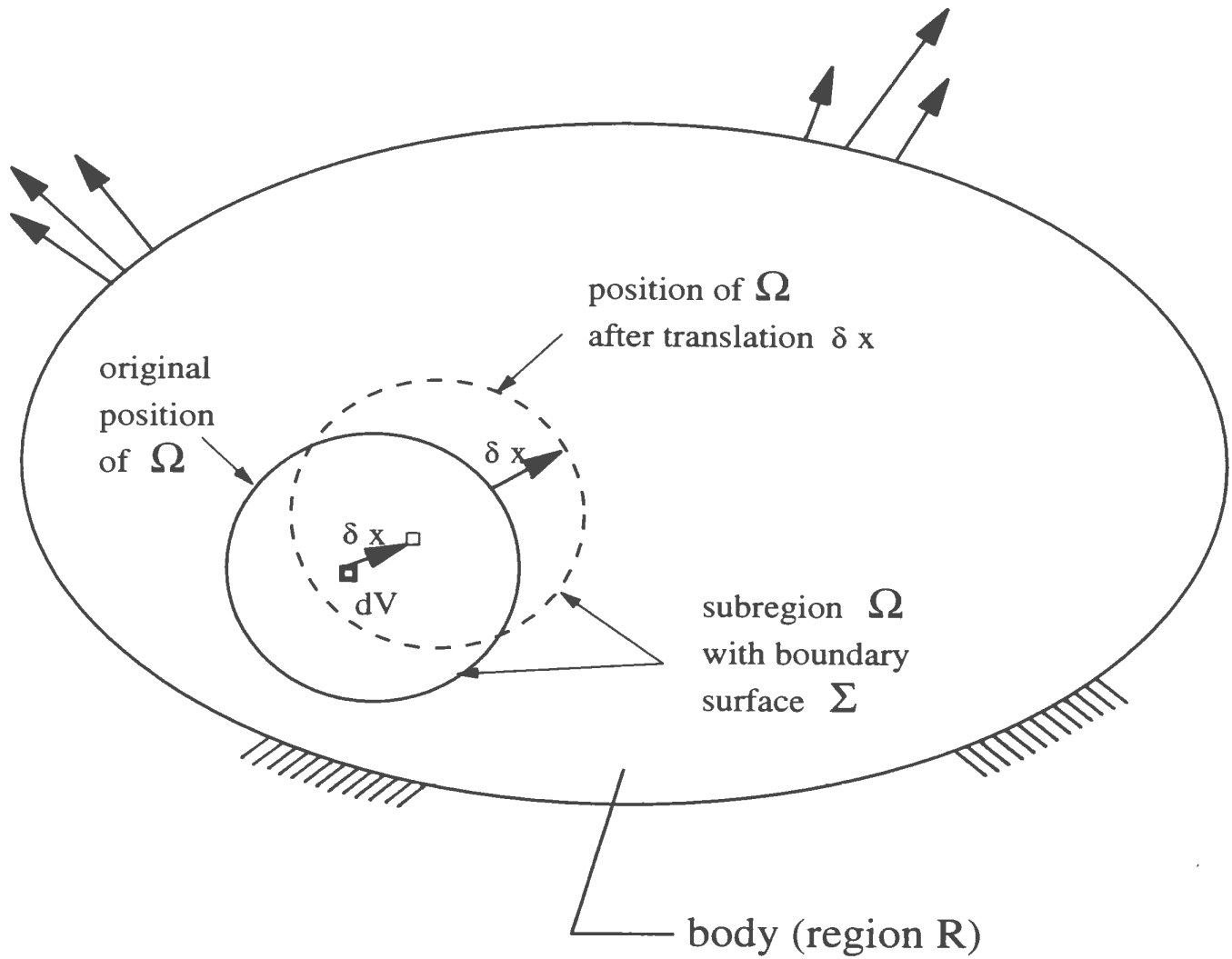


Figure 3.6: Translation of Subregion Ω with Respect to a Body R

The variation of the potential energy can be expressed as

$$\delta\Pi = \frac{\partial\Pi}{\partial x_k} \delta x_k \quad (3.28)$$

where x_k ($k=1, 2, 3$) are three-dimensional cartesian coordinates. By minimum potential energy principle,

$$\delta\Pi = \frac{\partial\Pi}{\partial x_k} \delta x_k = 0$$

Since the variation in x_k given by δx_k is chosen arbitrarily, it follows that

$$\frac{\partial\Pi}{\partial x_k} = 0. \quad (3.29)$$

Combining equations (3.27) and (3.29), we obtain

$$\int_{\Omega} W_{,k} dV - \int_{\Sigma} T_i u_{i,k} dA = 0. \quad (3.30)$$

The first conservation law given by equation (3.26) is then obtained by invoking the divergence theorem.

The first conservation law, equation (3.26), corresponds to Eshelby's (1956, 1970) energy momentum tensor equation. Rice's J -integral, defined to derive energy release rates for planar growth of two-dimensional defects in the X_1 direction, corresponds to the two-dimensional version of equation (3.26) and for $k = 1$ only.

Generalized two-dimensional J -integral expressed by equation (3.25) then corresponds to values of $k = 1, 2$.

3.2.2 Application to Three-Dimensional Cracked Bodies

For applying the integrals of equation (3.26) to cracked bodies, a part of the boundary of a subregion extending from one crack surface to the other, enclosing the crack tip, is considered. Equation (3.26) does not anymore represent the complete boundary of the subregion. The resulting values, generally non-zero, may be assigned to the components of vectors, denoted as \tilde{J} :

$$\tilde{J} = \int_{\Sigma} (W n_k - T_i u_{i,k}) dA \quad (k = 1, 2 \text{ or } 3). \quad (3.31)$$

The symbol tilde is used to distinguish the integrals from identical integrals subsequently to be defined per unit length of crack fronts.

Consider next a subregion Ω (Fig. 3.7) such that:

Σ_b : set of boundary points of Ω .

Σ : set of boundary points of Ω , excluding the defect surface.

Σ_d : set of defect boundary points of Ω .

Σ_t : set of defect tip boundary points.

Σ_s : set of defect boundary points, excluding the defect tip: separated by Σ_t into two disjunct subsets.

The first conservation law, equation (3.26), is expressed as

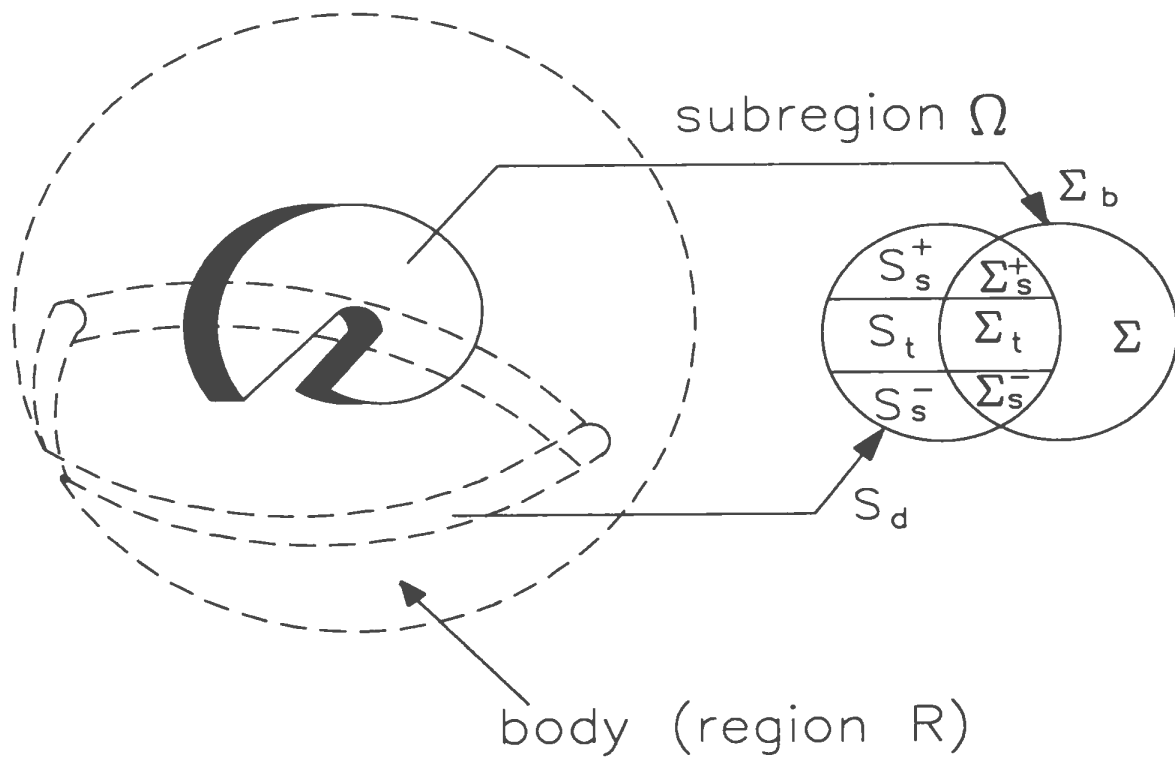


Figure 3.7: Typical Subregion in Relation to a Defect with an Associated Boundary Sets

$$\begin{aligned}
\int_{\Sigma_b} (W n_k - T_i u_{i,k}) dA &= \int_{\Sigma} (W n_k - T_i u_{i,k}) dA - \int_{\Sigma_d} (W n_k - T_i u_{i,k}) dA \\
&= 0
\end{aligned} \tag{3.32}$$

Furthermore,

$$\begin{aligned}
\tilde{J}_k &= \int_{\Sigma} (W n_k - T_i u_{i,k}) dA \\
&= \int_{\Sigma_d} (W n_k - T_i u_{i,k}) dA \\
&= \int_{\Sigma_s} (W n_k - T_i u_{i,k}) dA + \int_{\Sigma_t} (W n_k - T_i u_{i,k}) dA
\end{aligned} \tag{3.33}$$

A surface integral according to equation (3.33) is termed path independent if the integrand is unconditionally zero on Σ_s , such that equation (3.33) reduces to:

$$\begin{aligned}
\tilde{J} &= \int_{\Sigma} (W n_k - T_i u_{i,k}) dA \\
&= \int_{\Sigma_t} (W n_k - T_i u_{i,k}) dA.
\end{aligned} \tag{3.34}$$

This implies that the integrals are equal for all subregion Ω . If the integrand on Σ_s is not equal to zero, the integral is termed to be path dependent.

Fig. 3.8 shows a typical example of a subregion Ω that encloses a smoothly curved crack-tip. The coordinate axes are oriented in such a way that the flat notch surfaces are parallel to the x_1 - x_3 plane, and the notch front is perpendicular

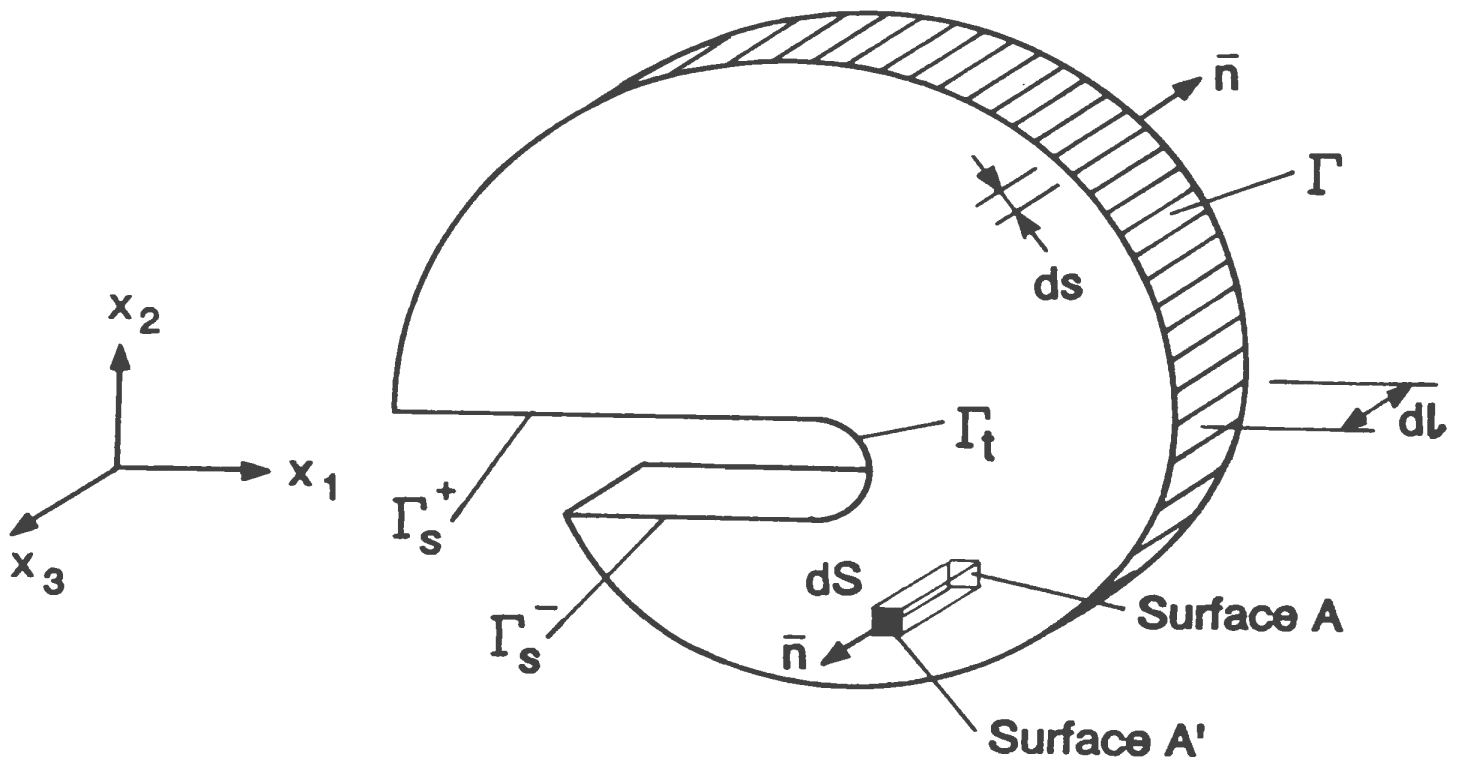


Figure 3.8: Subregion of Infinitesimal Thickness with a Smoothly Notched Defect

to the x_1 - x_2 plane at $x_3 = 0$. The dimension of the subregion in the x_3 direction is now reduced to an infinitesimal size, dl . A contour in the x_1 - x_2 plane defines the boundary of this subregion which is bounded by two surfaces A and A' parallel to this plane at $x_3 = 0$ and $x_3 = dl$, respectively. The contour is divided into three parts Γ_t , Γ_s and Γ , representing the notch tip, the flat notch surfaces and the remaining interior contour, respectively.

Application of equation (3.33) to this subregion yields:

$$\begin{aligned}\tilde{J}_k &= dl \int_{\Gamma} (W n_k - T_i u_{i,k}) ds + \int_{A+A'} (W n_k - T_i u_{i,k}) dA \\ &= dl \left[\int_{\Gamma_s} W n_k ds + \int_{\Gamma_t} W n_k ds \right].\end{aligned}\quad (3.35)$$

The integrals over A and A' are related according to:

$$\int_{A'} (W n_k - T_i u_{i,k}) dA = - \int_A (W n_k - T_i u_{i,k}) dA - dl \int_A (W n_k - T_i u_{i,k})_{,3} dA \quad (3.36)$$

where, the negative signs are due to opposite positive normal directions on A and A' . Substituting into equation (3.35) and dividing the result by dl , we find the \tilde{J} per unit crack-tip front length, denoted as J :

$$\begin{aligned}J_k &= \int_{\Gamma} (W n_k - T_i u_{i,k}) ds + \int_A (W \delta_{k3} - \sigma_{i3} u_{i,k})_{,3} dA \\ &= \int_{\Gamma_s} W n_k ds + \int_{\Gamma_t} W n_k ds\end{aligned}\quad (3.37)$$

where, as $n_1 = n_2 = 0$ and $n_3 = -1$ on A , the normal component in the surface integral is replaced by δ_{k3} (Kronecker's delta) and the traction component by $-\sigma_{i3}$. Therefore, equation (3.37) may be viewed as three-dimensional J -integral.

3.2.3 Energy Release Rate in Three-Dimensional Field

Based on the concept of energy release rate, the aspect pertaining to the path-independence of J -integral (Bakker, 1984) may be described as follows:

- (i) The energy release due to a virtual translation of $\Gamma_d (= \Gamma_s + \Gamma_t)$ in the x_1 direction is denoted by J_1 . Since only the notch tip part Γ_t of Γ_d is affected, there is no energy flow through the flat defect surface Γ_s , and the energy release is independent of Γ_s . Thus J_1 is path-independent.
- (ii) The energy release arising because of a virtual translation of Γ_d in the x_2 direction is denoted by J_2 . Since both Γ_t and Γ_s are affected, energy flows through both the surfaces, thus making J_2 path-dependent.
- (iii) A virtual translation of Γ_d in the x_3 direction, denoted by J_3 , is path-independent since no energy flow exists through Γ_d . Thus J_3 is unconditionally zero.

Given that a path-independent value is determined for the integral, a characteristic meaning can be associated with the three-dimensional formulations based on the potential energy rate. For the example discussed above, the vector components J_1 and J_3 are found to be path independent, i.e., the integrals over the contour Γ and associated area A are independent of the choice of Γ , while J_2 is always

equal to zero. Hence the J_1 component of equation (3.37) may be referred to as a three-dimensional J value.

Following the same procedure as the analysis of generalized two-dimensional J -integral, consider next the crack extension problem in a three-dimensional configuration as shown in Fig. 3.9. The solid curve represents the crack front contour in the initial state, while the dashed curve is the final crack front contour after a virtual crack extension has taken place. Let $O-X_1-X_2-X_3$ denote the fixed frame, with the origin O being at an arbitrary point along the crack front, and $O'-x_1-x_2-x_3$ be the moving frame, with the origin O' being at the point on the dashed curve, where the length of OO' is represented by Δl . Furthermore, the fixed coordinate system ($O - X_1 - X_2 - X_3$) is related to the moving system ($O' - x_1 - x_2 - x_3$) as follows:

$$\begin{aligned}
 X_1 &= l_1 x_1 + l_2 x_2 + l_3 x_3 + l_1 \Delta l \\
 X_2 &= m_1 x_1 + m_2 x_2 + m_3 x_3 + m_1 \Delta l \\
 X_3 &= n_1 x_1 + n_2 x_2 + n_3 x_3 + n_1 \Delta l
 \end{aligned} \tag{3.38}$$

where (l_i, m_i, n_i) are the direction cosines of the moving system axes x_i . For instance, $l_1 = \cos \theta_o$, $m_1 = \cos \phi_o$, $n_1 = \cos \psi_o$.

Similarly with equation (3.22), the energy release rate in three-dimensional configurations in terms of $O-X_1-X_2-X_3$ can be expressed as:

$$-\frac{d\Pi}{d(\Delta l)} = J_1 \cos(\theta_o) + J_2 \cos(\phi_o) + J_3 \cos(\psi_o) \tag{3.39}$$

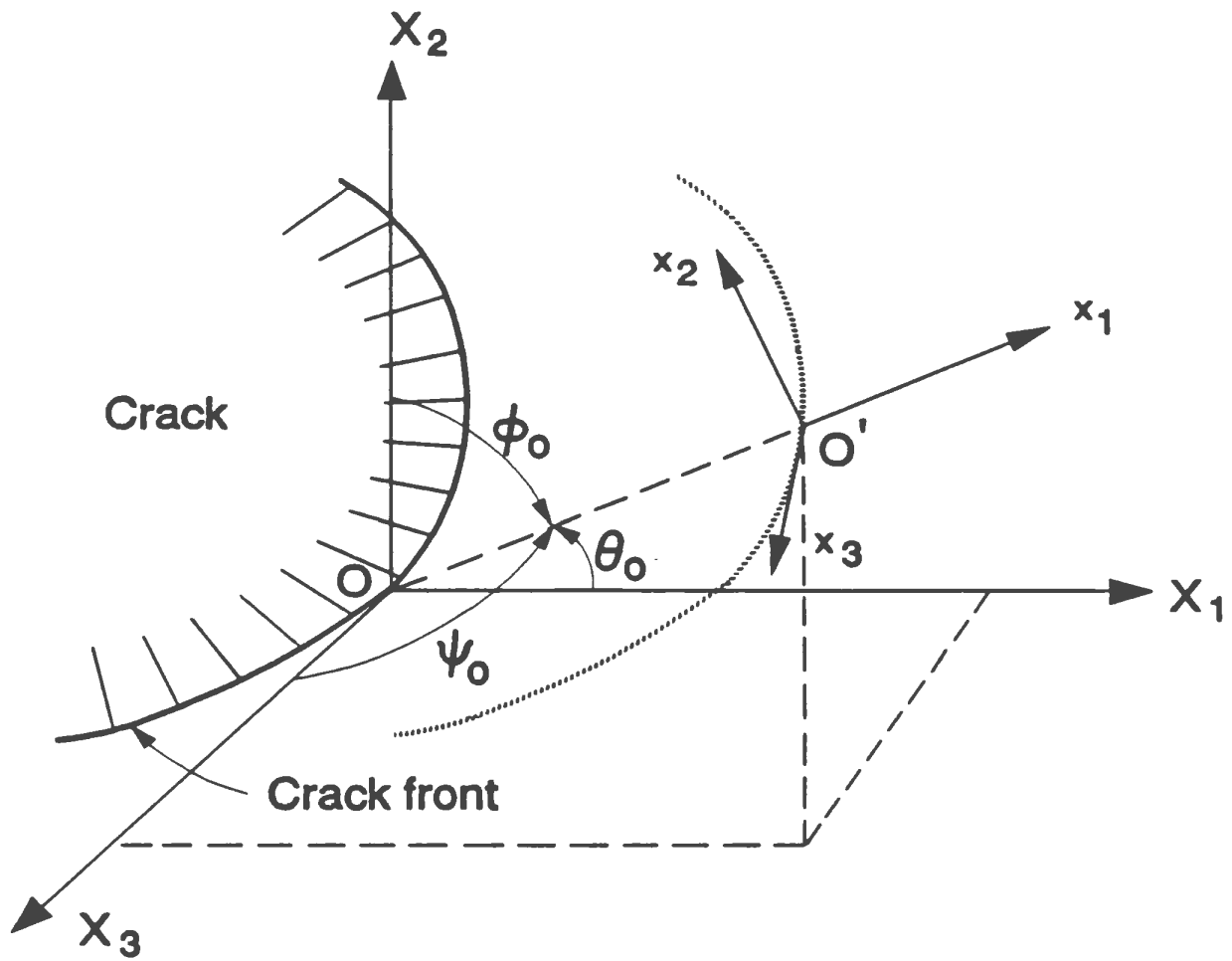


Figure 3.9: Schematic Representation for 3-D Crack Front

where θ_o , ϕ_o and ψ_o are the angles of line OO' with X_1 , X_2 and X_3 respectively.

For a straight-through cracked body (i.e. a finite-thickness plate with a through-crack) where the crack front is a straight line, it can be expected that OO' extends along X_1 direction and therefore, $\theta_o = 0$ and $\phi_o = \psi_o = \pi/2$. From equation (3.39), the energy release rate can be written as:

$$-\frac{d\Pi}{d(\Delta l)} = J_1. \quad (3.40)$$

From the aforementioned discussions it is clear that J_1 for three-dimensional loadings can be viewed as energy release rate for a finite-thickness cracked body. Equation (3.40) is central to the development of the $2\frac{1}{2}$ -Dimensional theory for practical pressure components with defects which would be described later in this thesis.

Chapter 4

Estimation of Mode I Crack Tip Plastic Zone Size

4.1 Introduction

Most of the classical methods of solution in fracture mechanics reduce a problem to two dimensions, i.e., plane stress or plane strain. A straight-through crack in finite-thickness plates may be viewed as a plane stress case when the thickness $B \leq \frac{1}{3\pi} \left(\frac{K_{cmax}}{\sigma_y} \right)^2$, or as a plane strain case when $B \geq 2.5 \left(\frac{K_{IC}}{\sigma_y} \right)^2$ (Ewalds and Wanhill, 1986). In general, the conditions at a crack tip for a specimen of finite-thickness indicate that there is neither plane stress nor plane strain condition present. The crack tip stress and strain are three-dimensional in such cases, the three-dimensional effects being essentially geometric.

It has been demonstrated that the plastic zone size at a crack tip is influenced by the crack tip constraint parameter (Wu and Seshadri, 1995a). The GLOSS method of analysis can also be used to evaluate the three-dimensional crack tip constraint parameter λ . The GLOSS technique is briefly discussed in the next section.

4.2 GLOSS Analysis

The GLOSS analysis, described by Seshadri (1991), is a simple and systematic method for carrying out inelastic evaluations of mechanical components and structures on the basis of two linear elastic finite element analyses. The mechanical component or structure is divided into “local” and “remainder” regions. Typically, “local” regions are subjected to a high strain concentrations while the “remainder” regions are predominantly elastic. The GLOSS method determines the constraint parameter, λ , which characterizes the manner in which the remainder region interacts with the local region.

A linear elastic finite element analysis of the structure is first carried out, and the elements with equivalent stress, σ_e , above the material yield stress, σ_y , are identified. The elastic modulus of each of these elements is modified from its original value of E_o to

$$E_s = E_o \frac{\sigma_y}{\sigma_e}. \quad (4.1)$$

The elastic moduli of all the other elements are kept unchanged.

A second linear elastic finite element analysis is then carried out with the modified set of moduli. If the highest stressed element in the structure has equivalent stress and strain $[(\sigma_e)_1, (\epsilon_e)_1]$ from the first analysis, and $[(\sigma_e)_2, (\epsilon_e)_2]$ from the second analysis, for example, then the normalized relaxation modulus \bar{E}_r is given by

$$\bar{E}_r = \frac{E_r}{E_o} = \frac{1}{E_o} \frac{(\sigma_e)_1 - (\sigma_e)_2}{(\epsilon_e)_1 - (\epsilon_e)_2} \quad (4.2)$$

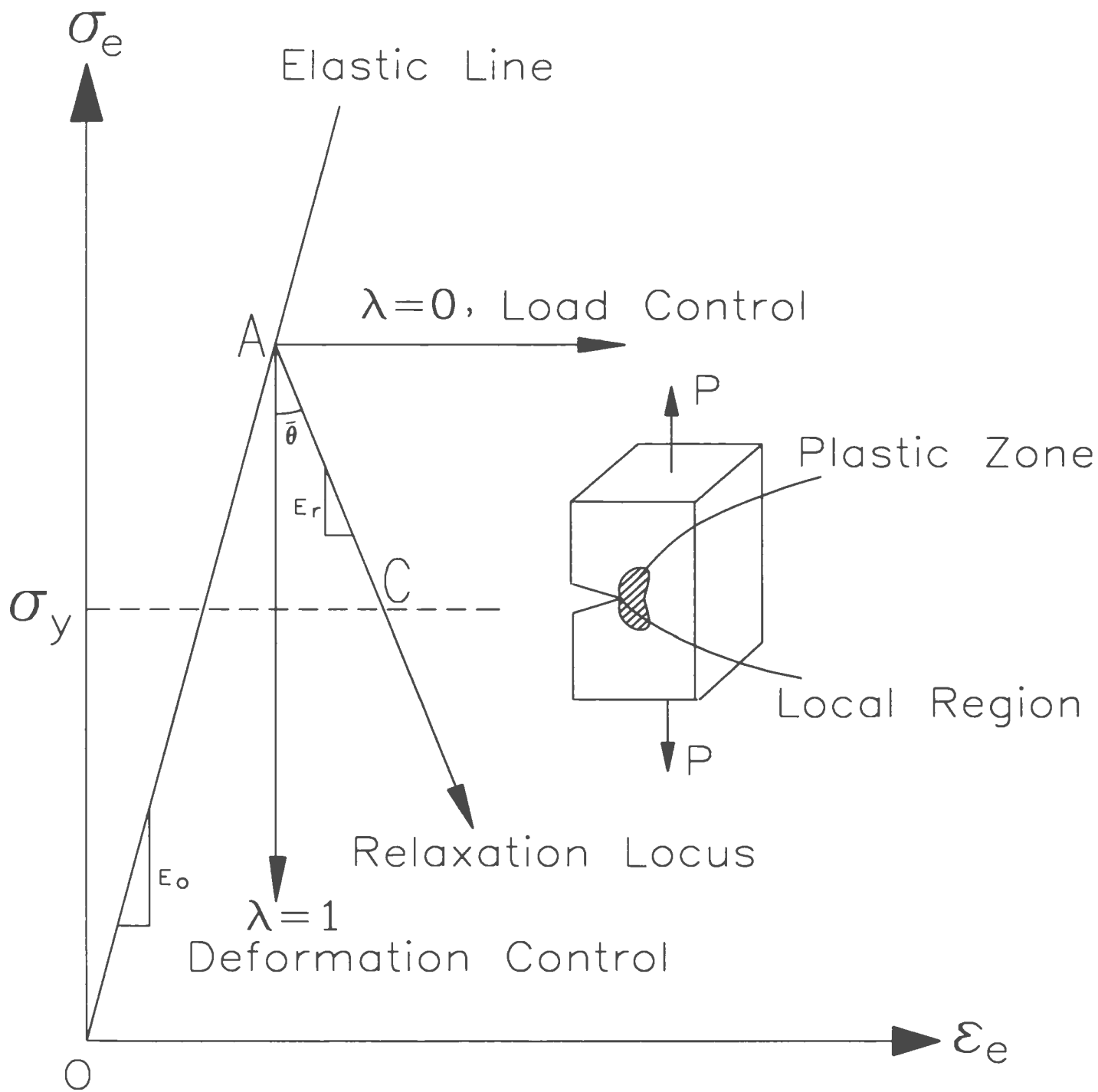


Figure 4.1: GLOSS Diagram - Local System Response in a Crack

The GLOSS theory essentially relates the multiaxial stress distribution in the local region to the uniaxial redistribution process. The varying degrees of interaction between the local and remainder regions are characterized by a “constraint parameter” which can be used in conjunction with the uniaxial model to generate inelastic results.

Key to GLOSS evaluations is the determination of the local region relaxation modulus. This can be accomplished by studying the relaxation locus on the GLOSS diagram. For small-to-moderate plastic zone sizes, the relaxation locus is almost linear in many practical component configurations. In other words, the local region relaxation modulus is dependent, to a first approximation, on the response of the remainder region. The local region response would therefore appear to be insensitive to the precise nature of the local region nonlinearity and the material constitutive relationship. The implication is quite significant in that the relaxation modulus can be determined using any convenient constitutive relationship that allows progressive relative softening of the local region. Therefore, GLOSS analysis can be used to predict inelastic response whether the inelasticity arises due to first stage creep, steady state creep, or even time-independent plasticity. Local region softening by systematically reducing the elastic modulus, for instance, is therefore an attractive prospect. The constraint parameter λ at local region may be then derived as (Fig. 4.1):

$$\lambda = \frac{\bar{E}_r}{\bar{E}_r - 1}. \quad (4.3)$$

The factor λ can be evaluated for any element in a similar manner.

4.3 Multiaxial Constraint

The concepts of load and deformation control can be illustrated on the GLOSS diagram (Fig. 4.1). For deformation control action, the relaxation locus AC in Fig. 4.1 would be vertical and therefore the value of λ would be equal to one. The implication is that a highly localized inelastic zone is surrounded by an entirely elastic remainder. It is precisely due to this reason that “shakedown” action occurs in mechanical components and structures. For load control action, on the other hand, the relaxation locus AC would be horizontal and hence the value of λ would be equal to zero. This situation is usually associated with a statically determinate action such as incipient collapse or net section yielding.

In most cases, however, the local region would exhibit a mixed-mode response, and the value of λ would vary between zero and one. A constant value of λ implies that the principal stress ratios are invariant along the relaxation line. For small to medium amounts of follow-up, the stress ratio changes are not significant. The assumption of proportional loading is implied along a relaxation line for which λ is constant, although in reality some departure from this is expected.

4.4 Normalized Constraint Parameter $\bar{\lambda}$

By stipulating the ideal plane strain conditions as a reference, the normalized constraint parameter $\bar{\lambda}$ can be defined as the ratio of the three-dimensional constraint parameter to the plane strain constraint parameter (no crack-tip deformation in the thickness direction) for a finite-thickness specimen:

$$\bar{\lambda} = \frac{\lambda}{\lambda_{\infty}} \quad (4.4)$$

where λ_{∞} represents the plane strain constraint parameter (corresponding to $B/a \rightarrow \infty$).

Based on two linear elastic finite element analyses (GLOSS analysis), for the three-dimensional finite element model illustrated in Fig. 4.2, a family of curves depicting $\bar{\lambda}$ vs. (B/a) is obtained for various loading conditions (Fig. 4.3).

It can be seen that when B/a is very small (i.e. $B/a \leq 0.05$), the plane stress condition is approached, i.e., $\bar{\lambda}_0$ is almost a constant, for constant loading. The subscript '0' adjacent to $\bar{\lambda}$ corresponds to the plane stress case ($B/a \rightarrow 0$). The three-dimensional crack-tip constraint parameter is bounded by the two-dimensional limiting cases of plane stress and plane strain. Therefore, the value of $\bar{\lambda}$ is between $\bar{\lambda}_0$ and one.

4.5 Approximate Method for Determining Crack-Tip Plastic Zone Size

It can be seen that the three-dimensional crack tip plastic zone size along $\theta = 0$ of the mid-section plane, r_y , meets the requirement that $r_{\infty} < r_y < r_0$, where r_0 and r_{∞} are plastic zone sizes along crack plane ($\theta = 0$) for plane stress and plane strain conditions, respectively.

For plane stress and plane strain conditions, the plastic zone sizes at the crack plane ($\theta = 0$) for mode I specimen with small-scale yielding are as follows (Anderson, 1991):

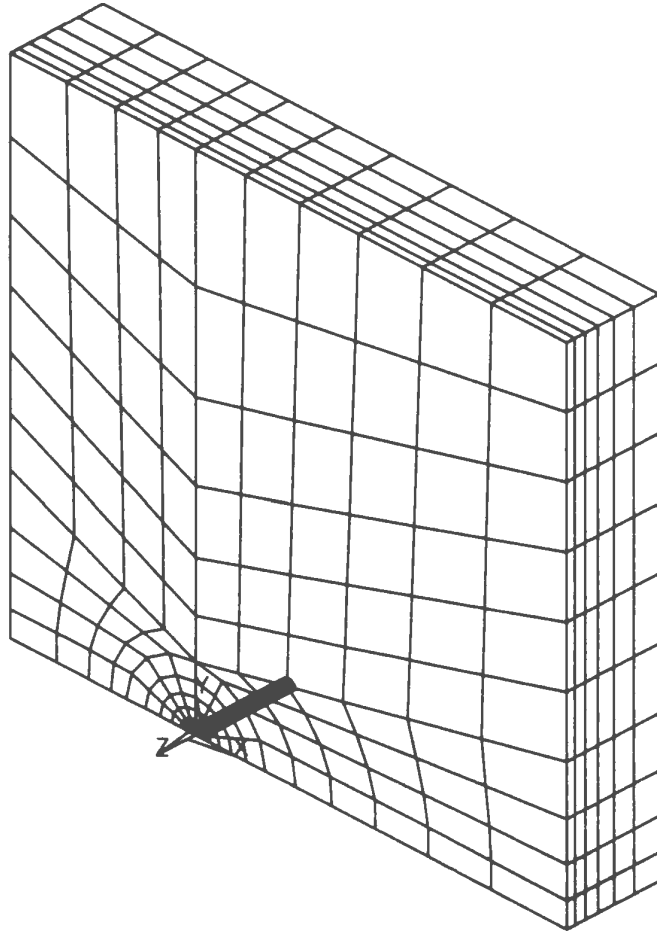


Figure 4.2: 3-D Finite Element Model

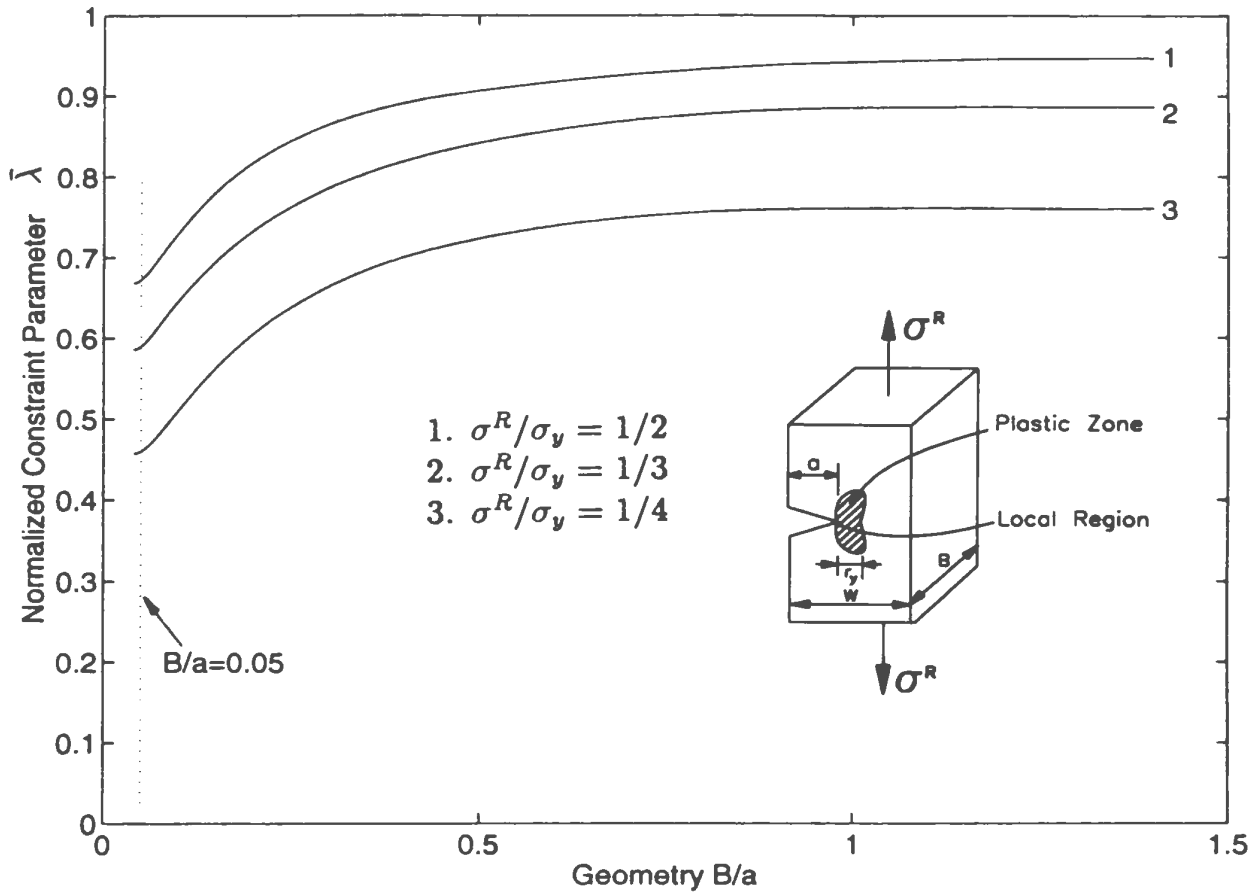


Figure 4.3: Normalized Constraint Parameter ($\bar{\lambda}$) vs. Geometry (B/a)

$$r_0 = \frac{1}{2\pi} \left(\frac{K_I}{\sigma_y} \right)^2 \quad (4.5)$$

and

$$r_\infty = \frac{(1 - 2\nu)^2}{2\pi} \left(\frac{K_I}{\sigma_y} \right)^2 \quad (4.6)$$

where K_I is the mode I stress intensity factor, and ν is the Poisson's ratio.

Assuming that the crack-tip plastic zone size is influenced by the crack-tip constraint parameter, the three-dimensional plastic zone size (r_y) can be estimated by the expression

$$r_y = r_\infty f(\bar{\lambda}) \quad (4.7)$$

where $f(\bar{\lambda})$ is, as yet, an undetermined function of the three-dimensional normalized crack tip constraint parameter $\bar{\lambda}$.

Equation (4.7) is prompted by the observation that when $\bar{\lambda} = 1$ the plane-strain condition is achieved, and the plastic-zone size $r_y = r_\infty$. As well, when $\bar{\lambda} = \bar{\lambda}_0$ corresponding to plane stress, $r_y = r_0$.

Comparing equation (4.7) with equations (4.5) and (4.6), we have:

$$f(1) = 1 \quad (4.8)$$

and

$$f(\bar{\lambda}_0) = 1/(1 - 2\nu)^2. \quad (4.9)$$

With an increase in the load, yielding at the crack plane becomes extensive and spreads to the lateral boundary ahead of the crack resulting in uncontained plastic flow. For this limiting case, r_y is identified with the crack ligament length ($W - a$). Therefore,

$$f(0) \simeq (W - a)/r_\infty. \quad (4.10)$$

A simple relationship between $f(\bar{\lambda})$ and $\bar{\lambda}$ can then be expressed as,

$$f(\bar{\lambda}) = C_1 + C_2 \bar{\lambda} + C_3 (\bar{\lambda})^2, \quad (4.11)$$

where C_1 , C_2 and C_3 can be determined from equations (4.8), (4.9) and (4.10). The constants are dependent on the specimen geometry, the material property and the loading conditions.

Therefore, equations (4.7) and (4.11) can be seen to provide an approximate estimation of the three-dimensional crack tip plastic zone size along $\theta = 0$ at the mid-section for mode I crack specimens. The procedure can also be used for evaluating the three-dimensional crack tip plastic zone size for different crack plane orientations ($0 \leq \theta \leq \pi$).

4.6 Remarks

An approximate method to evaluate the three-dimensional crack tip plastic zone size has been presented in this chapter. The expression for the estimation is based on LEFM results and therefore, the plastic zone size is small in comparison with the specimen crack ligament. The method presented in this chapter can be used to evaluate crack-tip plastic constraint parameters for many practical components.

Chapter 5

J-Estimation of Circular-Ended Notches

5.1 Introduction

An edge-crack problem can be viewed as the limiting case of circular-ended notch. Therefore, the edge-crack tip *J*-estimation may be obtained through the analysis of *J* for circular-ended notches. Approximate methods proposed here are based on the concept of the GLOSS technique. Following the approximate *J*-estimation of circular-ended notches, the edge-crack tip *J* in the limiting case is evaluated.

Key to this analysis is to determine the notch root stress and strain. Usually, numerical techniques, such as the inelastic finite element method and the boundary element method are used for obtaining the strain concentration at notches. However, numerical analysis can be time-consuming and expensive. From an engineering standpoint, a quicker and less expensive method is often preferable.

A commonly used method for the estimation of notch stress and strain is the Neuber's rule (Neuber, 1961). However, this rule has been shown to overestimate the strain concentration at notches. The GLOSS method of analysis is a practical

compromise between the elaborate methods (such as the inelastic finite element method) and the approximate analytical techniques. In this chapter, the notch root stress and strain are obtained for strain-hardening material behavior using GLOSS analysis and further, J -integral for smooth-ended notches is derived.

5.2 Notch Root Stress and Strain

For the sake of generality, the strain-hardening material behavior as governed by the modified Ludwik equation is assumed, i.e.,

$$\begin{aligned} \epsilon &= \frac{\sigma}{E_o} & \epsilon \leq \epsilon_y \\ \epsilon &= B\sigma^n & \epsilon > \epsilon_y \end{aligned} \tag{5.1}$$

where $B = \sigma_y^{1-n}/E_o$ and $\sigma_y = E_o\epsilon_y$. For a linear elastic material, $n = 1$ whereas for an elastic perfectly-plastic material, $n \rightarrow \infty$.

The underlying principle behind GLOSS evaluations lies in the determination of the relaxation modulus of the local region. The relaxation locus on the GLOSS diagram (Fig. 4.1) serves as an indicator for such a study. For small-to-moderate plastic zone sizes (i.e., follow-up angle $\bar{\theta} < 60^\circ$), the relaxation locus is found to be almost linear. The local region constraint can be characterized by the relaxation line AC , and therefore the constraint parameter, λ . The equation of line AC is:

$$\frac{\sigma_{ei} - \sigma_r}{\epsilon_{ei} - \epsilon_r} = \frac{\lambda}{\lambda - 1} E_o \tag{5.2}$$

where σ_{ei} is the highest equivalent stress in the first linear elastic finite element analysis and $\epsilon_{ei} = \sigma_{ei}/E_o$. The factors σ_r and ϵ_r correspond to the notch root stress and strain.

Based on the intersection of the local region relaxation line and strain-hardening material curve, the notch root stress and strain can be determined. By combining equations (5.1) and (5.2), notch root equivalent stress and strain can be obtained as

$$\lambda E_o B \sigma_r^n - (\lambda - 1) \sigma_r - \sigma_{ei} = 0$$

and (5.3)

$$\epsilon_r = B \sigma_r^n.$$

Particularly, for the linear material, $\sigma_r = \sigma_{ei}$ and $\epsilon_r = \sigma_{ei}/E_o$. For the elastic perfectly-plastic material, $\sigma_r = \sigma_y$ and $\epsilon_r = [\sigma_y + (\sigma_{ei} - \sigma_y)/\lambda]/E_o$.

5.3 *J*-Integral for Smooth-Ended Notches

Considering a flat-surfaced notch in a two-dimensional deformation field (Fig. 5.1), the *J*-integral may be evaluated along the curved notch tip Γ_r (Rice, 1968a).

The expression for two-dimensional *J*-integral is written as equation (2.6). Along the notch surface, since there is no traction, $T_i = 0$. This leads to

$$J = \int_{\Gamma_r} W dy$$

$$= \int_{-\pi/2}^{+\pi/2} W[\epsilon(\phi)] \rho_t(\phi) \cos(\phi) d\phi \quad (5.4)$$

where $W[\epsilon(\phi)]$ is the strain energy density of the notch end, $\rho_t(\phi)$ is the radius of curvature of the notch end, and ϕ is the angle included between the tangent to the notch end edge and the y -axis.

Considering strain-hardening material behavior, equation (5.1), the strain energy density is given by

$$\begin{aligned} W &= \int_0^\epsilon \sigma d\epsilon \\ \text{or } W &= \frac{1-n}{2(1+n)} \frac{(\sigma_y)^2}{E_o} + \frac{n}{n+1} \sigma \epsilon \end{aligned} \quad (5.5)$$

where $\sigma > \sigma_y$. For a linear elastic material, the strain energy density W_e is equal to $\frac{1}{2}\sigma\epsilon$. For a rigid plastic material, the strain energy density W_p is equal to $\sigma\epsilon$.

For approximations to the strain concentration through equation (5.4), Rice (1968a) considers a feature of the linear elastic problem of an ellipsoidal inclusion in an infinite matrix subjected to a uniform remote stress state. An ellipsoidal void in a material can be assumed to be an imagined inclusion with zero elastic moduli. Therefore, the surface strains for an elliptical hole in a linear elastic plate, loaded symmetrically so as to cause no shear or rotation of the imagined inclusion can be given by the expression (Eshelby, 1957):

$$\epsilon(\phi) = \epsilon_{max} \cos^2 \phi + \epsilon_{min} \sin^2 \phi. \quad (5.6)$$

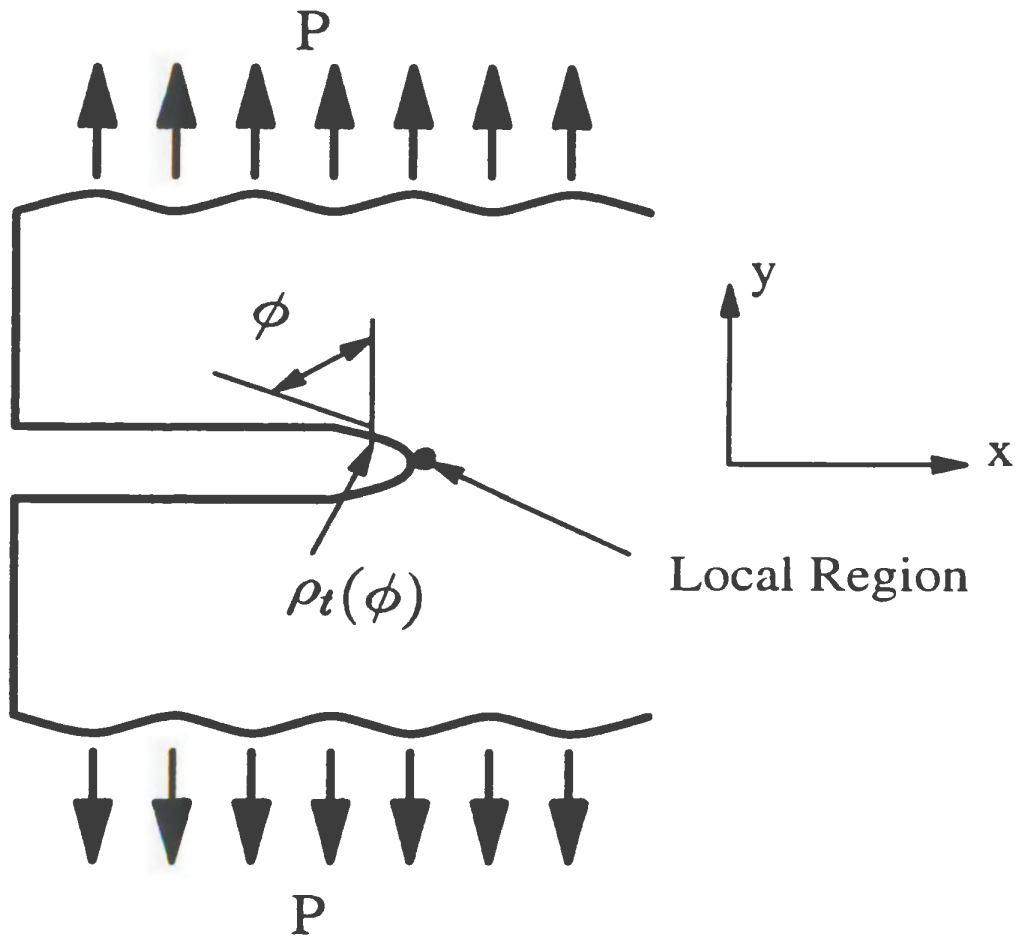


Figure 5.1: Typical Flat-surfaced Notch in a Two-dimensional Deformation Field

Here the ϕ notation is as in Fig. 5.1, ϵ_{max} is the strain at the semimajor axis ($\phi = 0, \pi$), and ϵ_{min} at the semiminor axis ($\phi = \pi/2, 3\pi/2$). Assuming ϵ_{min} to be small compared to ϵ_{max} , and postulating that the same interpretation of the surface strains holds good for the other cases also, equation (5.6) can be rewritten as:

$$\epsilon(\phi) = \epsilon_r \cos^2(\phi) \quad (5.7)$$

where the notch root strain ϵ_r corresponds to the maximum surface strain. Further, by combining equations (5.7) and (5.1), the corresponding expression for the surface stresses can be obtained as:

$$\sigma(\phi) = \sigma_r (\cos(\phi))^{2/n}. \quad (5.8)$$

The J -integral for notches can be derived from equations (5.4) through (5.8) as:

$$J = \frac{1-n}{2(1+n)} \frac{(\sigma_y)^2}{E_o} f_1 + \frac{n}{1+n} f_2 \sigma_r \epsilon_r, \quad (5.9)$$

where

$$f_1 = \int_{-\pi/2}^{+\pi/2} \rho_t(\phi) \cos(\phi) d\phi$$

$$f_2 = \int_{-\pi/2}^{+\pi/2} \rho_t(\phi) (\cos(\phi))^{3+2/n} d\phi.$$

Particularly, for a semi-circular end notch, $\rho_t(\phi) = \rho$ and therefore $f_1 = 2\rho$, $f_2 = \sqrt{\pi} \frac{\Gamma(2+1/n)}{\Gamma(5/2+1/n)} \rho$. On the basis of equations (5.3) and (5.9), J -integral for strain hardening material at the circular-ended notch can be evaluated.

5.4 J -Estimation Methods

A robust approximation is one which may seldom give an exact solution, but will be close enough for practical purposes. The solution will be relatively insensitive to inadequacies, uncertainties or variability in the input data which is typical of an industrial operating plant environment. Two approximate methods for the determination of J -integral are discussed here:

Method I: For the elastic perfectly-plastic material, notch root equivalent stress σ_r is equal to σ_y and equivalent strain ϵ_r is equal to $[\sigma_y + (\sigma_{ei} - \sigma_y)/\lambda]/E_o$. From equation (5.9) (when $n \rightarrow \infty$), elastic perfectly-plastic J_{e-p} of circular-ended notches can be obtained as

$$J_{e-p} = \frac{\sigma_y}{3E_o\lambda} [4(\sigma_{ei} - \sigma_y) + \lambda\sigma_y] \rho. \quad (5.10)$$

Comparing the elastic perfectly-plastic case with the linear elastic case in the notch root stress-strain curve (Fig. 5.2), the strain energy density W_{e-p} should be larger than W_e , and therefore, the area (A_1) of rectangle $BCFE$ should be larger than the area (A_2) of triangle ABD .

Based on the linear relaxation locus AC , following equation (5.3), the areas A_1 and A_2 are obtained as:

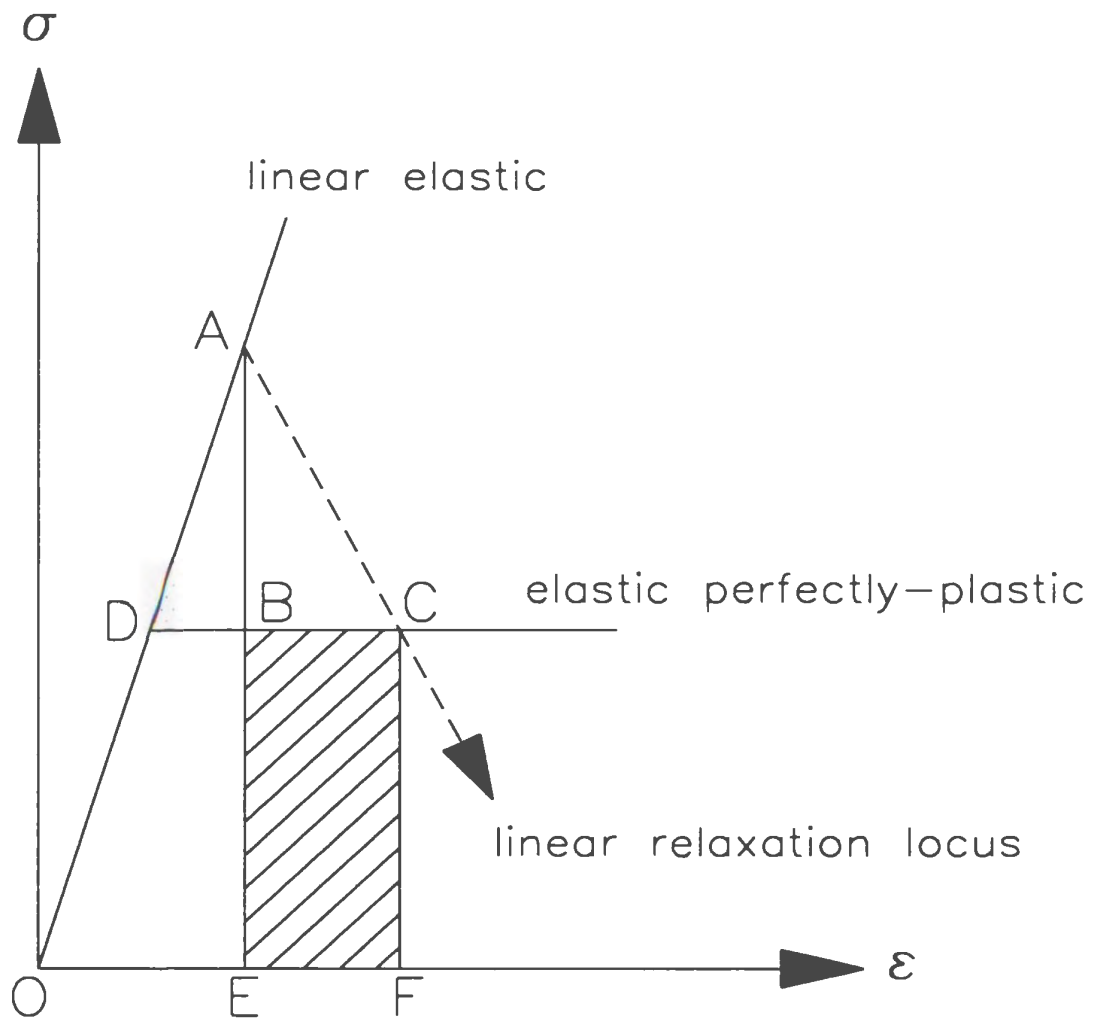


Figure 5.2: Notch Root Stress-Strain Curve

$$A_1 = \left[\frac{\sigma_y + (\sigma_{ei} - \sigma_y)/\lambda}{E_0} - \frac{\sigma_{ei}}{E_0} \right] \sigma_y \quad (5.11)$$

and

$$A_2 = \frac{1}{2} \frac{(\sigma_{ei} - \sigma_y)^2}{E_0}. \quad (5.12)$$

The GLOSS constraint parameter λ is then obtained as

$$\lambda \leq \frac{2}{\sigma_{ei}/\sigma_y + 1}. \quad (5.13)$$

For the condition $\lambda \geq 2/(\sigma_{ei}/\sigma_y + 1)$, J_{e-p} can be calculated from the constraint parameter $\lambda = 2/(\sigma_{ei}/\sigma_y + 1)$. Therefore, equation (5.10) can be rewritten as

$$J_{e-p} = \begin{cases} \frac{1}{3E_0} [2(\sigma_{ei})^2 - (\sigma_y)^2] \rho & \text{for } \lambda \geq \frac{2}{\sigma_{ei}/\sigma_y + 1} \\ \frac{\sigma_y}{3E_0\lambda} [4(\sigma_{ei} - \sigma_y) + \lambda\sigma_y] \rho & \text{for } \lambda \leq \frac{2}{\sigma_{ei}/\sigma_y + 1}. \end{cases} \quad (5.14)$$

Based on finite element evaluation (Wu and Seshadri, 1995b,c), it has been found that J for elastic perfectly-plastic material is larger than J for general strain-hardening material (Fig. 5.3). Considering strain-hardening material behavior in practice, for the purpose of safe design in engineering, equation (5.14) can be used for the elastic-plastic J -estimation of circular-ended notches.

Method II: Following the procedure used by Seshadri and Kizhatil (1995), an estimate of the elastic-plastic J based on the GLOSS constraint parameter, λ , is obtained as

$$J = \lambda J_e + (1 - \lambda) J_p. \quad (5.15)$$

Equation (5.15) is prompted by the observation that when the constraint parameter $\lambda = 0$, i.e., large plastic zone size is attained, $J \rightarrow J_p$, and when $\lambda = 1$, i.e., for constrained plasticity, $J = J_e$.

On the basis of equations (5.5) and (5.9), J_e and J_p are expressed as:

For linear elastic material:

$$J_e = \frac{8}{15} \frac{(\sigma_{ei})^2}{E_o} \rho. \quad (5.16)$$

For rigid plastic material:

$$J_p = \frac{4\sigma_y}{3E_o\lambda} [(\sigma_{ei} - \sigma_y) + \lambda\sigma_y] \rho. \quad (5.17)$$

Combining equations (5.15), (5.16) and (5.17), the elastic-plastic J can be obtained as follows:

$$J_{e/p} = \frac{8\lambda}{15} \frac{(\sigma_{ei})^2}{E_o} \rho + \frac{4(1 - \lambda)\sigma_y}{3E_o\lambda} [(\sigma_{ei} - \sigma_y) + \lambda\sigma_y] \rho \quad (5.18)$$

Equation (5.18) is another J -estimation of circular-ended notches. Equations (5.14) and (5.18) can, therefore, be considered as approximate J -estimations. The constraint parameter λ can be evaluated by GLOSS analysis for the notch root according to equations (4.1), (4.2) and (4.3).

Consider that the assumption of a linear relaxation locus is only suitable for small-to-moderate plastic zone sizes, i.e., follow-up angle is $0 \leq \bar{\theta} \leq 60^\circ$. From the GLOSS diagram (Fig. 4.1), the angle $\bar{\theta}$ can be calculated by the following expression

$$\bar{\theta} = \frac{\pi}{2} - \arctan(-\bar{E}_r). \quad (5.19)$$

Following equation (4.3), for a linear relaxation locus, the GLOSS constraint parameter is given by,

$$\frac{\sqrt{3}-1}{2} \leq \lambda \leq 1. \quad (5.20)$$

From Fig. 5.3, it is seen that J estimated by equation (5.18) is conservative up to loads close to limit loads. This corresponds to normalized load value of 0.9. Beyond this loading, the estimate given by equation (5.18) underestimates J . However, well-designed structural components rarely undergo such high loading, and hence this part of the curve should not be used in practice.

If a bilinear strain hardening material behavior is assumed for the numerical examples considered above, it is found that the elastic-plastic J estimated by nonlinear finite element analysis is lower than that for an elastic perfectly-plastic material as

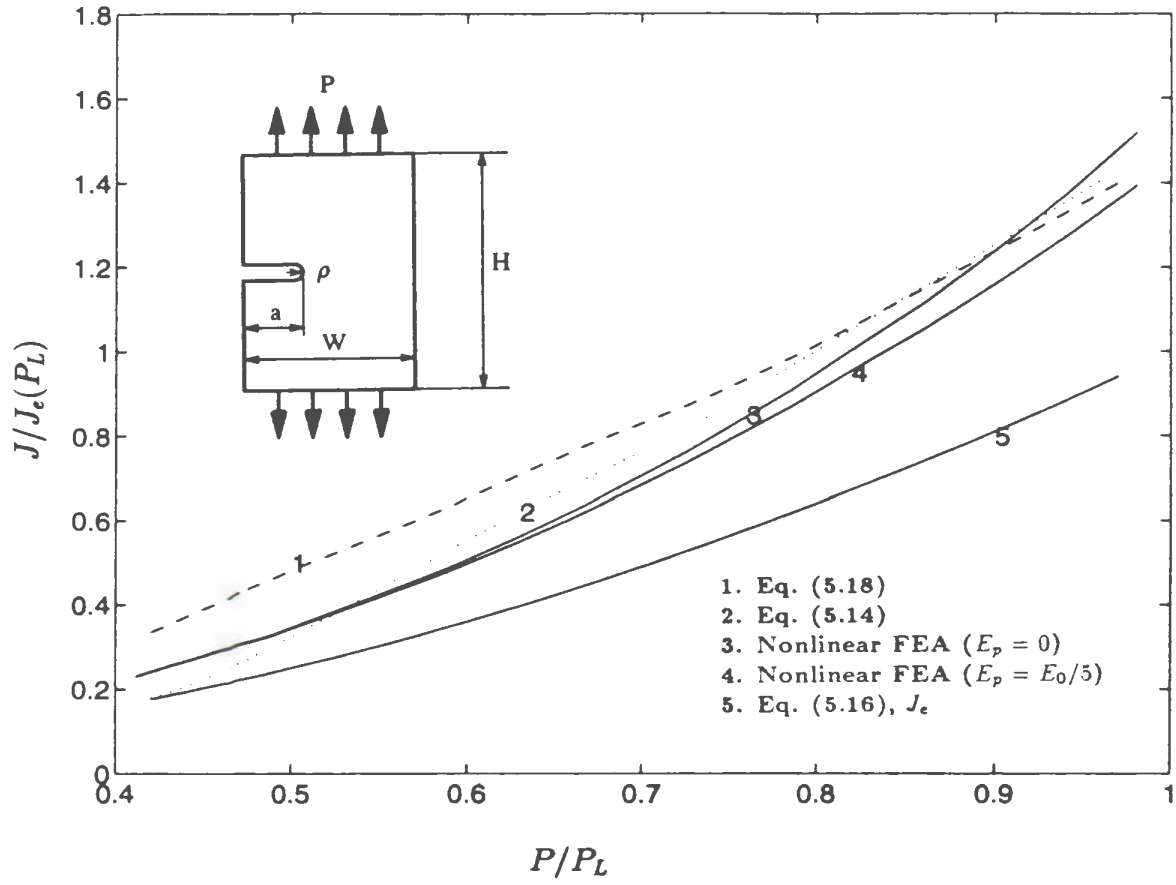


Figure 5.3: J vs. Load P for Single-Edge Circular Notch Specimen

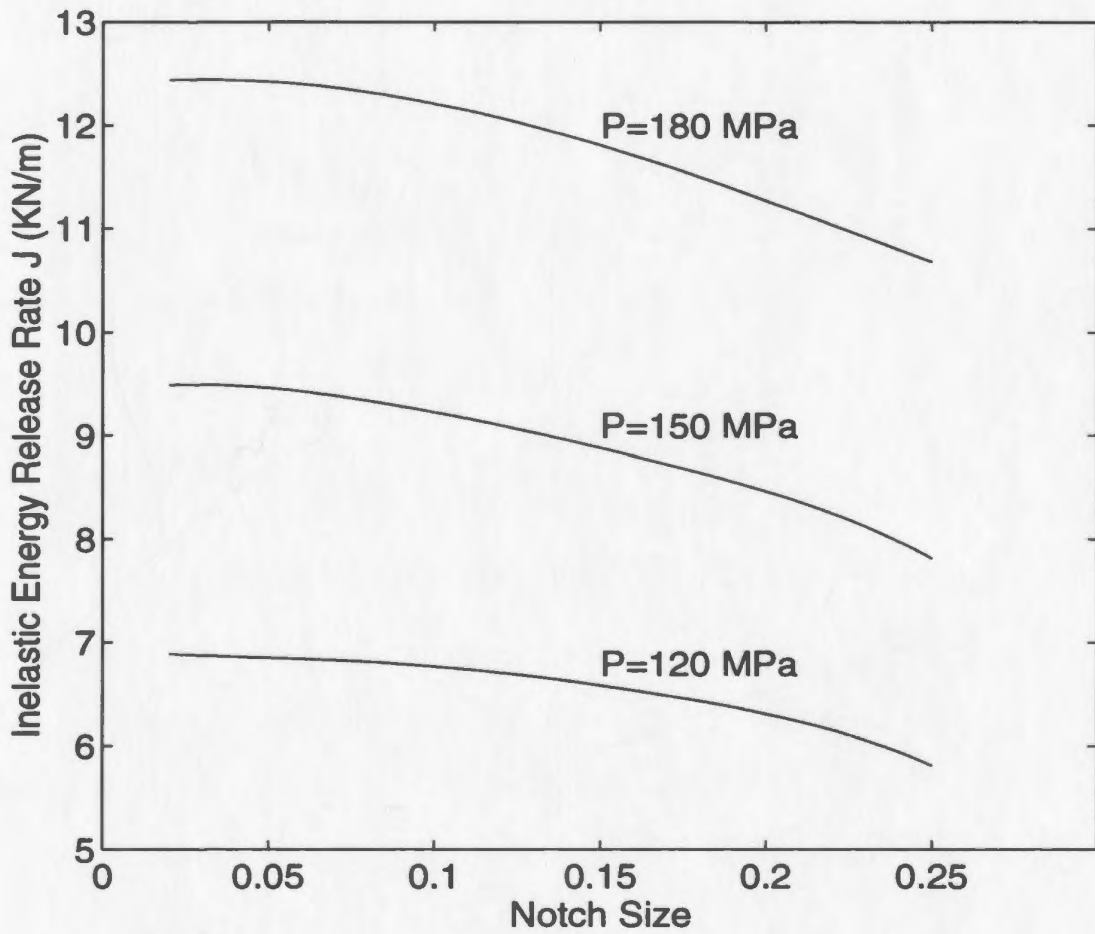


Figure 5.4: J vs. ρ/a for Single-Edge Circular Notch Specimen

shown in Fig. 5.3. An elastic perfectly-plastic curve can be defined by a slope of $E_p = 0$, whereas, a slope of $E_p = E_o/5$ depicts strain hardening. For the latter case, equation (5.18) would be conservative for larger values of load. For these reasons, equation (5.18) is recommended as the approximate estimation of J for circular-ended notches.

Based on equation (5.18), the J estimation for various notch sizes, ρ/a , is obtained and plotted in Fig. 5.4, and the edge-cracked components or structures are viewed as the limiting case of notched specimens. From Fig. 5.4, J -estimation for cracked components and structures can be approximately obtained from J of a small notch size (i.e., $\rho/a = 0.05$).

5.5 Remarks

Approximate methods for evaluating the elastic-plastic J for circular-ended notches are presented. The estimation of notch stress and strain is based on GLOSS linear relaxation locus, thus, the method proposed herein is applicable for small to medium amounts of local plastic zone at the notch root. The results obtained by these methods compare well with nonlinear finite element analysis for the numerical example considered. The methods presented in this chapter propose one simple way for evaluating the elastic-plastic J for cracked components and structures, and should also find use in performing quick design evaluations.

Chapter 6

A Simplified Three-Dimensional Model for Analyzing Pressure Vessels and Piping Components with Defects

6.1 Introduction

The current J -estimations for crack tips are based primarily on a biaxial loading condition in that a state of plane stress or plane strain is assumed depending on the physical situation. The appropriateness of the plane stress or plane strain approximations for practical three-dimensional configurations is an open issue. Surprisingly, very little of this work has been explored by fracture mechanics researchers. Dai (1989) has shown that a three-dimensional analysis which considers the specimen geometries and multiaxial loadings is necessary if one is to assure conservativeness of design. Recently, Schwartz (1993) has analyzed a circumferential flaw in a pressure vessel and has proposed that it is reasonable to expect that the tensile strain parallel to the crack front as opposed to zero (plane strain) or compressive (plane stress) could influence the constraint at the tip of the flaw.

The notion of $2\frac{1}{2}$ -Dimensional specimen proposed in this chapter is useful in representing cracked-components and structures that are subjected to special but common cases of practical three-dimensional loadings (Fig. 6.1) (Wu and Seshadri, 1996). The term “ $2\frac{1}{2}$ -Dimensional” implies that only partial three-dimensional effects are incorporated into the traditional two-dimensional cracked component models. Specifically, the remote loading in the direction along the crack front is considered in this chapter since this would cover many practical situations. The term $2\frac{1}{2}$ -D is borrowed from the “wire-frame graphics” terminology. The study essentially investigates the influence of out-of-plane loading on the crack tip constraint.

The effect of the remote field stress in the direction of the crack front on crack-tip constraint is examined for linear elastic materials. Appropriate correction factors that could be used in conjunction with existing experimental data are provided. Finally, pressure vessel and piping configurations with circumferential and longitudinal flaws are analyzed on the basis of the simplified theory developed here.

6.2 Crack Tip Constraint Parameter for $2\frac{1}{2}$ -D Specimens

The $2\frac{1}{2}$ -D model is used to describe a cracked body of finite-thickness subjected to three-dimensional remote loadings (σ_1^R , σ_2^R and σ_3^R). The remote stress σ_2^R would have a smaller influence on the stress field at the crack tip than σ_1^R and σ_3^R (Dai, 1989). We therefore assume that the influence of σ_2^R can be ignored. In order to investigate the influence of out-of-plane loading (σ_3^R) on crack tip constraint, the GLOSS method can be used to evaluate crack tip constraint parameter for $2\frac{1}{2}$ -D

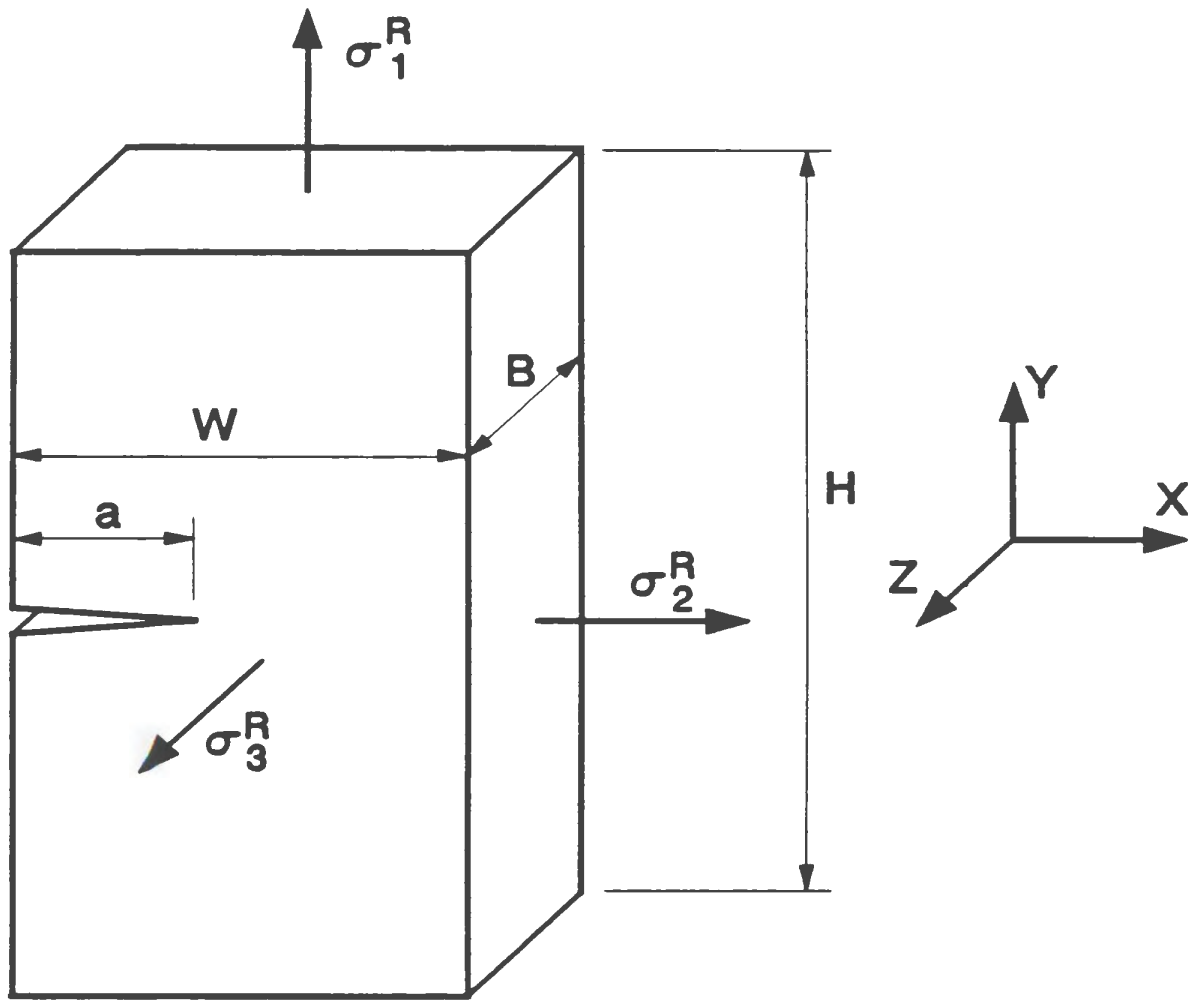


Figure 6.1: 2 $\frac{1}{2}$ -D Model

specimens.

The Generalized Local Stress Strain (GLOSS) method, based on reduced modulus technique, is a simple and systematic method for carrying out inelastic evaluations of mechanical components and structures on the basis of two linear elastic finite element analyses (Seshadri,1991).

From the GLOSS diagram (Fig. 4.1), the strains in equation (4.2) may be expressed by

$$(\epsilon_e)_1 = \frac{(\sigma_e)_1}{E_o} \quad \text{and} \quad (\epsilon_e)_2 = \frac{(\sigma_e)_2}{E_s} = \frac{(\sigma_e)_2}{E_o \frac{\sigma_y}{(\sigma_e)_1}}$$

Combining equations (4.2) and (4.3), the constraint parameter λ at crack tip can be obtained as

$$\lambda = \frac{(\sigma_e)_1/(\sigma_e)_2 - 1}{(\sigma_e)_1/\sigma_y - 1} \quad (6.1)$$

where $(\sigma_e)_1$, $(\sigma_e)_2$ are maximum equivalent stresses at the crack tip element from the first and second linear elastic finite element analyses, respectively, and σ_y is yielding stress. Following the procedure described in Chapter 4, the normalized constraint parameter, $\bar{\lambda}$, can be defined as described by equation (4.4). For a $2\frac{1}{2}$ -D single-edge cracked plate, the constraint parameter (λ) can be obtained for various geometric configurations (i.e., B/a) and remote field loadings (σ_1^R and σ_3^R) using the GLOSS method.

For the purpose of illustrating the influence of σ_3^R on the constraint parameter, the loading σ_1^R is set at $\bar{\sigma}_1^R = 1/3$. The results are shown in Table 6.1 where the normalized loadings are $\bar{\sigma}_1^R = \sigma_1^R/\sigma_y$ and $\bar{\sigma}_3^R = \sigma_3^R/\sigma_y$.

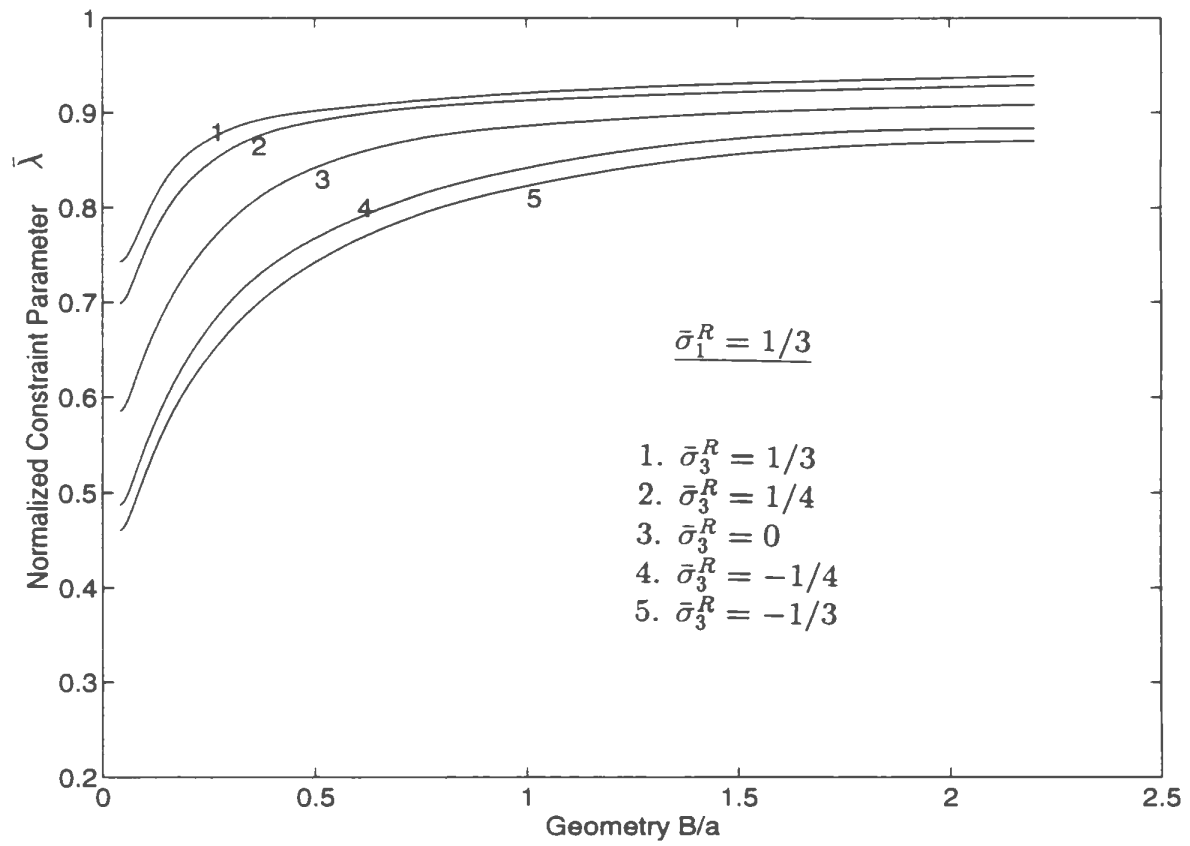


Figure 6.2: $\bar{\lambda}$ vs. B/a and $\bar{\sigma}_3^R$

From Fig. 6.2, it is seen that $\bar{\lambda}$ approaches a constant value when the specimens are very thin (i.e., $B/a=0.05$), and plane stress condition is said to have been attained. Furthermore, the value of $\bar{\lambda}$ increases with the tensile out-of-plane loading σ_3^R , but decreases with the compressive loading σ_3^R .

6.3 J -Estimation of $2\frac{1}{2}$ -D Specimens for Linear Elastic Materials

From the analysis of crack tip constraint parameter, it can be seen that the $\bar{\lambda}$ curves for the $2\frac{1}{2}$ -D component can be approximately viewed as the translation of the $\bar{\lambda}$ curve for the 2-D component according to the out-of-plane loading σ_3^R (Fig. 6.2). Therefore, $2\frac{1}{2}$ -D normalized constraint parameter can be expressed as

$$\bar{\lambda}^{(2\frac{1}{2}D)} = \bar{\lambda}^{(2D)} + \Delta\bar{\lambda} \quad (6.2)$$

where $\Delta\bar{\lambda}$ is due to the loading σ_3^R . It follows that the energy release rate J is also influenced by the crack-tip constraint parameter. Therefore, the $2\frac{1}{2}$ -D energy release rate (J) can be expressed as

$$J^{(2\frac{1}{2}D)} = J^{(2D)} + \Delta J \quad (6.3)$$

where ΔJ depends on the out-of-plane loading σ_3^R .

On the basis of the theoretical analysis of 3-D J -integral discussed in Chapter 3, the path-independent integral J_1 can be viewed as the energy release rate for $2\frac{1}{2}$ -D specimens (i.e. a through-cracked body where the crack front is a straight line).

From equation (3.37), the path-independent integral J_1 of the $2\frac{1}{2}$ -D configuration can be expressed as

$$J_1 = \int_{\Gamma} [W n_1 - (T_1 u_{1,1} + T_2 u_{2,1} + T_3 u_{3,1})] ds - \int_A (\sigma_{13} u_{1,1} + \sigma_{23} u_{2,1} + \sigma_{33} u_{3,1})_{,3} dA \quad (6.4)$$

where the first term is a line integral and the second term is a surface integral.

On the surface A , where the remote stress σ_3^R is applied, the stress state can be described as:

$$\sigma_{13} = 0, \quad \sigma_{23} = 0, \quad \sigma_{33} = \sigma_3^R,$$

and n_k, T_k along the path Γ can be represented by:

$$n_1 = dX_2/ds, \quad n_2 = -dX_1/ds, \quad n_3 = 0$$

and

$$T_1 = \sigma_{11} n_1 + \sigma_{12} n_2, \quad T_2 = \sigma_{12} n_1 + \sigma_{22} n_2, \quad T_3 = 0.$$

Therefore, the energy release rate for $2\frac{1}{2}$ -D specimens can be expressed as

$$J_1 = \int_{\Gamma} [W n_1 - (T_1 u_{1,1} + T_2 u_{2,1})] ds - \int_A \sigma_3^R \frac{\partial \epsilon_3^{(s)}}{\partial X_1} dA \quad (6.5)$$

where $\epsilon_3^{(s)}$ is the strain on the surface A along the σ_3^R direction.

The identity

$$\int_A \sigma_3^R \frac{\partial \epsilon_3^{(s)}}{\partial X_1} dA = 0 \quad (6.6)$$

holds for any 2-D problem ($\sigma_3^R = 0$). Therefore, the $2\frac{1}{2}$ -D energy release rate can be approximately expressed as

$$J^{(2\frac{1}{2}D)} = J^{(2D)} - \int_A \sigma_3^R \frac{\partial \epsilon_3^{(s)}}{\partial X_1} dA. \quad (6.7)$$

The above equation is valid for inelastic materials in the sense of Rice's original development.

Equation (6.7) calculates the energy release rate on the surface A only. Although J has a small variation along the thickness, J based on equation (6.7) can be approximately viewed as an averaged $2\frac{1}{2}$ -D energy release rate.

For linear elastic materials, the strain $\epsilon_3^{(s)}$ on the surface A can be expressed as:

$$\epsilon_3^{(s)} = \frac{1}{E_o} [\sigma_{33} - \nu(\sigma_{11} + \sigma_{22})]^{(s)} = \frac{1}{E_o} [\sigma_3^R - \nu(\sigma_{11} + \sigma_{22})^{(s)}] \quad (6.8)$$

where σ_{11} and σ_{22} are normal stresses in the X_1 and X_2 directions on the surface A , respectively.

Traditional fracture mechanics methods have been confined primarily to two-dimensional configurations. For the two-dimensional mode I cracked specimens, the crack-tip stress state within the K -dominated zone near crack tip is given as (Anderson, 1991):

$$\begin{aligned}
\sigma_{11} &= \frac{K_I}{\sqrt{2\pi r}} \cos\left(\frac{\theta}{2}\right) \left[1 - \sin\left(\frac{\theta}{2}\right) \sin\left(\frac{3\theta}{2}\right) \right] \\
\sigma_{22} &= \frac{K_I}{\sqrt{2\pi r}} \cos\left(\frac{\theta}{2}\right) \left[1 + \sin\left(\frac{\theta}{2}\right) \sin\left(\frac{3\theta}{2}\right) \right] \\
\sigma_{33} &= \begin{cases} 0 & \text{plane stress} \\ \nu(\sigma_{11} + \sigma_{22}) & \text{plane strain} \end{cases}
\end{aligned} \tag{6.9}$$

where K_I is the mode I stress intensity factor, and r and θ are polar coordinates, where the origin is located at crack tip. K_I depends on the remote stress σ_1^R and the geometry only.

In most of the current literature, the stress system parallel to the crack face is assumed not to disturb the crack. Therefore, only the uniaxial remote stress σ_1^R is considered to be important in the traditional analysis (Broek, 1986). However, for $2\frac{1}{2}$ -D specimens, the remote stress σ_3^R could have significant influence on the stress state at the crack tip as will be shown next.

In a manner similar to the analysis of two-dimensional linear elastic fracture mechanics, the stress state near the crack tip for $2\frac{1}{2}$ -D specimens can be expressed as:

$$\sigma_{ij} = C r^{-\frac{1}{2}} f_{ij}(\theta) \tag{6.10}$$

where the parameter C would depend on the loading condition and the crack geometry.

Although the geometric configuration of a $2\frac{1}{2}$ -D specimen is the same as a 2-D specimen, the loading conditions are different in that σ_3^R is applied. Therefore, the stress state near the crack-tip in the proposed $2\frac{1}{2}$ -D configurations can be expressed as:

$$\begin{aligned}\sigma_{11} &= \frac{K_I^*}{\sqrt{2\pi r}} \cos\left(\frac{\theta}{2}\right) \left[1 - \sin\left(\frac{\theta}{2}\right) \sin\left(\frac{3\theta}{2}\right)\right] \\ \sigma_{22} &= \frac{K_I^*}{\sqrt{2\pi r}} \cos\left(\frac{\theta}{2}\right) \left[1 + \sin\left(\frac{\theta}{2}\right) \sin\left(\frac{3\theta}{2}\right)\right]\end{aligned}\tag{6.11}$$

where K_I^* represents the equivalent stress intensity factor for $2\frac{1}{2}$ -D specimens and depends on σ_1^R , σ_3^R and the geometric configuration.

For the linear elastic material behavior, $\epsilon_3^{(s)}$ within the crack tip K -dominated zone can be obtained by combining equations (6.8) and (6.11) as:

$$\epsilon_3^{(s)} = \frac{1}{E_o} \left[\sigma_3^R - 2\nu K_I^* \cos\left(\frac{\theta}{2}\right) / \sqrt{2\pi r} \right].\tag{6.12}$$

Since J_1 is independent of the path, for the sake of convenience, Γ may be chosen as a circle of radius r_K with its center being at crack tip (Fig. 6.3). The relationship of coordinate systems is given by

$$\begin{aligned}X_1 &= r \cos(\theta) \\ X_2 &= r \sin(\theta).\end{aligned}\tag{6.13}$$

The strain $\epsilon_3^{(s)}$ can be estimated by equation (6.12) when the radius r_K is confined within the K -dominated zone.

Therefore, if σ_3^R is considered to be a constant, the surface integral can be expressed as:

$$\begin{aligned} \int_A \sigma_3^R \frac{\partial \epsilon_3^{(s)}}{\partial X_1} dA &= \lim_{r_o \rightarrow 0} \int_{r_o}^{r_K} \int_{-\pi}^{\pi} \sigma_3^R \frac{\partial \epsilon_3^{(s)}}{\partial X_1} r dr d\theta \\ &= -\frac{8\sqrt{r_K}}{3\sqrt{2\pi}E_0} \nu \sigma_3^R K_I^* \end{aligned} \quad (6.14)$$

where a small circle with radius r_o is assumed to be located at the crack tip that excludes the crack tip itself and hence singular points in the stress-strain field from the subregion (Fig. 6.3).

Substitution of equation (6.14) into equation (6.7) leads to the expression:

$$J_e^{(2\frac{1}{2}D)} = J_e^{(2D)} + \frac{8\sqrt{r_K}}{3\sqrt{2\pi}E_0} \nu \sigma_3^R K_I^* \quad (6.15)$$

where the subscript 'e' represents validity for linear elastic range.

In the two-dimensional linear elastic fracture mechanics, the normal stress along $\theta = 0$ can be obtained as:

$$\sigma_{22} = K_I / \sqrt{2\pi r} + \sigma_1^R = \sigma_1^R \left(\beta \sqrt{\frac{a}{2r}} + 1 \right)$$

where β is the geometric factor ($\beta \geq 1$). The radius r must be small when compared

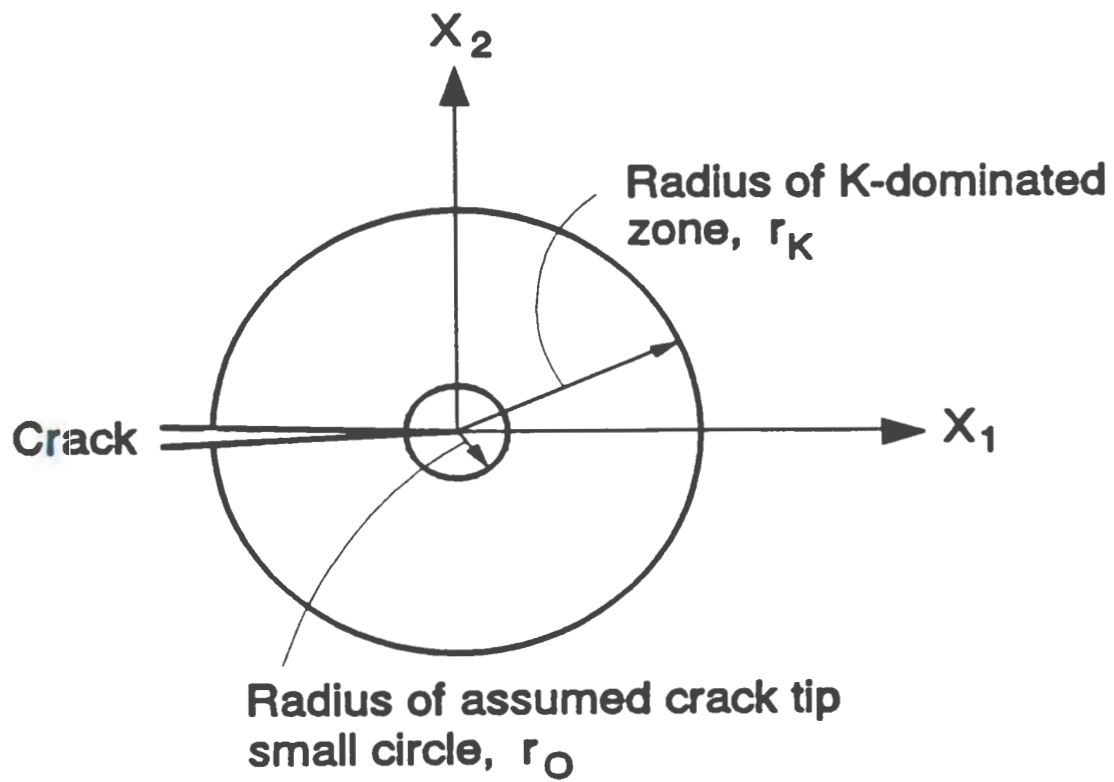


Figure 6.3: Consideration of Crack Tip Singularity

to the crack length, a , in order for the singular term to dominate. If the K -dominated zone is defined as the region where the first term is at least 5 times the second term, the size of this zone is $r_K = a/50$.

For the $2\frac{1}{2}$ -D situation, the same K -dominated zone size can be assumed and substituted into equation (6.15) since the stress state distributions near the crack tip would be similar. Therefore, the linear elastic energy release rate for $2\frac{1}{2}$ -D specimens can be obtained as:

$$\begin{aligned} J_e^{(2\frac{1}{2}D)} &= J_e^{(2D)} + \frac{4}{15} \sqrt{\frac{a}{\pi}} \frac{\nu}{E_0} \sigma_3^R K_I^* \\ &= \frac{(K_I)^2}{E_0} + \frac{4}{15} \sqrt{\frac{a}{\pi}} \frac{\nu}{E_0} \sigma_3^R K_I^* \end{aligned} \quad (6.16)$$

where $J_e^{(2D)} = (K_I)^2/E_0$ (for plane stress).

The crack tip stress distribution for the two-dimensional geometry is given by equation (6.10) as $\sigma_{ij} = K_I r^{-\frac{1}{2}} f_{ij}(\theta)$. The introduction of the remote field stress σ_3^R is assumed not to affect the distribution $f_{ij}(\theta)$. Rather, it is anticipated that the magnitude of K_I would be affected. Therefore, it is postulated that the crack tip stress distribution for $2\frac{1}{2}$ -D configuration would be given by $\sigma_{ij} = K_I^* r^{-\frac{1}{2}} f_{ij}(\theta)$. In effect, self-similarity of the stress distribution is preserved.

In equation (6.16), K_I is the traditional two-dimensional crack-tip stress intensity factor which depends on the geometry and the remote field loading σ_1^R . However, K_I^* represents $2\frac{1}{2}$ -D crack-tip equivalent stress intensity factor which depends on the geometry and the simplified remote field loadings σ_1^R and σ_3^R .

For the special case of a linear elastic material, $J = G$. Also,

$$J_e^{(2\frac{1}{2}D)} = \frac{(K_I^*)^2}{E_0} \quad (6.17)$$

for $2\frac{1}{2}$ -D mode I loading (σ_1^R and σ_3^R present).

Combining equations (6.16) and (6.17), the equivalent stress intensity factor for $2\frac{1}{2}$ -D is obtained as

$$K_I^* = \sqrt{(K_I)^2 + (K_0)^2} + K_0 \quad (6.18)$$

wherein $K_I = \beta \sigma_1^R \sqrt{\pi a}$ and $K_0 = \frac{2\nu}{15\pi} \beta \sigma_3^R \sqrt{\pi a}$. Equation (6.18) can be used to evaluate the crack tip stress intensity factor for practical $2\frac{1}{2}$ -D configurations such as pressure vessels or piping with a circumferential or a longitudinal flaw.

If μ is defined as the ratio of σ_3^R to σ_1^R in the $2\frac{1}{2}$ -D model, with $K_I^* = \psi_k K_I$ in equation (6.18), the parameter ψ_k is equal to $[0.014\mu + \sqrt{1 + (0.014\mu)^2}]$ when $\nu = 0.33$. Therefore, ψ_k can find use in the adaptation of ASTM E-399 K_{Ic} tests for the $2\frac{1}{2}$ -D specimens.

6.4 Size Requirement For Plane Strain Fracture Toughness Testing

Based on the ASTM Standard Test Method for Plane-Strain Fracture Toughness (ASTM Standard E 399-83, 1984), the specimen size requirement in the traditional two-dimensional model is:

$$a, B, W - a \geq 2.5 \left(\frac{K_I}{\sigma_y} \right)^2 \quad (6.19)$$

where a is the crack length, B is the thickness of cracked specimen, and $W-a$ is the crack ligament length. However, for $2\frac{1}{2}$ -D specimens, the specimen size requirement would be influenced by the loading σ_3^R as compared to the traditional two-dimensional situation.

The von Mises yield criterion states that yielding will occur when

$$(\sigma_1 - \sigma_2)^2 + (\sigma_2 - \sigma_3)^2 + (\sigma_3 - \sigma_1)^2 = 2\sigma_y^2 \quad (6.20)$$

where σ_1 , σ_2 and σ_3 are the principal stresses. For $2\frac{1}{2}$ -D specimens, the principal stresses on surface A are:

$$\begin{aligned} \sigma_1 &= \frac{K_I^*}{\sqrt{2\pi r}} \cos \frac{\theta}{2} \left(1 + \sin \frac{\theta}{2}\right) \\ \sigma_2 &= \frac{K_I^*}{\sqrt{2\pi r}} \cos \frac{\theta}{2} \left(1 - \sin \frac{\theta}{2}\right) \\ \sigma_3 &= \sigma_3^R. \end{aligned} \quad (6.21)$$

Therefore the plastic zone size can be derived by substituting Eq. (6.21) into Eq. (6.20):

$$r(\theta) = \left[\frac{K_I^*(1 + \cos \theta + \frac{3}{2}(\sin \theta)^2)}{2\sqrt{2\pi}\sigma_3^R \cos \frac{\theta}{2} + 2\sqrt{\pi}\sqrt{\sigma_y^2(1 + \cos \theta) + \frac{3}{2}(\sigma_y^2 - (\sigma_3^R)^2)(\sin \theta)^2}} \right]^2. \quad (6.22)$$

Along the crack plane, $\theta = 0$, the $2\frac{1}{2}$ -D plastic zone size can be obtained as:

$$r_y^* = \frac{1}{2\pi} \left(\frac{K_I^*}{\sigma_3^R + \sigma_y} \right)^2. \quad (6.23)$$

Comparing with the traditional two-dimensional plastic zone size (for plane stress), equation (6.23) can be rewritten as

$$r_y^* = \frac{1}{2\pi} \left(\frac{K_I^*}{\sigma_y} \right)^2 \frac{1}{(1 + \bar{\sigma}_3^R)^2}. \quad (6.24)$$

Therefore, similar to equation (6.19), the $2\frac{1}{2}$ -D specimen size requirement for plane strain K_{Ic}^* testing can be expressed as:

$$a, B^*, W - a \geq \frac{2.5}{(1 + \bar{\sigma}_3^R)^2} \left(\frac{K_I^*}{\sigma_y} \right)^2. \quad (6.25)$$

Let B_c be termed as the critical thickness for plane strain in the fracture toughness testing. The thickness size requirement in order to obtain a valid K_{Ic} for the traditional two-dimensional specimens is given by:

$$B \geq B_c = 2.5 \left(\frac{K_I}{\sigma_y} \right)^2. \quad (6.26)$$

The critical thickness in the traditional specimens can therefore be obtained as:

$$\left(\frac{B_c}{a}\right)_{2D} = 2.5\pi\beta^2(\bar{\sigma}_1^R)^2. \quad (6.27)$$

For the $2\frac{1}{2}$ -D specimen, combining equations (6.18) and (6.25), the critical thickness in $2\frac{1}{2}$ -D can be obtained as:

$$\left(\frac{B_c}{a}\right)_{2\frac{1}{2}D}^* = 2.5\pi\beta^2 \left(\frac{\sqrt{(\bar{\sigma}_1^R)^2 + \left(\frac{2\nu}{15\pi}\bar{\sigma}_3^R\right)^2} + \frac{2\nu}{15\pi}\bar{\sigma}_3^R}{1 + \bar{\sigma}_3^R} \right)^2. \quad (6.28)$$

The theoretical expression, Eq. (6.28), can be verified by using the GLOSS analysis, the results of which are presented in Table 6.1. For the single-edge cracked specimen ($a/W = \frac{1}{3}$), the geometry factor β is approximately equal to 1.78. From Eq. (6.27), $(\frac{B_c}{a})_{2D}$ is 2.76 when $\bar{\sigma}_1^R$ is fixed at $1/3$. From Fig. 6.2, it is seen that the curve 3 corresponds to the 2-D situation ($\sigma_3^R = 0$), and $B_c/a = 2.76$ corresponds to $\bar{\lambda} = 0.92$. However, the same value of 0.92 for $\bar{\lambda}$ corresponds to $B_c/a = 1.45$ in curve 1 ($\bar{\sigma}_3^R = 1/3$) and $B_c/a = 1.75$ in curve 2 ($\bar{\sigma}_3^R = 1/4$). Based on Eq. (6.28), the theoretical values of B_c/a are 1.59 and 1.80 for $\bar{\sigma}_3^R = 1/3$ and $1/4$, respectively. It can therefore be seen that the theoretical estimates of the critical thickness for the $2\frac{1}{2}$ -D configurations compare well with the results of the GLOSS analysis.

6.5 Numerical Examples

6.5.1 Analysis of Practical Pressure Vessels and Piping Components with Defects

Three-dimensional pressure vessels and piping components with defects (i.e., a circumferential or a longitudinal flaw in a pressure vessel) differ from the conventional fracture specimens in one significant manner: the stresses parallel to the crack front are tensile. The analysis of such flaws is of importance in the evaluation of the fracture integrity of welds in nuclear reactor pressure vessels, which contain only circumferential welds. Some practical three-dimensional pressure vessels and piping components ($2\frac{1}{2}$ -D model) are analyzed in this section to illustrate the effect of stresses parallel to the crack front.

The ANSYS (1992) finite element computer-program has been used for performing linear as well as nonlinear analyses. While the ANSYS finite element program has been used in fracture mechanics, it has mainly been based on the traditional two-dimensional fracture mechanics results. The crack tip element is only valid for the two-dimensional in-plane loading conditions (i.e., $\sigma_3^R=0$). Therefore, commercial finite element programs are not suitable for calculating fracture parameters (i.e., K and J) of the $2\frac{1}{2}$ -D model.

Theoretical estimates of J_e for the $2\frac{1}{2}$ -D model are compared with the theoretical results of J_e for the traditional two-dimensional fracture model. For elastic-plastic materials, the robust estimate of $J_{e/p}$ for $2\frac{1}{2}$ -D model is also presented.

6.5.2 Circumferential Flaw in a Pressure Vessel

In this study, a pressure vessel with a circumferential flaw is treated as a cylinder having an internal radius, R_i , of 100 mm and a wall thickness, W , of 10 mm. The flaw with a crack length, a , of 2.5 mm in the radial direction ($a/W = 0.25$) is assumed to be circumferentially continuous.

The material behavior is assumed to be elastic perfectly-plastic. The following values of material constants are used in all analyses: Young's modulus (E_0) = 2.11×10^5 MN/ m^2 , Poisson's ratio (ν) = 0.3, and yield stress (σ_y) = 488.43 MN/ m^2 . The traditional fracture model considers the longitudinal loading only (2-D model), and the proposed $2\frac{1}{2}$ -D model considers the combined circumferential and longitudinal loadings.

For the limiting case of a continuous circumferential flaw, the problem can be considered as a plane strain case. Therefore, theoretical linear elastic J_e of the traditional 2-D model (longitudinal loading condition) is:

$$J_e^{(2D)} = \frac{K_I^2(1 - \nu^2)}{E_0} \quad (6.29)$$

where $K_I = \beta p_i \frac{R_i^2}{R_o^2 - R_i^2} \sqrt{\pi a}$ and $\beta = 1.12 - 0.231(a/W) + 10.55(a/W)^2 - 21.72(a/W)^3 + 30.39(a/W)^4$ (Ewalds and Wanhill, 1986).

Based on the proposed J theory for $2\frac{1}{2}$ -D specimens,

$$J_e^{(2\frac{1}{2}D)} = (K_I^*)^2 / E_0 \quad (6.30)$$

where the subscript 'e' stands for the linear elastic behavior. For the combined

loading (circumferential and longitudinal) condition, the equivalent stress intensity factor K_I^* is given by $K_I^* = \sqrt{K_I^2 + K_0^2} + K_0$ and $K_0 = \frac{2\nu}{15\pi} \beta p_i \frac{R_i}{W} \sqrt{\pi a}$. Therefore linear elastic J_e can be obtained by Eq. (6.30).

The inelastic energy release rate (J) is calculated by the ANSYS finite element program for the traditional 2-D fracture model, and by robust approximate method (Seshadri and Kizhatil, 1995) for the 2 $\frac{1}{2}$ -D configuration.

The finite element model for the two-dimensional cracked specimen of the assumed geometry is generated by using ANSYS software. Only the upper half of the vessel is considered because of symmetry conditions. The computed J -integral values are normalized with the value of $(a\sigma_y)$, i.e., $\bar{J} = J/(a\sigma_y)$, and normalized load is designated as p_a/σ_y , where p_a is the remote axial stress applied on the top of the model. For the axisymmetric combined load case, p_a is a function of the internal pressure (p_i) of the vessel, and can be expressed as $p_a = p_i R_i^2 / (R_o^2 - R_i^2)$ in which R_i and R_o are the inner and outer radii of the vessel.

The robust approximate method for estimating J (Seshadri and Kizhatil, 1995) is based on the concepts of the GLOSS (Seshadri, 1991) and the GLOSS R-Node (Seshadri and Fernando, 1992) techniques. An estimate of the elastic-plastic J based on the GLOSS constraint parameter (λ) is obtained as

$$J = \lambda J_e + (1 - \lambda) J_p \quad (6.31)$$

or

$$J = J_e \left[\lambda + (1 - \lambda) \frac{\delta^{(2)} P_L}{\delta^{(1)} P} \right] \quad (6.32)$$

where $\delta^{(1)}$ is the load-point displacement from a linear elastic finite element analysis at some arbitrary load (P), $\delta^{(2)}$ is the load-point displacement from the second linear elastic finite element analysis with the moduli of all element modified according to

$$E_s = \left[\frac{(\sigma_e)_{ref}}{\sigma_e} \right] E_o. \quad (6.33)$$

The equivalent reference stress, $(\sigma_e)_{ref}$, can be approximately obtained by using the engineering beam theory as (Appendix C.1)

$$(\sigma_e)_{ref} = \frac{P_a}{\frac{a}{W}(\sqrt{1 + (\frac{W-a}{a})^2} - 1)}. \quad (6.34)$$

The intersection of the equivalent stress distributions from the two analyses gives the r-node stress (which will be discussed later in this thesis), σ_{r-n} , which can then be used to scale the applied load (P) in order to obtain the limit load (P_L); i.e.,

$$P_L = P \frac{\sigma_y}{\sigma_{r-n}}.$$

The r-node stress is obtained as $\sigma_{r-n} = 82 \text{ MN}/m^2$ for an internal pressure of $p_i = 10 \text{ MN}/m^2$, and the corresponding limit load, $(p_i)_L = 59.56 \text{ MN}/m^2$. The load-point longitudinal displacements from two linear elastic finite element analyses are $\delta^{(1)} = 3.03 \times 10^{-3} \text{ mm}$ and $\delta^{(2)} = 3.21 \times 10^{-3} \text{ mm}$.

Although the constraint parameter (λ) can be obtained for small to medium plastic zone sizes using GLOSS analysis, it is possible to obtain robust approxima-

tions for the variation of λ with the normalized load (P/P_L), and the relationship can be expressed as (Seshadri and Kizhatil, 1995):

$$\lambda = \begin{cases} 1 & \text{for } 0 \leq P/P_L \leq 0.5 \\ 2[1 - (P/P_L)] & \text{for } 0.5 \leq P/P_L \leq 1.0 \end{cases} \quad (6.35)$$

or

$$\lambda = \sqrt{1 - (P/P_L)^2}. \quad (6.36)$$

Robust estimates of the $2\frac{1}{2}$ -D configuration and the inelastic finite element analysis results of the 2-D model are shown in Fig. 6.4.

6.5.3 Longitudinal Flaw in a Pressure Vessel

A pressure vessel with a longitudinal flaw is also treated as a cylinder having an internal radius, R_i , of 100 mm and a wall thickness, W , of 10 mm. The longitudinal flaw with a crack length, a , of 2.5 mm in the radial direction ($a/W = 0.25$) is assumed to be continuous and present in the inner surface of the vessel. The length of the crack is assumed to be equal to the meridional length of the vessel. Therefore, the problem can be viewed as one of plane strain.

The material behavior is assumed to be elastic perfectly-plastic. The material constants used for the present analysis are the same as those defined in the case of the problem with a circumferential flaw. The traditional fracture model considers the circumferential loading only (2-D model), and the proposed $2\frac{1}{2}$ -D model

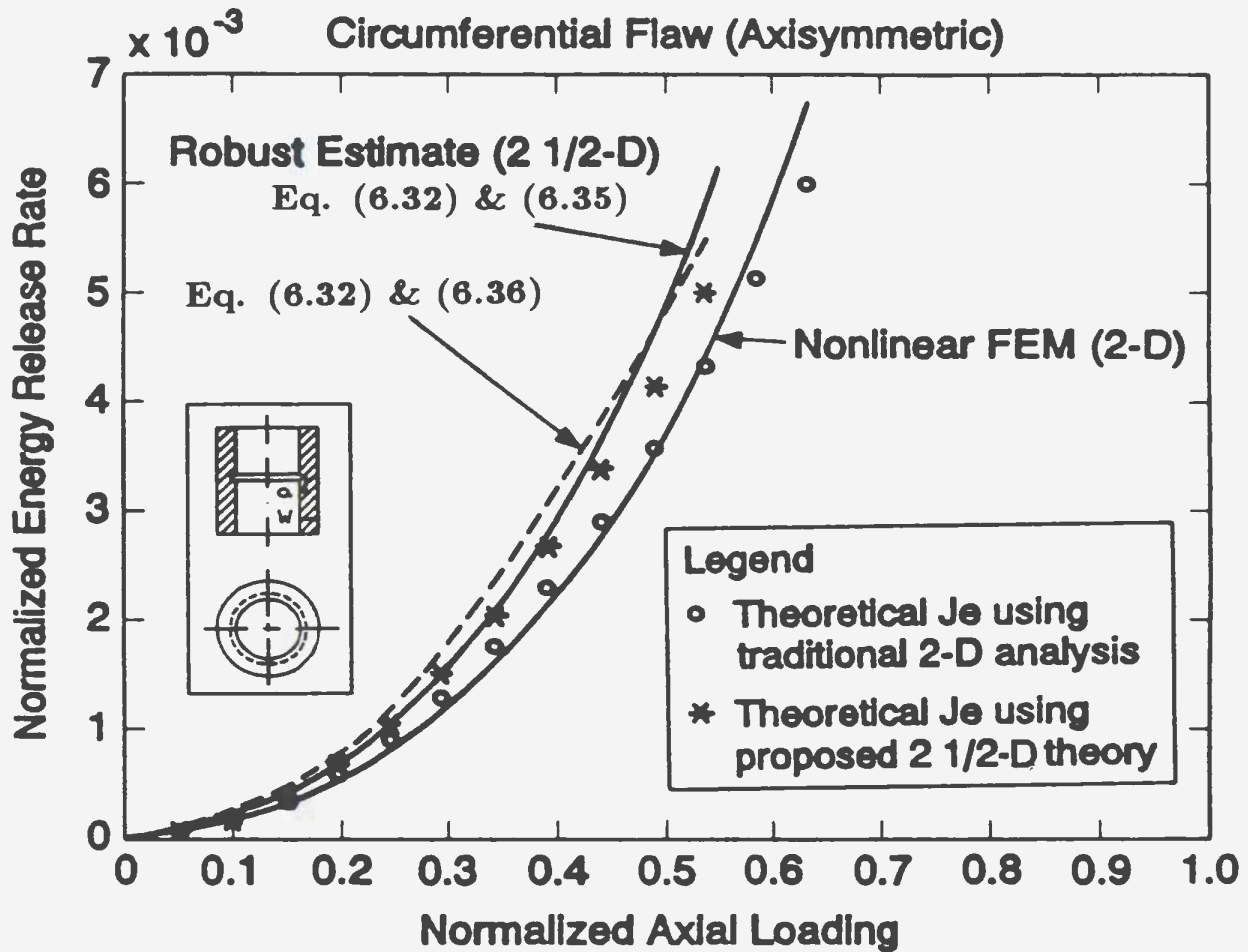


Figure 6.4: Cylinder or Pipe with a Circumferential Flaw Subjected to Internal Pressure - $J/(a\sigma_y)$ vs. p_a/σ_y

considers the combined circumferential and longitudinal loadings.

The theoretical linear elastic J_e under the circumferential loading (2-D model) can be expressed as:

$$J_e^{(2D)} = \frac{K_I^2(1 - \nu^2)}{E_o}$$

where $K_I = \beta p_i \frac{R_i}{W} \sqrt{\pi a}$ and $\beta = 1.12 - 0.231(a/W) + 10.55(a/W)^2 - 21.72(a/W)^3 + 30.39(a/W)^4$ (Ewalds and Wanhill, 1986).

For the combined loading (circumferential and longitudinal) case, the equivalent stress intensity factor K_I^* is given by $K_I^* = \sqrt{K_I^2 + K_0^2} + K_0$ and $K_0 = \frac{2\nu}{15\pi} \beta p_i \frac{R_i^2}{(R_i + R_o)W} \sqrt{\pi a}$. The linear elastic J_e for the $2\frac{1}{2}$ -D configuration can therefore be obtained by Eq. (6.30).

For the traditional 2-D model, inelastic energy release rate (J) can be obtained by nonlinear finite element analysis. Again, the finite element model of the assumed geometry is generated by using ANSYS software. Only the symmetric half of the vessel is considered. The eight-noded isoparametric elements are selected and six crack tip elements are used. The radius of the first array of elements at the tip of crack is 0.5 mm ($=0.2a$), and the ratio of size of the second row of elements to the first row is 0.5.

The computed J -integral values are again normalized with the value of $(a\sigma_y)$ and normalized load is designated as σ_θ/σ_y , in which σ_θ is the applied hoop stress. The factor σ_θ is a function of the internal pressure (p_i) of the vessel, and can be given by $\sigma_\theta = p_i R_i/W$.

The robust approximate procedure for estimating J of $2\frac{1}{2}$ -D configuration is the same as the one discussed in the case of the circumferential flaw. Based on the limit

analysis of a thick-walled cylinder subjected to an internal pressure, the equivalent reference stress, $(\sigma_e)_{ref}$, can be approximately obtained as (Appendix C.2)

$$(\sigma_e)_{ref} = \frac{\sqrt{3}}{2} \left[\frac{p_i}{\ln\left(\frac{R_o}{R_i+a}\right)} \right]. \quad (6.37)$$

The r-node stress is obtained as $\sigma_{r-n} = 165 \text{ MN}/m^2$ for an internal pressure of $p_i = 10 \text{ MN}/m^2$, and the corresponding limit load, $(p_i)_L = 29.6 \text{ MN}/m^2$. The load-point circumferential displacements from two linear elastic finite element analyses are $\delta^{(1)} = 3.40 \times 10^{-2} \text{ mm}$ and $\delta^{(2)} = 3.51 \times 10^{-2} \text{ mm}$.

Robust estimates of the $2\frac{1}{2}$ -D configuration and inelastic finite element analysis results of the 2-D configuration are shown in Fig. 6.5.

6.6 Remarks

In this chapter, a $2\frac{1}{2}$ -D model that accounts for the remote field stress σ_3^R is developed. The stress intensity factor corresponding to the aforementioned configuration is also derived. A correction factor that can be used in conjunction with the available two-dimensional results and the ASTM E-399 formula is provided.

The results obtained by the postulated $2\frac{1}{2}$ -D theory and the robust approximate method are given for practical $2\frac{1}{2}$ -D configurations such as pressure vessels and piping that contain a circumferential or a longitudinal flaw.

It can be seen that the remote field stress σ_3^R has a significant effect on the crack-tip constraint, and neglecting its influence would likely lead to unconservative situations.

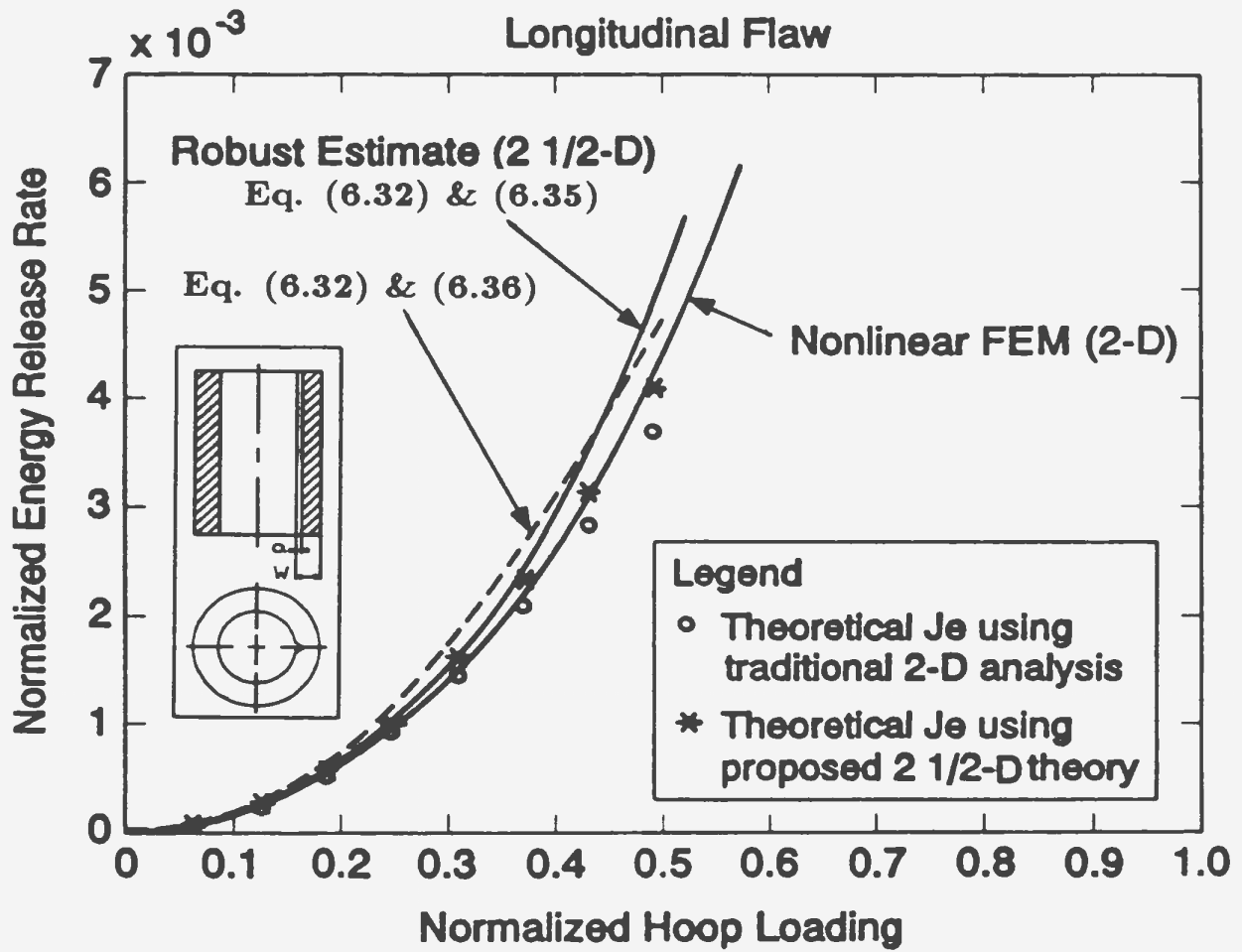


Figure 6.5: Cylinder or Pipe with a Longitudinal Flaw Subjected to Internal Pressure - $J/(a\sigma_y)$ vs. σ_θ/σ_y

Table 6.1: Constraint Parameter λ of $2\frac{1}{2}$ -D Specimens

$a = 2$ in, $W = 6$ in, $H = 12$ in
 $E_o = 30 \times 10^6$ psi, $\nu = 0.3$, $\sigma_y = 60 \times 10^3$ psi

| GEOMETRY B/a | LOADING $\bar{\sigma}_1^R = \frac{1}{3}$ | | | | |
|-------------------|---|----------------------------------|------------------------|-----------------------------------|-----------------------------------|
| | $\bar{\sigma}_3^R = \frac{1}{3}$ | $\bar{\sigma}_3^R = \frac{1}{4}$ | $\bar{\sigma}_3^R = 0$ | $\bar{\sigma}_3^R = -\frac{1}{4}$ | $\bar{\sigma}_3^R = -\frac{1}{3}$ |
| 0.03 | 0.470 | 0.443 | 0.371 | 0.309 | 0.292 |
| 0.05 | 0.470 | 0.443 | 0.372 | 0.310 | 0.293 |
| 0.075 | 0.482 | 0.458 | 0.389 | 0.327 | 0.309 |
| 0.125 | 0.512 | 0.490 | 0.424 | 0.363 | 0.345 |
| 0.25 | 0.550 | 0.534 | 0.481 | 0.425 | 0.406 |
| 0.5 | 0.569 | 0.562 | 0.531 | 0.484 | 0.468 |
| 1.0 | 0.581 | 0.576 | 0.559 | 0.531 | 0.519 |
| 2.0 | 0.591 | 0.585 | 0.572 | 0.557 | 0.548 |
| 4.0 | 0.623 | 0.612 | 0.593 | 0.577 | 0.572 |
| ∞^* | 0.631 | 0.631 | 0.631 | 0.631 | 0.631 |

* $B/a \rightarrow \infty$ represents ideal plane strain condition (all $u_3 = 0$)

Chapter 7

Robust J Estimation - Design Perspectives

7.1 Introduction

Two approaches are commonly administered for analyzing problems in elastic-plastic fracture mechanics. One approach expresses the inelastic energy release rate (J) or the crack opening displacement (COD) as a function of the behavior of the uncracked component or structure. Typical examples of such methods are the COD method (PD6493, 1980) and the EnJ method (Turner, 1984b). An alternate approach is to express J or COD as a function of the stress-strain behavior. In this case, the load-deflection behavior of the cracked component or structure would be required. Evidently, the former approach is similar to conventional structural analysis and is usually restricted to linear elastic analysis augmented by rigid plastic limit analysis. Computational fracture studies fall under the category of the latter approach (Turner, 1984a). United Kingdom's $R6$ (Dowling and Townley, 1975) and $EPRI$ (Kumar et al., 1981) approaches, however, are based on the analyses of cracked specimens.

There is a correlation between the extent of crack-tip plasticity and the load-deflection behavior of a cracked component. For small-scale yielding at the crack-tip, the load-deflection behavior is linear and the linear elastic fracture mechanics (LEFM) theory applies. When the plastic zone surrounding the crack tip becomes larger, the LEFM assumptions do not strictly apply since the load-deflection behavior is nonlinear. When plasticity spreads across the cross-section and large deformation occurs, then the concept of limit loads for rigid plastic materials becomes useful.

Determination of inelastic energy release rate (J) for a cracked component involves the use of inelastic finite element analyses, and can be time-consuming and possibly expensive. From a design standpoint there is an incentive to develop robust approximate methods that are simple to use and yet provide acceptable results. A robust method is presented here that is based on the GLOSS method (Seshadri, 1991) and the r-node concept (Seshadri and Fernando, 1992).

The robust design method is applied to a single-edge crack specimens (SEC), compact tension specimens (CT) and single edge notched bend specimens (SENB). The effect of strain-hardening and creep is also addressed in this chapter.

7.2 Redistribution Nodes (R-Nodes)

The apparently disconnected concepts of the reference stress, limit load and ASME stress classification can be unified by using the idea of redistribution nodes (r-nodes) (Seshadri and Marriott, 1993). Redistribution nodes are load-controlled locations in a structure. On the GLOSS diagram, Fig. 4.1, these can be identified as locations where the follow-up angle $\bar{\theta}$ is equal to 90 degrees (Seshadri, 1991; Seshadri and

Fernando, 1992). On account of the load-controlled nature, the equivalent stress values at the r-nodes are linearly proportional to the external tractions irrespective of the material constitutive relationships. In other words, any two stress distributions satisfying equilibrium with externally applied tractions will intersect at the r-nodes. This feature is useful in the practical determination of the r-nodes and the corresponding r-node equivalent stress.

For a component or a structure that develops a single r-node prior to collapse, it is possible to obtain the limit load by simply scaling the external load or moment. For a component or a structure that requires formation of a discrete number of independent plastic zones to cause collapse, an equal number of r-node peaks can be considered (Seshadri, 1996).

In the former case, the r-node can be represented by a uniaxial bar of a prescribed material behavior. It is, however, assumed here that the material is elastic perfectly-plastic. Since σ_{r-n} is load-controlled, it would be linearly proportional to the externally applied tractions (Seshadri and Fernando, 1992),

$$\sigma_{r-n} = \mu P \quad (7.1)$$

where μ is a constant of proportionality that would depend on the geometry of the component or structure. Plastic collapse would occur when σ_{r-n} reaches yield,

$$\sigma_y = \mu P_L. \quad (7.2)$$

By eliminating μ between equations (7.1) and (7.2), the limit load can be obtained

as

$$P_L = P \frac{\sigma_y}{\sigma_{r-n}}. \quad (7.3)$$

In the case of combined remote field loadings, equation (7.3) can be written as

$$\langle P, M \rangle_L = \langle P, M \rangle \frac{\sigma_y}{\sigma_{r-n}}.$$

The r-nodes can be approximately located by using the following procedure:

- A linear elastic finite element analysis is carried out for the mechanical component or structure.
- The elastic moduli of all elements are modified according to the equation

$$E_{sj} = \left[\frac{\sigma_{arb}}{\sigma_{ej}} \right] E_o \quad (7.4)$$

where “j” stands for the element number and σ_{arb} is an arbitrary stress value. A second linear elastic finite element analysis is then carried out.

- On the basis of the two linear elastic analysis, the r-nodes are identified.

Limit loads can then be determined by using the expression

$$P_L = \left[\frac{\sigma_y}{\bar{\sigma}_n} \right] P$$

where $\bar{\sigma}_n$, referred to as the “combined r-node stress”, can be defined as the average of the peak r-node stresses. The number of r-node peaks corresponds to the

number of independent plasticity nucleation centers responsible for the collapse of the mechanical component or structure. Seshadri (1996) has developed guidelines for determining the r-node peaks that lead to collapse.

7.3 Robust Determination of J

From the LEFM analysis, elastic energy release rate for a component or structure can be expressed as (Anderson, 1991)

$$J_e = G = \frac{K_I^2}{E'} \quad (7.5)$$

where E' is equal to E_o for plane stress case while E' is equal to $E_o/(1 - \nu^2)$ for plane strain situation. Equation (7.5) can be rewritten as (Seshadri and Kizhatil, 1995)

$$J_e = \frac{\beta^2(\sigma_1^R)^2\pi a}{E'} \quad (7.6)$$

where σ_1^R is the remote field stress, usually load-controlled in nature. σ_1^R can be replaced by the r-node equivalent stress for multiaxial remote stress field. By introducing the concept of r-nodes, equation (7.5) can be expressed as

$$J_e = R_e\sigma_{r-n}\epsilon_{r-n} \quad (7.7)$$

where the r-node equivalent strain $\epsilon_{r-n} = \sigma_{r-n}/E_o$, and the parameter R_e can be expressed as:

$$R_e = \frac{E_o}{E'} \frac{K_I^2}{(\sigma_{r-n})^2}. \quad (7.8)$$

The general expression of energy release rate for elastic, elastic-plastic and plastic domains can be expressed as:

$$\begin{aligned} J_e &= R_e \sigma_{r-n} \epsilon_{r-n} \\ J_{e/p} &= R_{e/p} \sigma_{r-n} \epsilon_{r-n} \\ J_p &= R_p \sigma_{r-n} \epsilon_{r-n} \end{aligned} \quad (7.9)$$

where R_e , $R_{e/p}$, and R_p are defect-size parameters for linear elastic, elastic-plastic, and fully plastic situations, respectively. The challenge now is to determine the defect size parameters R_e , $R_{e/p}$ and R_p for a range of plastic-zone sizes.

The quantity R_e can be readily obtained from equation (7.8) as

$$J_e = R_e E_o (\epsilon_{r-n})^2. \quad (7.10)$$

It can be seen that the $J_e(\epsilon_{r-n})$ curve is a parabola. As well, the fully plastic $J_p(\delta)$ can be shown to be a straight line that passes through the origin (Bucci et al., 1972). Similarly, the fully plastic $J_p(\epsilon_{r-n})$ is also a straight line passing through the origin (Fig. 7.1). If the two curves intersect at $\epsilon_{r-n} = \epsilon_{r-n}^*$, where ϵ_{r-n}^* is as yet undetermined, we can stipulate that

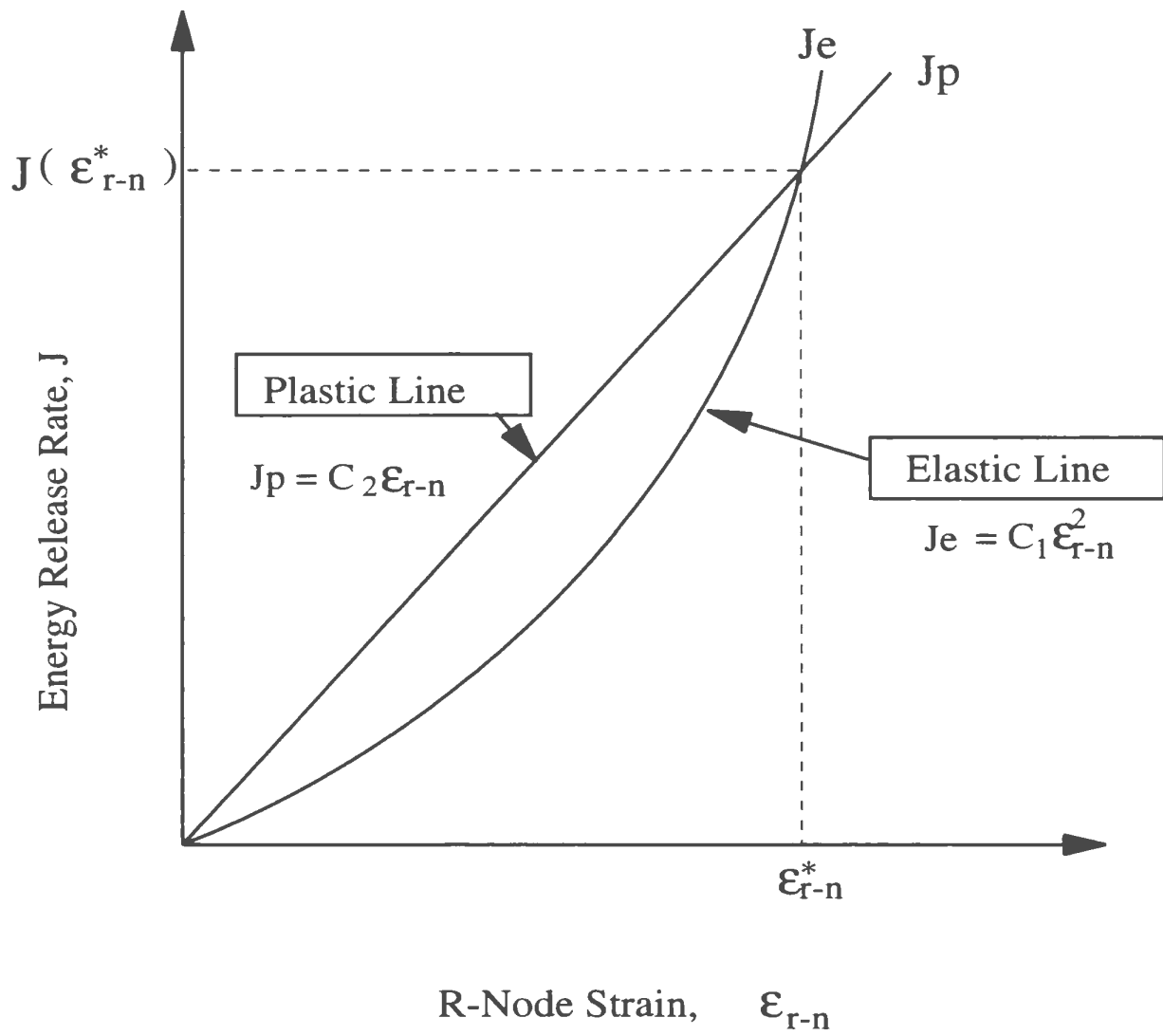


Figure 7.1: Energy Release Rate (J) vs. R-Node Strain (ϵ_{r-n})

$$J_e(\epsilon_{r-n}^*) = J_p(\epsilon_{r-n}^*).$$

The method of establishing the value of ϵ_{r-n}^* will be discussed later.

The fully plastic J_p can therefore be expressed as

$$J_p = R_e E_o \epsilon_{r-n}^* \epsilon_{r-n}. \quad (7.11)$$

Comparing with the general expression, $J_p = R_p \sigma_{r-n} \epsilon_{r-n}$, R_p can be expressed as:

$$R_p = \frac{\epsilon_{r-n}^*}{\epsilon_{r-n}} R_e = \frac{P^*}{P} R_e \quad (7.12)$$

where $P^* = P_L \frac{\epsilon_{r-n}^*}{\epsilon_y}$.

It can be seen that the elastic-plastic $J_{e/p}$ is related to the linear elastic J_e and the fully plastic J_p at the two extremities. Based on the constraint parameter (λ), robust estimates of $J_{e/p}$ can be obtained as:

$$\begin{aligned} J_{e/p} &= \Phi(\lambda) J_e + \Psi(\lambda) J_p \\ &= \Phi(\lambda) J_e + [1 - \Phi(\lambda)] J_p \end{aligned} \quad (7.13)$$

where $\Phi(\lambda)$ is as yet an undetermined function of λ .

It is known that when the constraint parameter $\lambda = 0$, corresponding to net section yielding, $J \rightarrow J_p$; and when $\lambda = 1$, corresponding to small-scale crack-tip plasticity, $J = J_e$. Therefore, we have

$$\Phi(1) = 1 \quad \text{and} \quad \Phi(0) = 0.$$

Although the constraint parameter λ can be obtained for small to medium plastic zone sizes using the GLOSS analysis, it is possible to obtain robust approximations for the variation of λ with the normalized load P/P_L . Based on the load-displacement curves for many cracked component configurations, these curves can be bounded by two extremes, i.e., linear elastic response and rigid plastic response. Even at a load corresponding to one-half of the limit load, the global load-displacement behavior is essentially linear (Fig. 7.2). The linear behavior corresponds to small-scale plasticity and LEFM assumptions. Therefore for $0 < P/P_L < \frac{1}{2}$, the value of constraint parameter λ can be assumed to be equal to one. When $P/P_L \rightarrow 1$, net section yielding is assumed to occur and λ becomes equal to zero.

Another interpretation is that if the load at first yield is P_{y1} (on the global $P - \delta$ curve), the shakedown load would be approximately $P_s = 2P_{y1}$. For practical components with cracks, $P_s \leq P_L$, so that the first yield load can be approximated as $P_{y1} = P_L/2$. Therefore until a load of $P_L/2$ is reached, the global $P - \delta$ behavior can essentially be assumed to be linear elastic.

For $0.5 \leq P/P_L \leq 1$, the actual load versus displacement curve is a smooth-curve bounded by linear elastic ($\lambda = 1$) and rigid plastic ($\lambda = 0$) load-deflection responses.

For a given component, let the loading path 0-1-2 along path @ (Fig. 7.2)

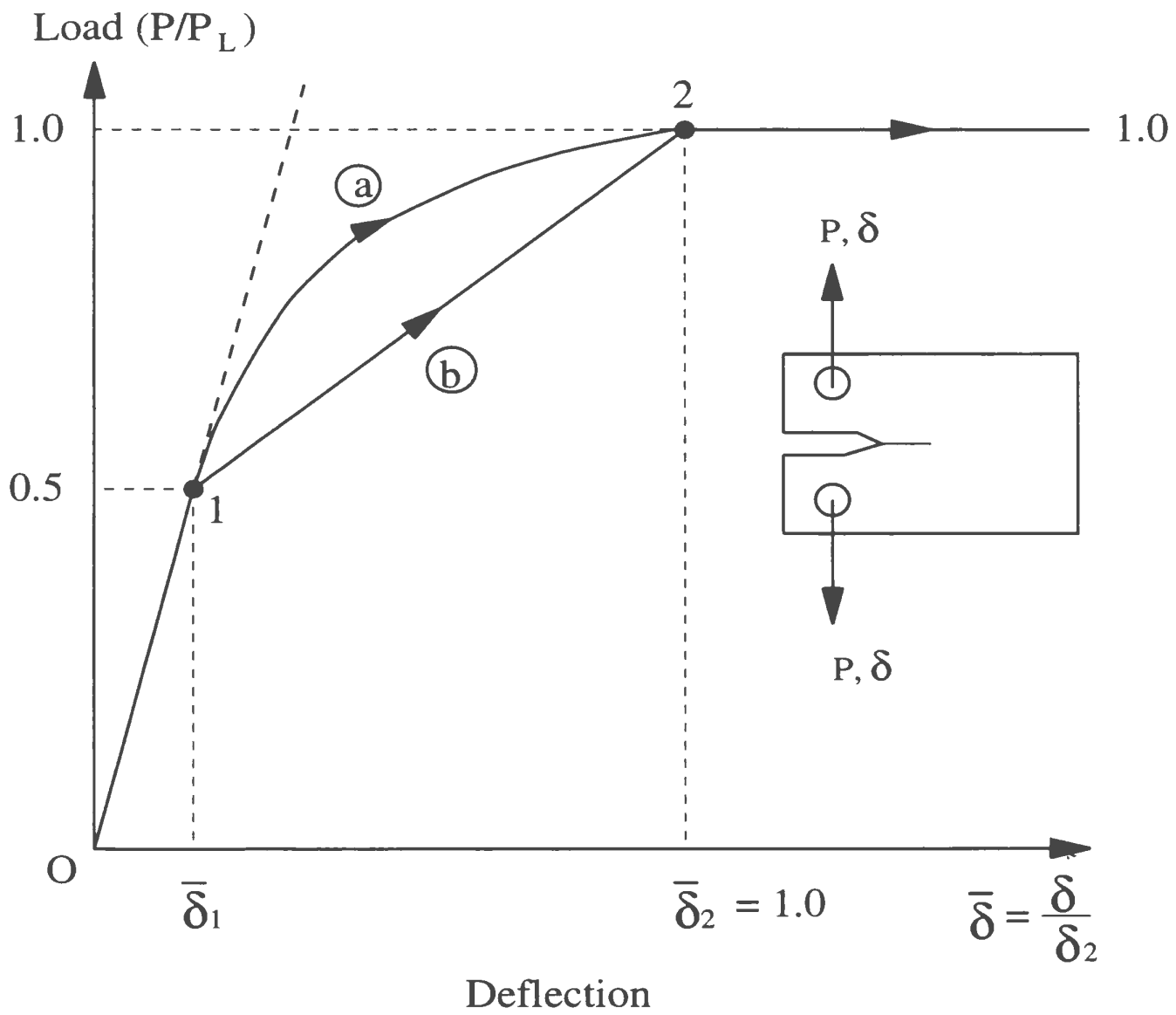


Figure 7.2: Typical Load-Displacement ($P - \delta$) Record

correspond to the actual curve, while 0-1-2 along path (b) describe the postulated linear approximation. For a given value of P/P_L , δ computed along path (b) is greater than δ computed along path (a). Therefore the computation of J using path (b) would be more conservative than other actual $P - \delta$ paths.

Thus, normalized load P/P_L is linearly related to normalized load point displacement $\bar{\delta}$, and can be expressed as:

$$P/P_L = \begin{cases} 0.5 \bar{\delta}/\bar{\delta}_1 & \text{for } 0 \leq \bar{\delta} \leq \bar{\delta}_1 \\ 0.5 (\bar{\delta} - 2\bar{\delta}_1 + 1)/(1 - \bar{\delta}_1) & \text{for } \bar{\delta}_1 \leq \bar{\delta} \leq 1 \\ 1.0 & \text{for } \bar{\delta} \geq 1. \end{cases} \quad (7.14)$$

Fig. 7.3 shows the variation of λ with normalized deflection $\bar{\delta}$. In comparison with actual curve (a), curve (b) implies a softer crack-tip constraint, and therefore a large plastic zone, except at $\bar{\delta} = \bar{\delta}_1$ and 1.0 .

These variations can be expressed as

$$\lambda = \begin{cases} 1.0 & \text{for } 0 \leq \bar{\delta} \leq \bar{\delta}_1 \\ (1 - \bar{\delta})/(1 - \bar{\delta}_1) & \text{for } \bar{\delta}_1 \leq \bar{\delta} \leq 1.0 \\ 0 & \text{for } \bar{\delta} \geq 1.0. \end{cases} \quad (7.15)$$

Using equations (7.14) and (7.15), a relationship between the constraint parameter (λ) with normalized load (P/P_L) can be obtained by eliminating $\bar{\delta}$, and can be expressed as:

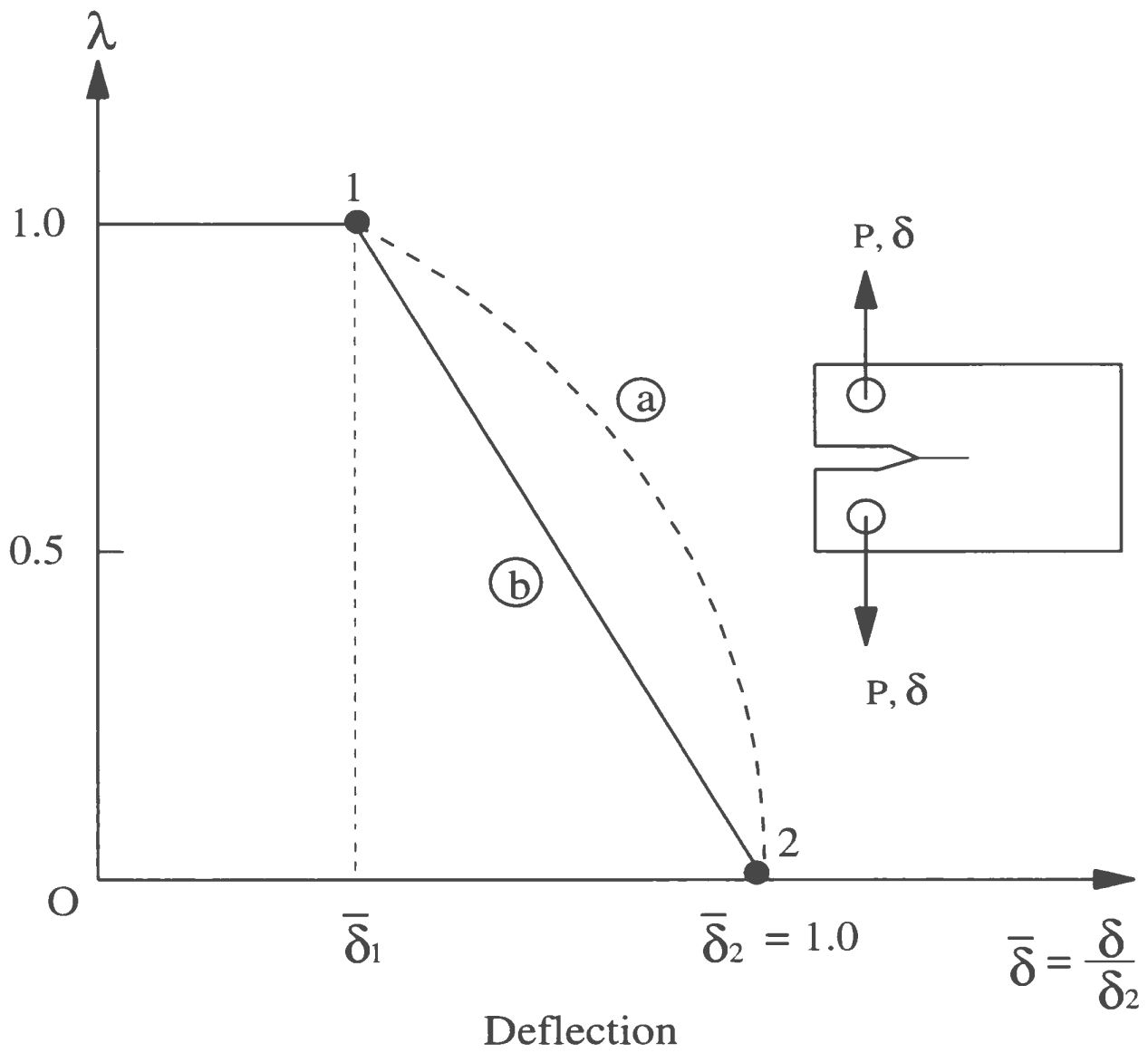


Figure 7.3: Constraint Parameter (λ) vs. load point displacement (δ)

$$\lambda = \begin{cases} 1 & \text{for } 0 \leq P/P_L \leq 0.5 \\ 2[1 - (P/P_L)] & \text{for } 0.5 \leq P/P_L \leq 1.0 \\ 0 & \text{for } P/P_L \geq 1.0. \end{cases} \quad (7.16)$$

The variation is shown in Fig. 7.4. It is postulated that the variation described by equation (7.16) bounds real $\lambda - P/P_L$ curve for practical mechanical components and structures, such that the J -estimates are conservative.

Consider next the variation of $\Phi(\lambda)$ with P/P_L . For loads below the shakedown threshold, the crack-tip plastic-zone is small and the load-deflection behavior is almost linear. Therefore, for $0 \leq P/P_L \leq \frac{1}{2}$, $\Phi(\lambda) = 1$. Beyond $P/P_L = \frac{1}{2}$, the $\Phi(\lambda)$ versus P/P_L would be smooth for well-designed components and structures. As well, the first derivative would be continuous and the second derivative negative, in order to incorporate the convexity of the curve (Fig. 7.5).

Prescribing a linear variation of $\Phi(\lambda)$ versus P/P_L , i.e.,

$$\Phi(\lambda) = \lambda = 2(1 - P/P_L) \quad (7.17)$$

would lead to a conservative estimate of J , evaluated by the expression

$$J = \lambda J_e + (1 - \lambda) J_p. \quad (7.18)$$

Combining equations (7.16) and (7.18), $R_{e/p}$ can be expressed as:

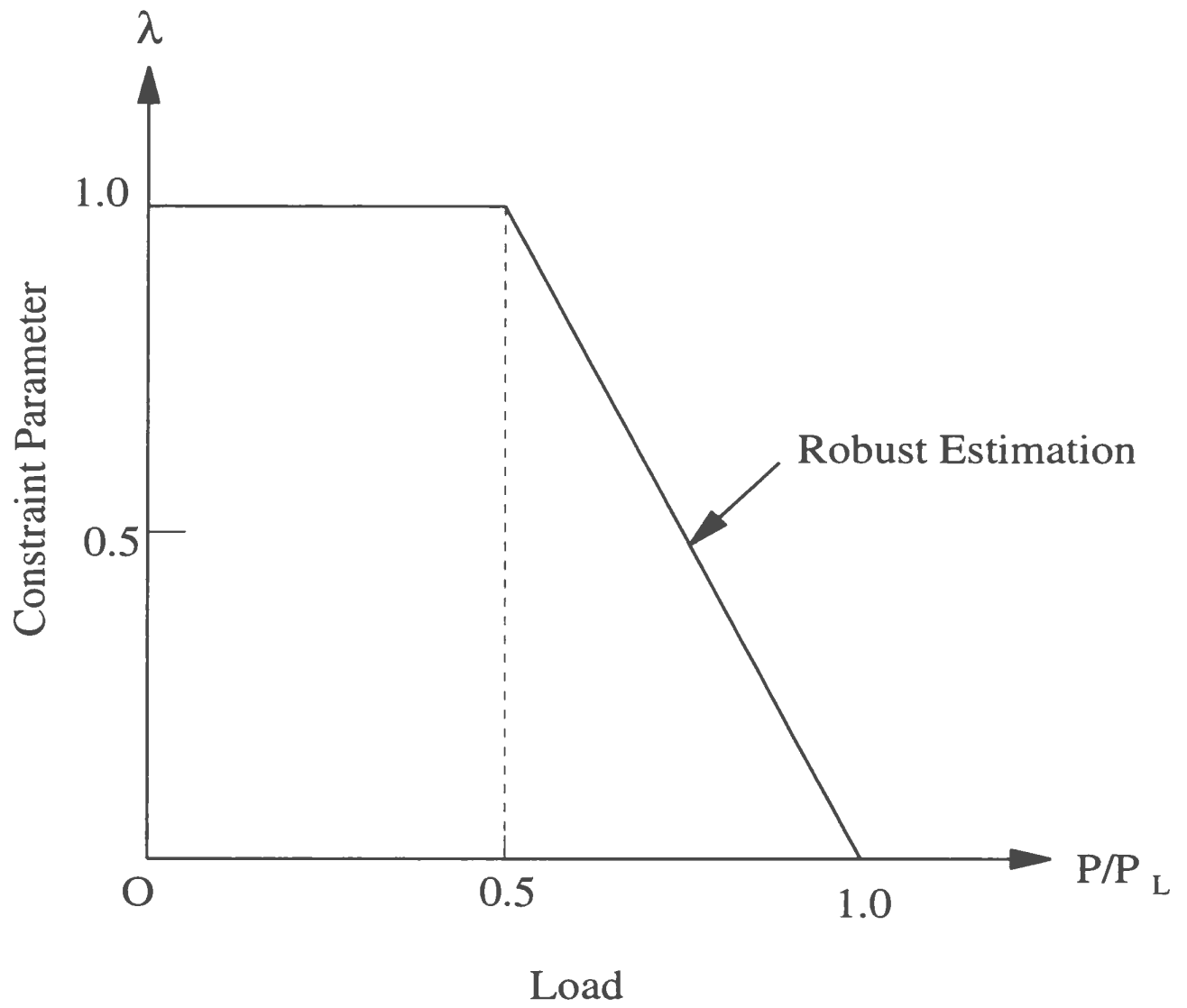


Figure 7.4: Constraint Parameter (λ) vs. Normalized Load (P/P_L)

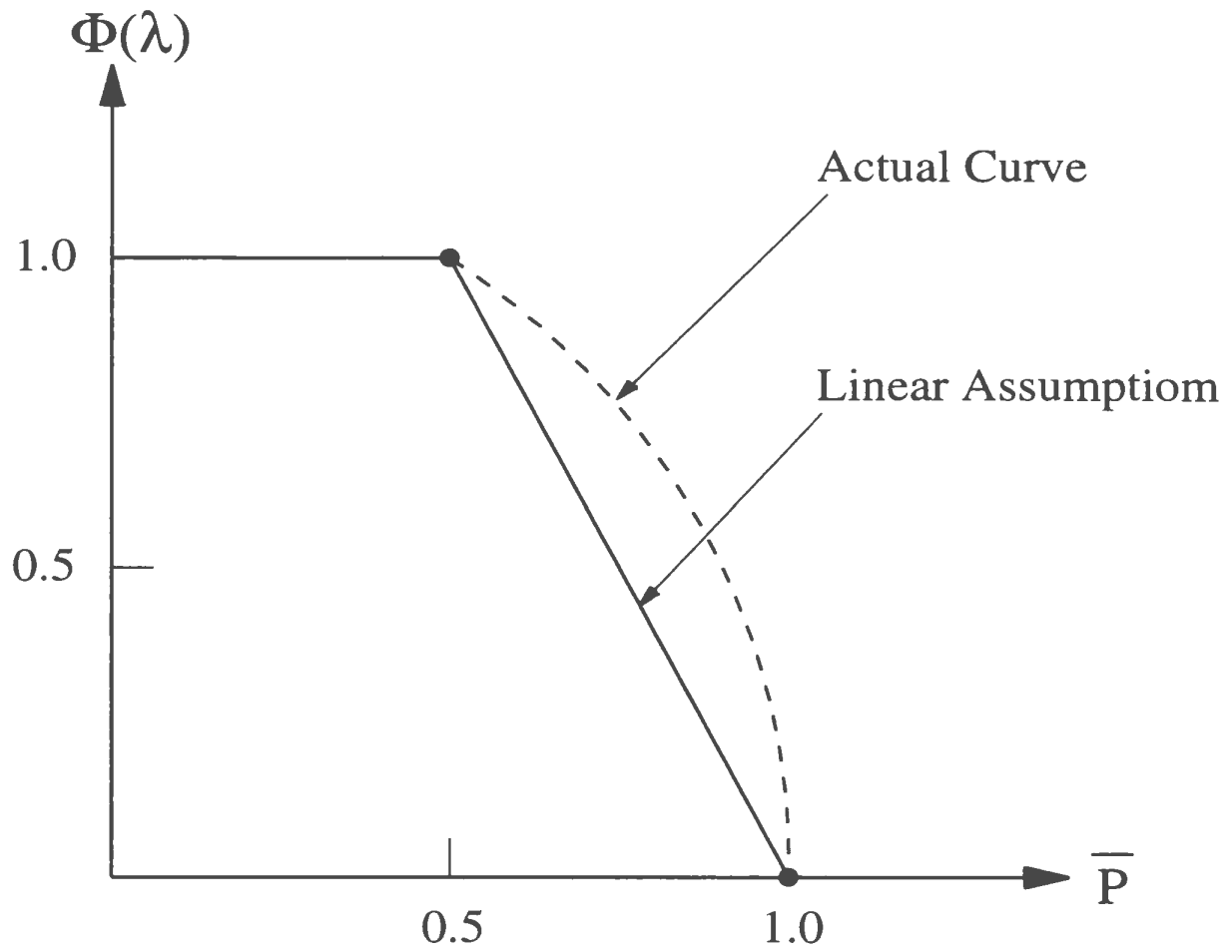


Figure 7.5: $\Phi(\lambda)$ vs. Normalized Load P/P_L

$$R_{e/p} = \begin{cases} R_e & \text{for } 0 \leq \bar{P} \leq 0.5 \\ R_e[\bar{P}^*(2 - \frac{1}{\bar{P}}) + 2(1 - \bar{P})] & \text{for } 0.5 \leq \bar{P} \leq 1.0 \end{cases} \quad (7.19)$$

where $\bar{P} = P/P_L$ and $\bar{P}^* = P^*/P_L$ are the normalized loads.

7.4 Estimation of J and C^* for Design Purposes

It can be seen from Fig. 7.1 that the parabolic curve $J_e(\epsilon_{r-n})$ intersects the straight line $J_p(\epsilon_{r-n})$ at $\epsilon_{r-n} = \epsilon_{r-n}^*$. Therefore,

$$R_{e/p}/R_e = [\bar{P}^*(2 - \frac{1}{\bar{P}}) + 2(1 - \bar{P})] \quad \text{for } 0.5 \leq \bar{P} \leq 1.0 . \quad (7.20)$$

The defect-size parameters for elastic, elastic-plastic and fully plastic fracture processes can be expressed as follows:

For $\bar{P} \leq 0.5$,

$$R_{e/p}/R_e = 1.0 . \quad (a)$$

For $0.5 < \bar{P} < 1.0$,

$$R_{e/p}/R_e = [\bar{P}^*(2 - \frac{1}{\bar{P}}) + 2(1 - \bar{P})] . \quad (b)$$

For $\bar{P} \rightarrow 1.0$,

$$R_{e/p}/R_e \rightarrow \bar{P}^* . \quad (c)$$

It is clear from the robust construction that $R_{e/p} < R_p$, leading to the inequality:

$$\bar{P}^* > 2\bar{P}. \quad (7.21)$$

Given that $\bar{P} < 1$, the above inequality is satisfied if $\bar{P}^* \geq 2$. This leads to the relationship

$$\epsilon_{r-n}^* \geq 2\epsilon_y. \quad (7.22)$$

For the purpose of design, we can set

$$\epsilon_{r-n}^* = 2\epsilon_y. \quad (7.23)$$

The defect-size parameters can be obtained by modifying equation (7.19) using the relationship given by equation (7.23), i.e.,

$$R_{e/p} = \begin{cases} R_e & 0 \leq \bar{P} \leq 0.5 \\ R_e(6 - 2\bar{P} - \frac{2}{\bar{P}}) & 0.5 \leq \bar{P} \leq 1.0 \end{cases} \quad (7.24)$$

The elastic-plastic energy release rate can now be expressed as:

$$J_{e/p} = \begin{cases} R_e \sigma_{r-n} \epsilon_{r-n} & 0 \leq \bar{P} \leq 0.5 \\ R_e \sigma_{r-n} \epsilon_{r-n} (6 - 2\bar{P} - \frac{2}{\bar{P}}) & 0.5 \leq \bar{P} \leq 1.0 \end{cases} \quad (7.25)$$

or

$$\bar{J} = \begin{cases} (\bar{\epsilon}_{r-n})^2 & 0 \leq \bar{\epsilon}_{r-n} \leq 0.5 \\ 2\bar{\epsilon}_{r-n}[3\bar{\epsilon}_{r-n} - (\bar{\epsilon}_{r-n})^2 - 1] & 0.5 \leq \bar{\epsilon}_{r-n} \leq 1.0 \\ 2(\bar{\epsilon}_{r-n})^2 & \bar{\epsilon}_{r-n} \geq 1.0 \end{cases} \quad (7.26)$$

where $\bar{J} = J/J_e(\epsilon_y)$ and $\bar{\epsilon}_{r-n} = \epsilon_{r-n}/\epsilon_y$. Equation (7.26) is the robust design curve for the analysis and design of elastic-plastic fracture problems and is illustrated in Fig. 7.6.

There is a direct analogy between sub-creep temperature fracture and time-dependent creep crack growth. The parameter C^* is defined by replacing the strains with strain rates. Following equation (7.9), the parameter C^* can be expressed as

$$C^* = R\sigma_{r-n}\dot{\epsilon}_{r-n} \quad (7.27)$$

where $\dot{\epsilon}_{r-n} = A(\sigma_{r-n})^n$ for second stage creep. Using equations (7.24) and (7.27), the foregoing expression becomes

$$C^* = \begin{cases} R_e A(\sigma_{r-n})^{n+1} & \text{for } 0 \leq \bar{P} \leq 0.5 \\ R_e A(\sigma_{r-n})^{n+1}(6 - 2\bar{P} - 2/\bar{P}) & \text{for } 0.5 \leq \bar{P} \leq 1.0 \end{cases} \quad (7.28)$$

where equation (7.28) corresponds to the second stage creep.

Just as J characterizes the crack tip fields in an elastic or elastic-plastic material, the C^* uniquely defines crack tip condition in a viscous material. Thus the time-dependent crack growth rate in a viscous material should depend only on the value of C^* . Experimental studies (Landes and Begley, 1976, Nikbin et al., 1976,

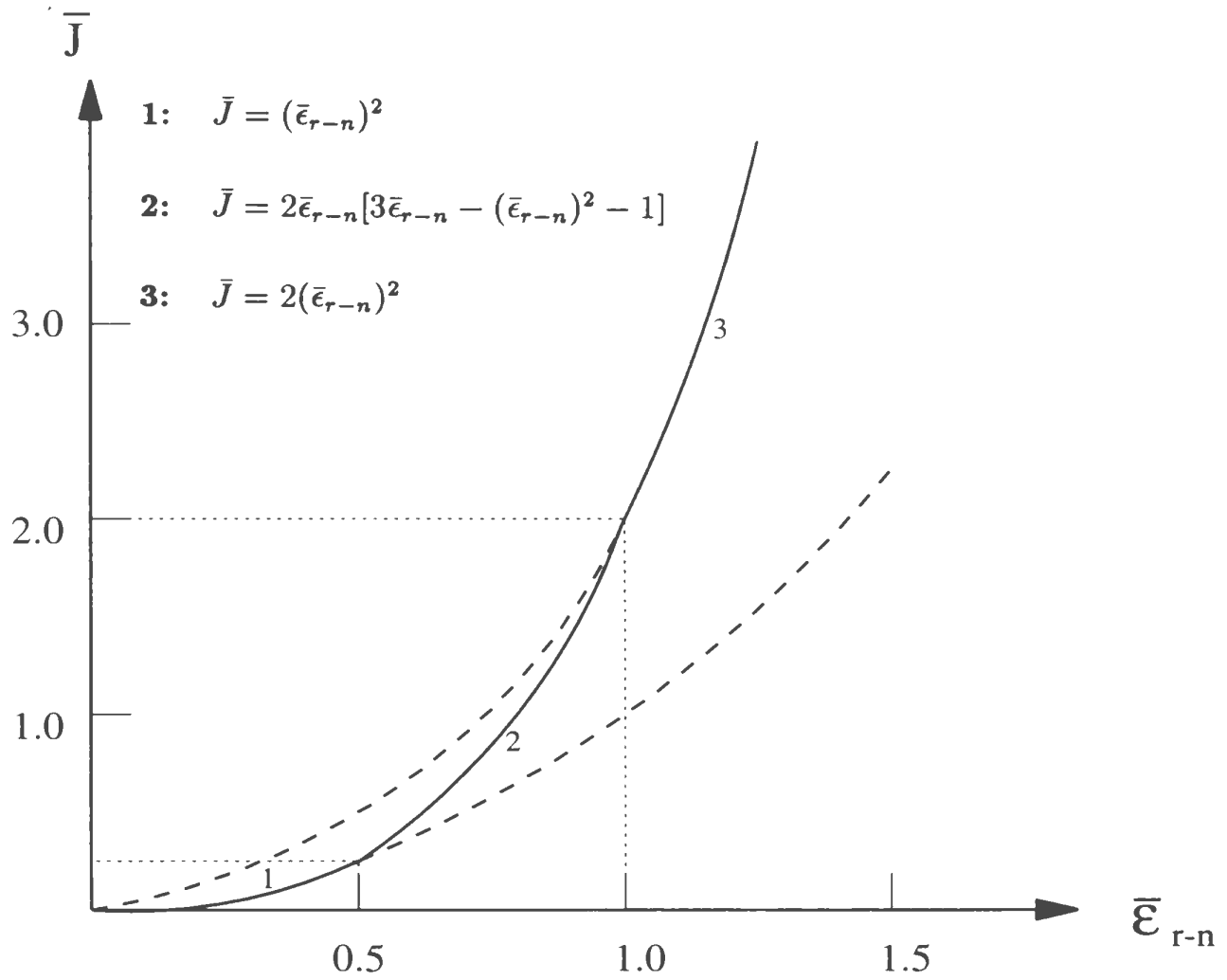


Figure 7.6: Robust J Design Curve

Riedel, 1989) have shown that creep crack growth rates correlate very well with C^* , provided steady state creep is the dominant deformation mechanism in the specimen. The creep crack growth rate follows a power law:

$$\dot{a} = \gamma(C^*)^m \quad (7.29)$$

where γ and m are material constants. In many materials, $m \simeq n/(n + 1)$.

7.5 Numerical Examples

7.5.1 Single-Edge Crack Specimen

Analysis Model: A single-edge crack specimen under tension with width $W=50$ mm, height $H=100$ mm in plane strain is analyzed. There are two different crack lengths considered in the analysis: crack length $a = 10$ mm ($a/W = 0.2$) and $a = 20$ mm ($a/W = 0.4$). Elastic perfectly-plastic material behavior is assumed with $\sigma_y = 488.43$ MN/m² and $E_0 = 2.11 \times 10^5$ MN/m².

The finite element model of an assumed geometry is generated using the ANSYS software. Only the symmetric half of the specimen is considered. Eight-noded isoparametric elements are chosen and eight fans of elements cover the crack tip. All finite element calculations are performed using the ANSYS software program.

The GLOSS R-Node analyses are performed, and the equivalent stress distributions obtained along the symmetry plane from the first and second linear elastic finite element analyses are plotted in Fig. 7.7 and Fig. 7.8. Since failure by plastic collapse occurs by net section yielding along the symmetry plane, the r-node stress along this section is used in the calculations. For the configuration with $a/W = 0.2$,

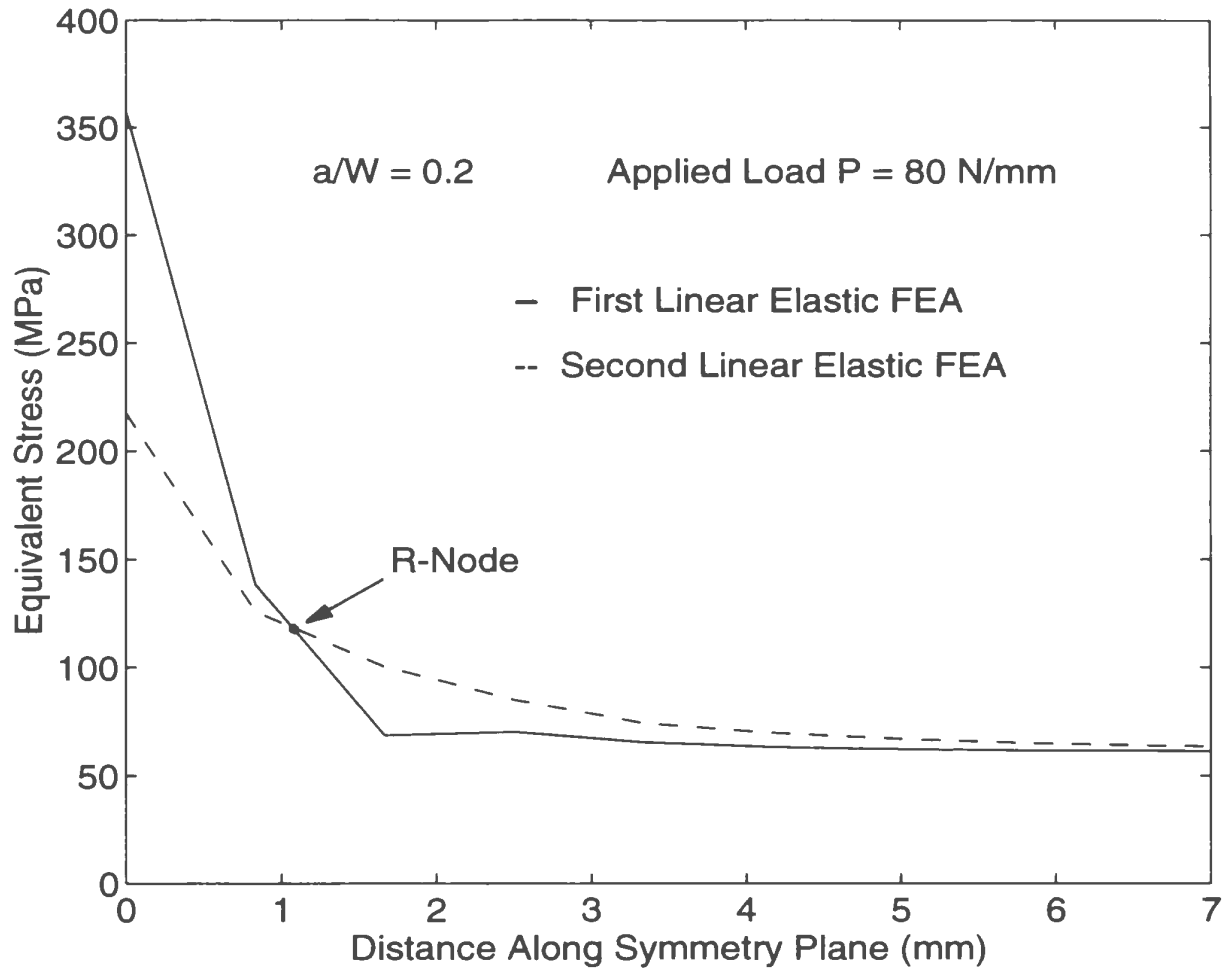


Figure 7.7: Determination of σ_{r-n} for SEC Specimen with $a/W=0.2$

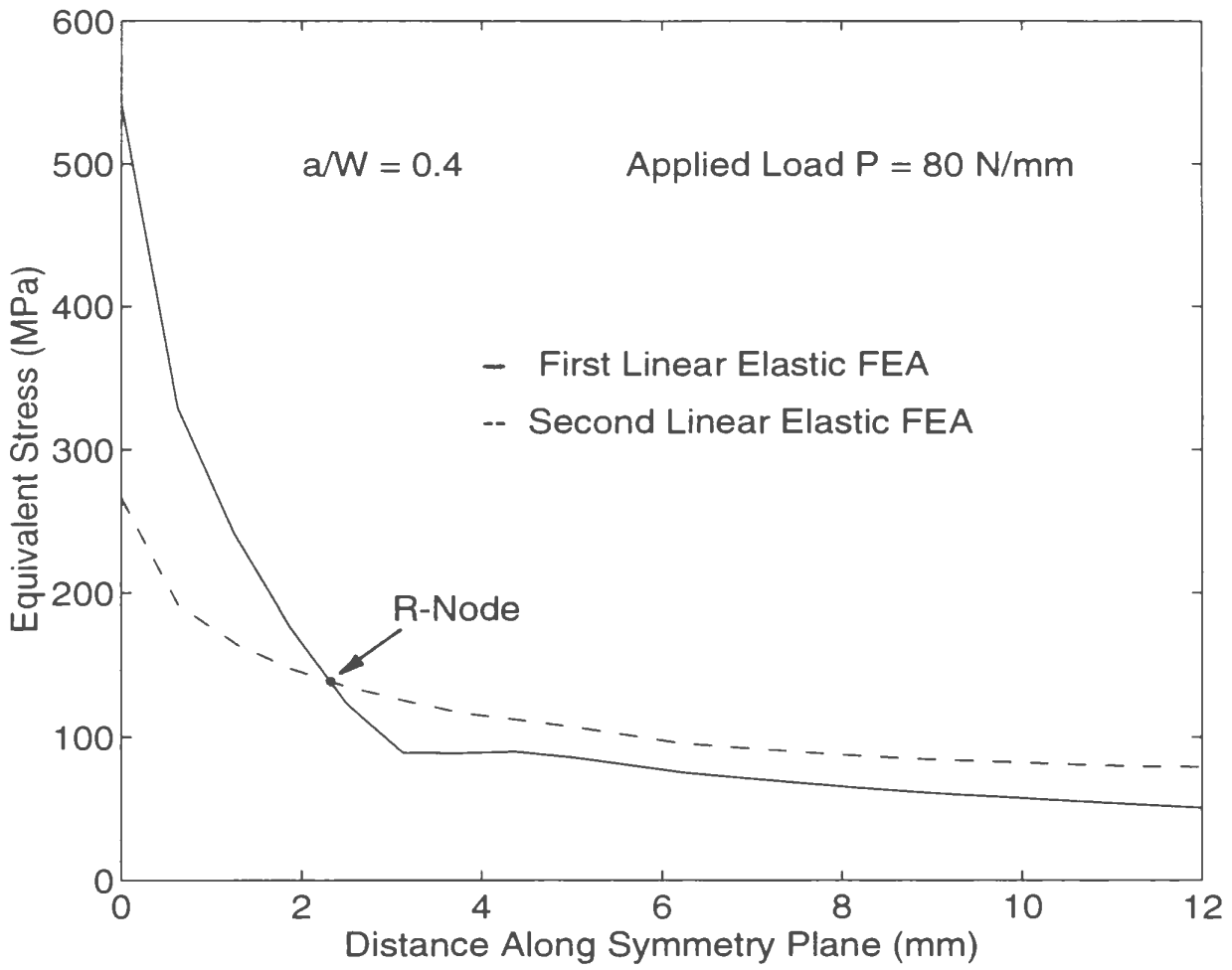


Figure 7.8: Determination of σ_{r-n} for SEC Specimen with $a/W=0.4$

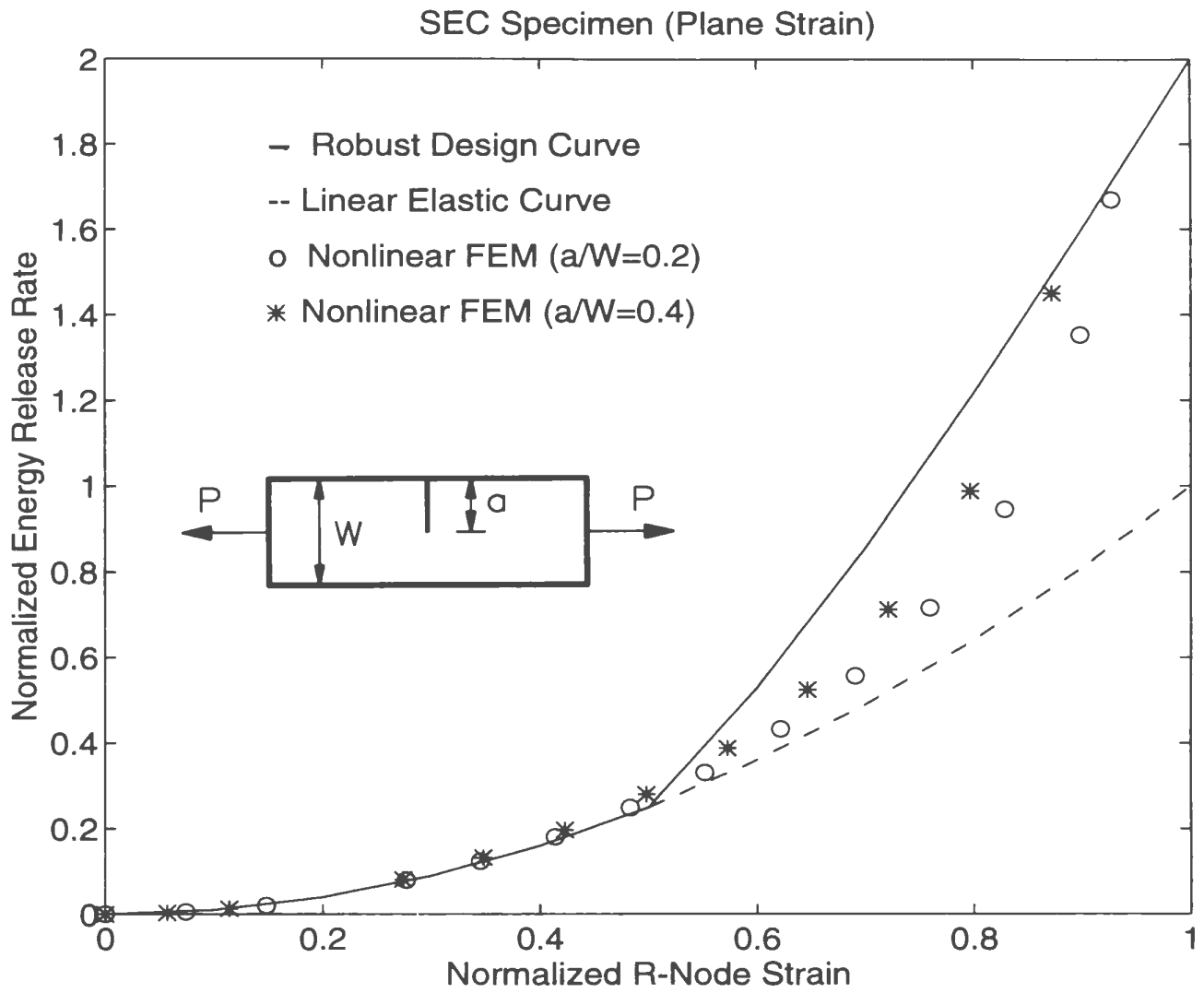


Figure 7.9: $J/J_e(\epsilon_y)$ vs. $\epsilon_{r-n}/\epsilon_y$ for SEC Specimen

the r-node stress is obtained as $\sigma_{r-n} = 119 \text{ MN}/m^2$ for an external tensile load of $P = 80 \text{ N}/mm$, and the corresponding limit load, $P_L = 328 \text{ N}/mm$. For the configuration with $a/W = 0.4$, the r-node stress is obtained as $\sigma_{r-n} = 139 \text{ MN}/m^2$ for an external tensile load of $P = 80 \text{ N}/mm$, and the corresponding limit load, $P_L = 281 \text{ N}/mm$.

The normalized $J/J_e(\epsilon_y)$ values corresponding to normalized r-node strain $\epsilon_{r-n}/\epsilon_y$ obtained by nonlinear finite element analyses and robust J design method are plotted in Fig. 7.9. It can be seen that the robust J design estimates are conservative up to loads close to net section collapse. This corresponds to normalized r-node strain values of 0.88 and 0.93 for crack lengths $a/W = 0.4$ and 0.2 , respectively. Beyond this strain threshold, the robust design curve underestimates J . Well-designed structural components, however, rarely undergo such extensive yielding and this part of the curve would not be relevant in practice.

7.5.2 Compact Tension Specimen

Analysis Model: A standard compact tension specimen subjected to a tensile load, with width $W=100 \text{ mm}$, height $H=120 \text{ mm}$, and thickness $B=50 \text{ mm}$ and in plane strain is analyzed. Two different crack lengths are prescribed: crack length $a = 50 \text{ mm}$ ($a/W=0.5$) and $a = 55 \text{ mm}$ ($a/W=0.55$). Elastic perfectly-plastic material behavior is again assumed with $\sigma_y = 488.43 \text{ MN}/m^2$ and $E_0 = 2.11 \times 10^5 \text{ MN}/m^2$.

The finite element model for the assumed geometry is generated by using the ANSYS software. Only the symmetric half of the specimen is considered. Eight-noded isoparametric elements are chosen and nine crack tip elements are used.

Similar to the analysis of single-edge crack specimen, r-node stresses along the symmetry crack plane can be obtained using the GLOSS R-Node analyses.

Fig. 7.10 shows normalized $J/J_e(\epsilon_y)$ values corresponding to the normalized r-node strain $\epsilon_{r-n}/\epsilon_y$ computed by the nonlinear finite element analyses and robust J design method. It can be seen that the proposed robust J design curve is conservative.

7.5.3 Single Edge Notched Bend Specimen

Analysis Model: A single edge notched bend specimen with crack length $a=50$ mm, width $W=100$ mm, $S=400$ mm in plane stress with thickness $B=3$ mm is analyzed. Elastic perfectly-plastic material behavior is assumed with $\sigma_y = 488.43$ MN/m² and $E_0 = 2.11 \times 10^5$ MN/m².

The finite element model for the assumed geometry is generated by considering the symmetric half of the specimen. Eight-noded isoparametric elements are chosen and eight crack tip elements are used.

Normalized $J/J_e(\epsilon_y)$ values corresponding to the normalized r-node strain $\epsilon_{r-n}/\epsilon_y$ obtained from inelastic finite element analyses and the robust J design method are plotted in Fig. 7.11. It is seen that robust J design point is conservative up to loads close to net section collapse. This corresponds to normalized r-node strain value of 0.95.

7.6 Consideration of the Effect of Strain-hardening

In the development of the robust J design method, the material behavior is assumed to be elastic perfectly-plastic (no strain-hardening). However, if the material be-

CT Specimen (Plane Strain)

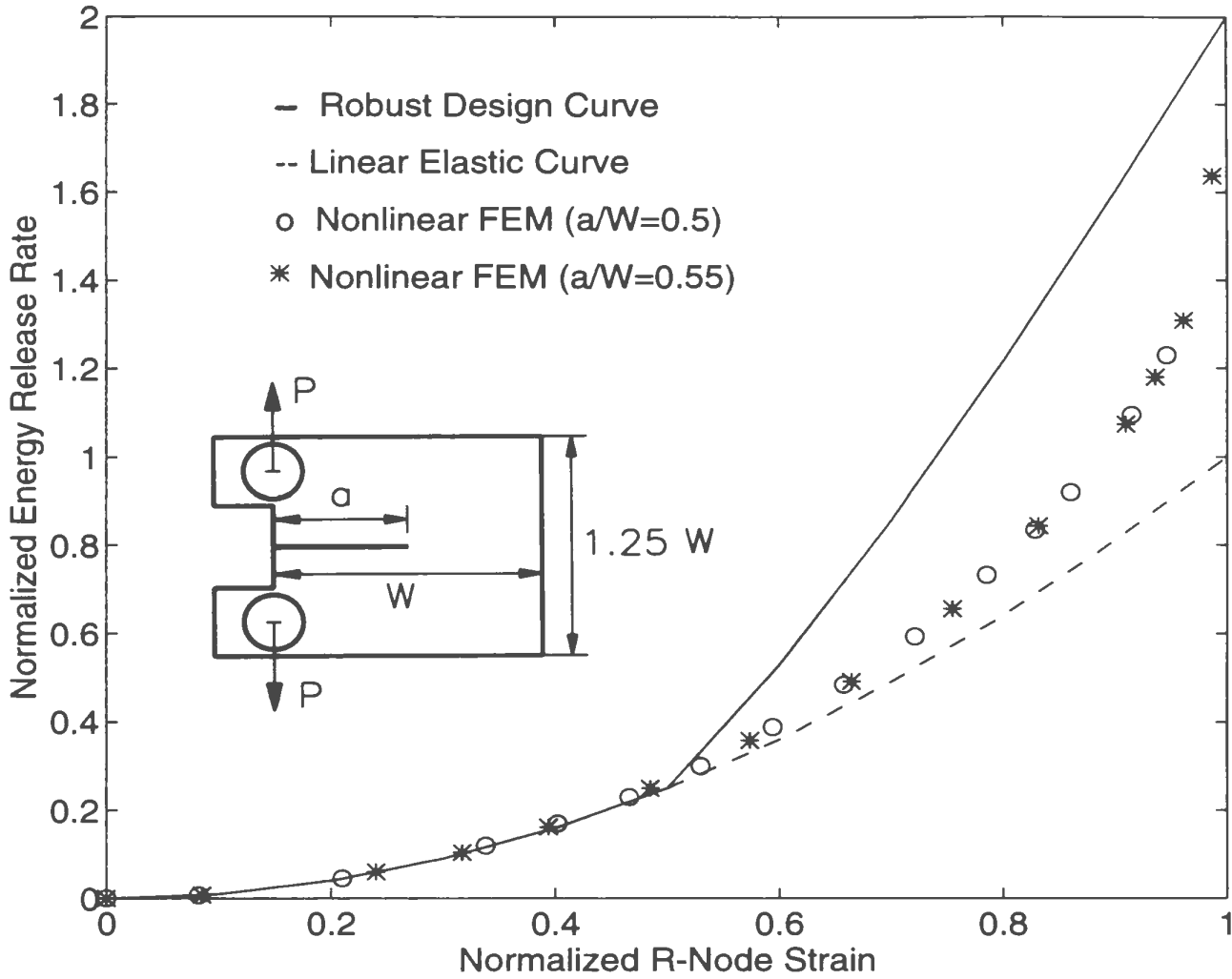


Figure 7.10: $J/J_e(\epsilon_y)$ vs. $\epsilon_{r-n}/\epsilon_y$ for CT Specimen

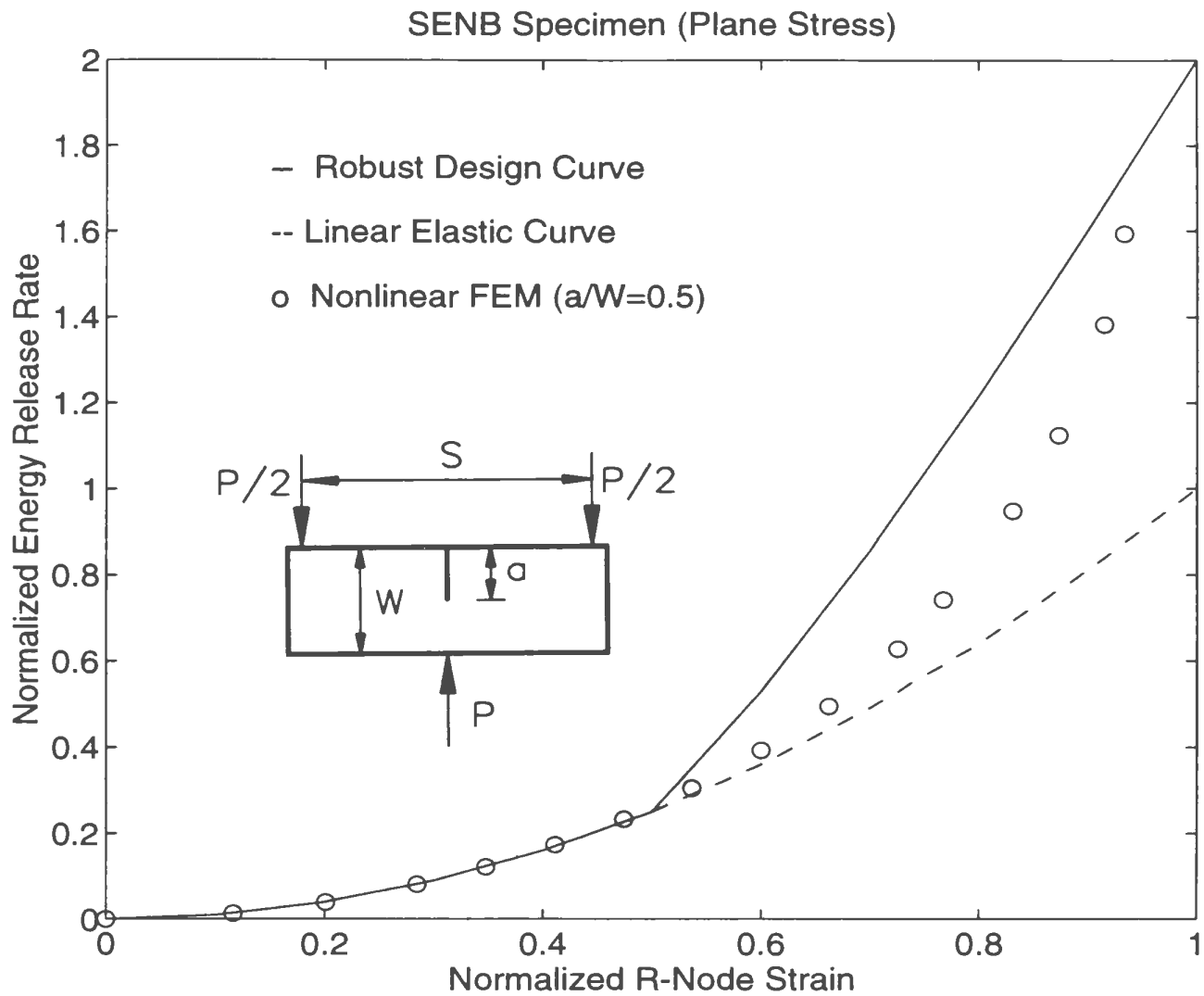


Figure 7.11: $J/J_e(\epsilon_y)$ vs. $\epsilon_{r-n}/\epsilon_y$ for SENB Specimen

havior is elastic-plastic (strain-hardening) then the approach needs to be modified.

For many strain-hardening materials, the stress-strain behavior can be represented by using the Ramberg-Osgood relationship:

$$\frac{\epsilon}{\epsilon_o} = \frac{\sigma}{\sigma_o} + \alpha \left(\frac{\sigma}{\sigma_o} \right)^n \quad (7.30)$$

where σ_o is a reference value stress that is usually equal to the yield strength, $\epsilon_o = \sigma_o/E_o$, α is a dimensionless constant, and n is the strain hardening exponent.

By equating the strain energy densities, the strain-hardening curve can be represented by an equivalent elastic perfectly-plastic curve in which σ_y^* is the assumed yield stress (Fig. 7.12), i.e., area of A_1 should approximately be equal to the area of A_2 . Therefore, σ_y^* can be determined by the equation:

$$\int_{\sigma_o}^{\sigma_y^*} \left(\epsilon - \frac{\sigma}{E_o} \right) d\sigma = \int_{\epsilon_y^*}^{\epsilon_f} (\sigma - \sigma_y^*) d\epsilon \quad (7.31)$$

where $(\sigma_y^*, \epsilon_y^*)$ and (σ, ϵ) are satisfied with strain-hardening curve, and ϵ_f is the fracture strain.

Another method for determining σ_y^* is akin to the K_{Ic} test procedure. For several strain-hardening materials, there is a gradual increase in the non-linearity. In Fig. 7.13, the load P_5 is determined by drawing a secant line from the origin O , with a slope 5 percent less than that of the tangent OA to the initial part of the load-displacement curve. The corresponding stress is then assumed to be equal to the assumed yield stress σ_y^* .

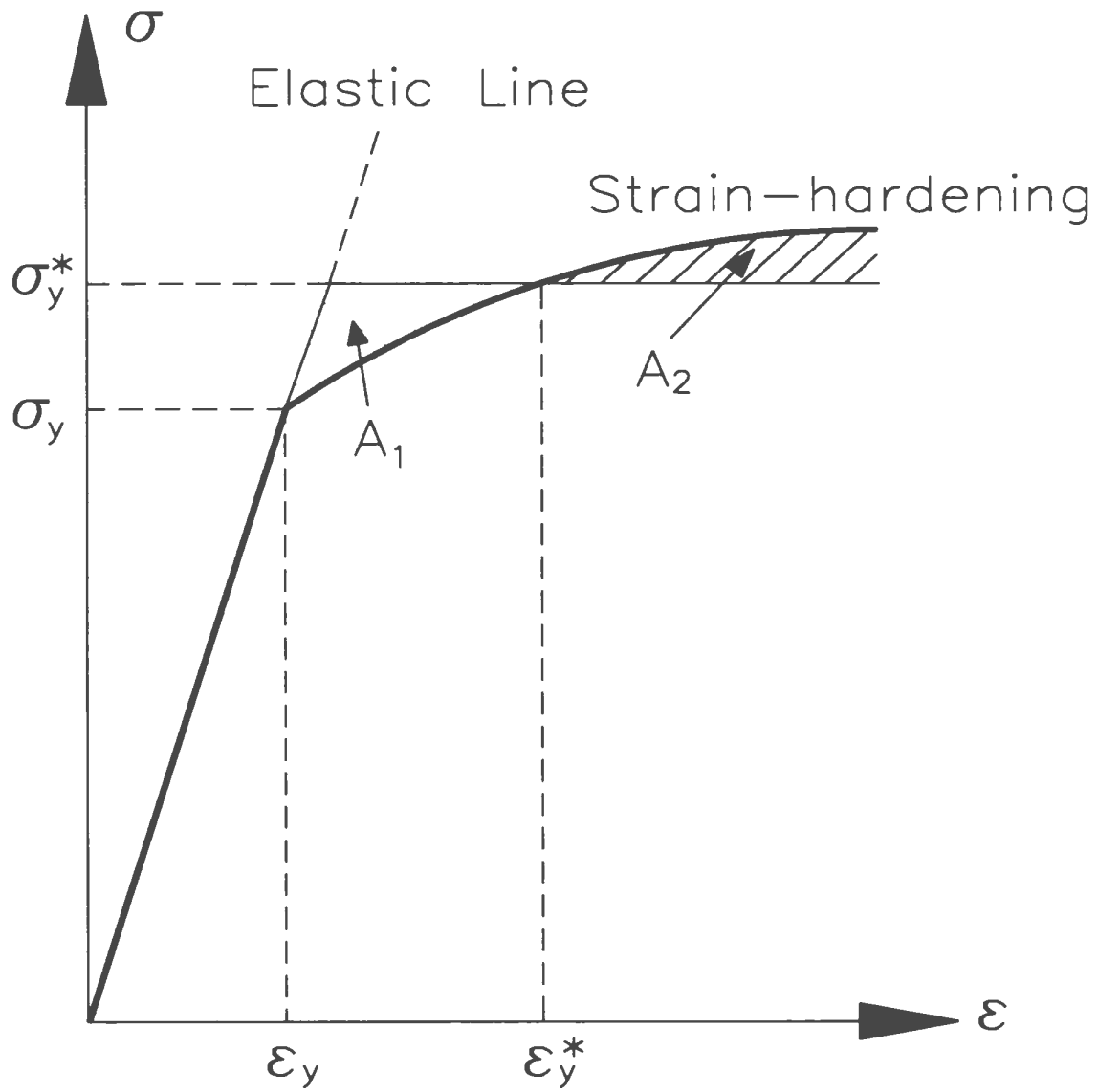


Figure 7.12: Equivalent Elastic Perfectly-Plastic Curve to Strain-hardening

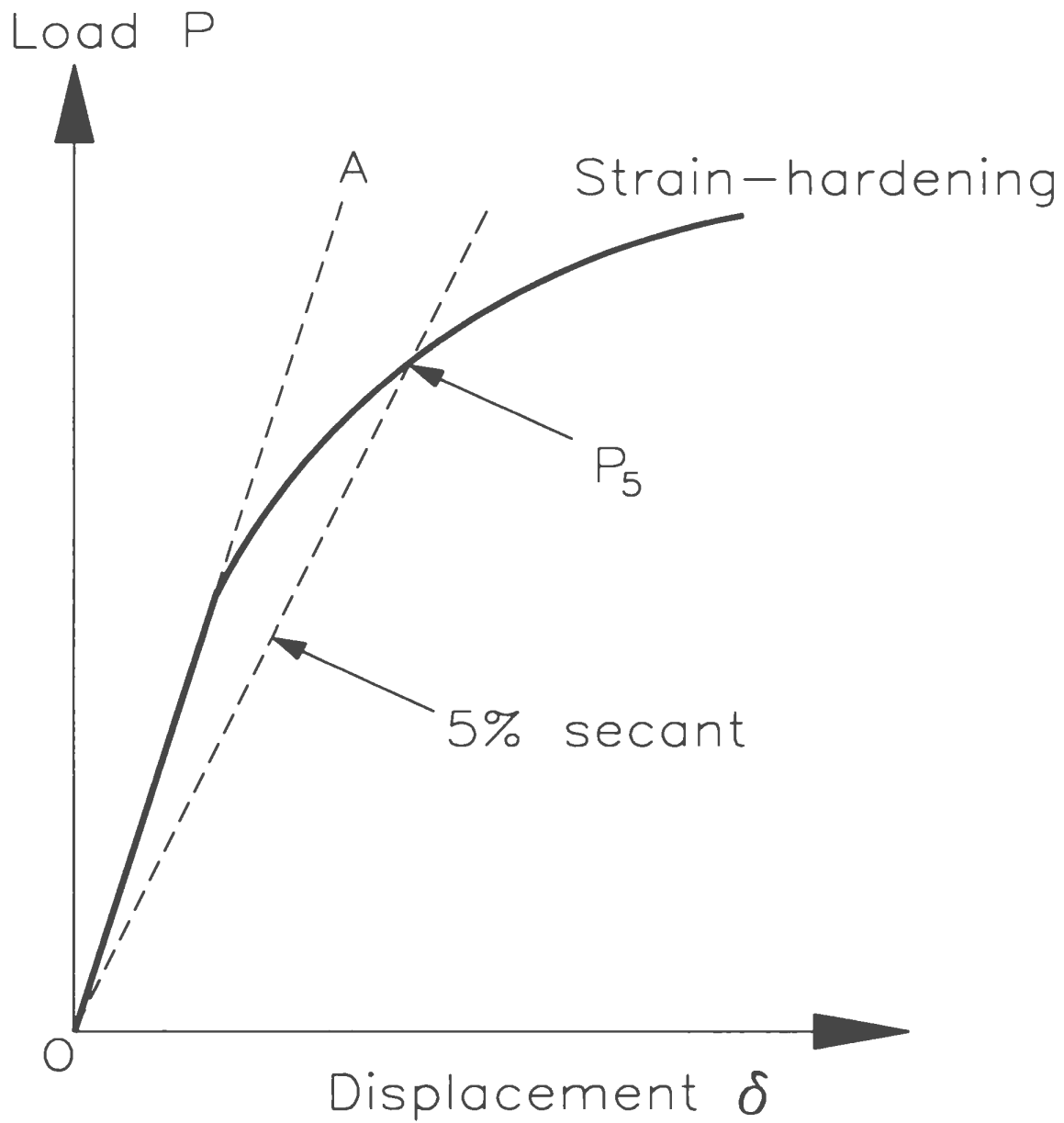


Figure 7.13: Determination of P_5 for Strain-hardening Behaviors

7.7 Remarks

A robust method for estimating the elastic-plastic energy release rate has been presented in this chapter which is suitable for the purpose of design. The method is based on the results of LEFM (linear elastic fracture mechanics) analysis and limit analysis.

The estimations of J made by the robust method are compared with inelastic finite element analysis results for the single-edge crack specimen (SEC), the compact tension specimen (CT) and the single edge notched bend specimen (SENB). The comparisons are reasonable from a design standpoint.

The method is suitable for complex geometries and multiaxial loading conditions that are often encountered in practice.

Chapter 8

Conclusions

8.1 Contributions of the Thesis

Although fracture is one of the principle modes of failure when the material is brittle and the temperature is low, there is considerable design interest in ductile materials and at high temperatures. Evolving methodologies for evaluating fracture assessment parameters for various geometries, loading conditions and materials thus become key ingredients for designing mechanical components and structures.

This thesis lays emphasis on developing simpler and cost efficient techniques, otherwise termed as “robust methods”, for providing conservative fracture assessments. Especially where the operational overheads such as computational time and cost of analysis warrant a high premium, robust techniques serve as viable alternatives over conventional analyses.

Most of the research work that has been carried out so far focuses on two-dimensional idealizations such as plane stress and plane strain. Such idealizations, though may appear to be seemingly simple, yet might not replicate the in-situ conditions with the required accuracy. For instance, conventional understanding has been that the out-of-plane loading (σ_3^R) parallel to the crack front does not

have any effect on the crack growth in a two-dimensional fracture model. It is demonstrated in this thesis that such an assumption might lead to unconservative results. To this end, a simplified three-dimensional model that incorporates the out-of-plane loading and is applicable to practical pressure vessels and piping component configurations is proposed. The results of the study confirm that the remote field stress, σ_3^R , has a significant effect on the crack-tip constraint and therefore, should not be neglected.

A robust design method for estimating the elastic-plastic energy release rate based only on linear elastic fracture analysis and limit analysis is presented in this thesis. The proposed design curves are applicable for elastic, elastic-plastic and perfectly plastic components with defects.

In essence, the following are the original contributions made by this thesis:

- The GLOSS analysis is used for determining the mode I three-dimensional crack-tip plastic zone size. The crack-tip constraint parameter is determined on the basis of two linear elastic analyses. Based on this, the three-dimensional crack-tip plastic zone size can be approximately evaluated. The proposed methodology is suitable for complex geometry and multiaxial loading conditions.
- Approximate methods for determining the J of circular-ended notches are developed. The notch root stress and strain are obtained in conjunction with the GLOSS technique. In this context, an edge-cracked component or structure is viewed as the limiting case of a circular-ended notched specimen. The methods suggested provide a simple way for evaluating elastic-plastic J for cracked components and structures.

- A $2\frac{1}{2}$ -D model that accounts for the out-of-plane remote stress-field, σ_3^R , is developed. The model can be used for analyzing practical pressure vessels and piping components with a circumferential flaw or a longitudinal flaw. A correction factor is recommended so that the conventional two-dimensional results can be adapted, taking into account the out-of-plane remote stress-field.
- A robust method for estimating the elastic-plastic energy release rate has been developed. The method is suitable for analyzing complex geometries and multiaxial loading conditions that are often encountered in real life situation. The effects of strain-hardening and creep are also included.
- The proposed methods are validated by means of a number of numerical examples of practical significance and the results are found to be encouraging.

The robust methods developed in this thesis demonstrate a simple and systematic approach for performing the integrity assessments of structures and components with defects. The proposed methods come in handy for practising engineers involved in routine design and analysis. Since the methods proposed in this thesis do not require high cost, time and computer memory, they also pave way for quick and conservative design assessments. Research in this thesis points out that neglecting the out-of-plane remote stress is unconservative and would likely lead to premature failures and potential damage. The effect of out-of-plane loading should be considered in the related design codes.

8.2 Future Research

The usefulness of robust techniques has been asserted in the previous chapters. As engineers spend most of their time in improving existing designs, apart from evolving newer designs, robust methods would serve as an effective means to keep pace with the “design - redesign - improve” cycle. It would be therefore highly rewarding to pursue research in this area. The methods developed can be applied to configurations that are not specifically addressed in this thesis. This would further serve for benchmarking and validating the application of these methods.

Further experimental study should focus on three-dimensional pressure vessels and piping components with defects. The J estimates based on the research in this thesis should compare with the experimental results, and some design perspectives should emerge from the work.

References

Ainsworth, R. A., 1984, "The Assessment of Defects in Structures of Strain Hardening Materials," *Engineering Fracture Mechanics*, Vol. 19, No. 4, pp. 633-642.

Amestoy, M., Bui, H. D., and Labbens, R., 1981, "On the Definition of Local Path Independent Integrals in Three-Dimensional Crack Problems," *Mechanics Research Communications*, Vol. 8 (4), pp. 231-236.

Anderson, T. L., 1991, *Fracture Mechanics - Fundamentals and Applications*, CRC Press Inc..

ANSYS User's Manual for Revision 5.0, 1992, Swanson Analysis Systems Inc., Houston, PA, U.S.A..

ASTM Standard E 399-83, 1984, "Standard Test Method for Plane-Strain Fracture Toughness of Metallic Materials," 1984 Annual Book of ASTM Standard, Vol. 03.01, pp. 519-554.

Bakker, A., 1984, *The Three-Dimensional J-Integral: An Investigation into Its Use for Post-Yield Fracture Safety Assessment*, Ph.D. Thesis, Delft University of Technology, Delft, The Netherlands.

Broek, D., 1986, *Elementary Engineering Fracture Mechanics*, 4th ed.,

Martinus Nijhoff Publishers, Netherlands, pp. 75-81.

Bucci, R. J., Paris, P. C., Landes, J. D., and Rice, J. R., 1972, "*J* Integral Estimation Procedures," ASTM STP 514, pp. 40-69.

Burgreen, D., 1968, Design Method for Power Plant Structures, C. P. Press, Jamaica, N.Y..

Chiarelli, M., and Frediani, A., 1993, "A Computation of the Three-Dimensional *J*-Integral for Elastic Materials with a View to Applications in Fracture Mechanics," *Engineering Fracture Mechanics*, Vol. 44, No. 5, pp. 763-788.

Dai, L., 1989, "Fracture Assessment of Mechanical Components Under Multiaxial Loading," Master's Thesis, University of Regina, Regina, Canada.

Dowling, A. R., and Townley, C. H. A., 1975, "Effect of Defects on Structural Failure: a Two-criteria Approach," *Int. J. Pres Ves. & Piping*, **3**, pp. 77-107.

Ellyin, F., and Kujawski, D., 1987, "Notch Root Stress/Strain Prediction for Elastic-Plastic Loading," *Res Mechanica*, Vol. 20, pp. 177-190.

Eshelby, J. D., 1956, "A Continuum Theory of Lattice Defects," in: Solid State Physics: *Advances in Research and Applications*, Vol. 3, Seitz, F. and Turnbull, D. (ed's), Academic Press, pp. 79-144.

Eshelby, J. D., 1957, "The Determination of the Elastic Field of an Ellipsoidal Inclusion and Related Problems," *Proceeding of the Royal Society*, London, Series A, Vol. 241.

Eshelby, J. D., 1970, "The Energy Momentum Tensor in Continuum

- Mechanics,” in: *Inelastic Behavior of Solids*. Kanninen et al. (ed.), McGraw-Hill.
- Ewalds, H. L., and Wanhill, R. J. H., 1986, *Fracture Mechanics*, Edward Arnold Ltd.
- Hardrath, H. F., and Ohman, L., 1953. “A Study of Elastic and Plastic Stress Concentration Factors due to Notches and Fillets in Flat Plates,” NACA Report 117.
- Kikuchi, H., and Miyamoto, H., 1982, “On the Three-Dimensional J Integrals,” *Bull. Fract. Mech. Lab.*, Science University of Tokyo, **1**, pp.46-73.
- Kishimoto, K., Aoki, S., and Sakata, M., 1980, “On the Path Independent Integral- \tilde{J} ,” *Engineering Fracture Mechanics*, Vol. 13, pp. 841-850.
- Kizhatil, R. K., 1993, *Robust Approximate Methods for Inelastic Analysis of Mechanical Components*, Ph.D. Thesis, University of Regina, Regina, Canada.
- Knowles, J. K., and Sternberg, E, 1972, “On a Class of Conservation Laws in Linearized and Finite Elastostatics,” *Archive for Rational Mechanics and Analysis*, Vol. 44, pp. 187-211.
- Kumar, V., German, M. D., and Shih, C. F., 1981, *An Engineering Approach for Elastic Plastic Fracture Analysis*, EPRI Palo Alto, Calif., Report No. NP-1931.
- Landes, J. D., and Begley, J. A., 1976, “A Fracture Mechanics Approach to Creep Crack Growth,” ASTM STP 590, pp. 128-148.

Marriott, D. L., 1992, Beyond Finite Element Analysis, Professional Development Session 3, *11th Symposium on Engineering Applications of Mechanics*, University of Regina, Regina, Canada.

Molski, K., and Glinka, G., 1981, "A Method of Elastic-Plastic Stress and Strain Calculation at a Notch Root," *Mater. Sci. Eng.*, Vol. 50, pp. 93-100.

Narasimhan, R., and Rosakis, A. J., 1988, Three Dimensional Effects near a Crack Tip in a Ductile Three Point Bend Specimen - Part I: A Numerical Investigation, Division of Engineering and Applied Science, California Institute of Technology, SM Report 88-6.

Neuber, H., 1961, "Theory of Stress Concentration for Shear-Strained Prismatical Bodies with Arbitrary Nonlinear Stress-Strain Laws," *ASME Journal of Applied Mechanics*, Vol. 28, pp. 544-550.

Newman, J. C., Bigelow, C. A., and Sivakumar, K. N., 1993, "Three-Dimensional Elastic-Plastic Finite-Element Analyses of Constraint Variations in Cracked Bodies," *Engineering Fracture Mechanics*, Vol. 46, No. 1, pp. 1-13.

Nikbin, K. M., Webster, G. A., and Turner, C. E., 1976, ASTM STP 601, pp. 47-62.

PD 6493, 1980, Guidance on Some Methods for the Derivation of Acceptance Levels for Defects in Fusion Welded Joints, BSI, London.

Rice, J. R., 1968a, "A Path Independent Integral and the Approximate Analysis of Strain Concentration by Notches and Cracks," *ASME Journal of Applied Mechanics*, Vol. 35, pp. 379-386.

- Rice, J. R., 1968b, "Mathematical Analysis in the Mechanics of Fracture," *Treatise on Fracture*, Vol. 2, ed., Liebowitz, H., Academic Press. pp. 191-311.
- Rice, J. R., Paris, P. C., and Merkle, J. G., 1973, "Some Further Results on *J*-Integral Analysis and Estimates," *Progress in Flaw Growth and Fracture Toughness Testing*, ASTM STP 536, pp. 231-245.
- Rice, J. R., and Rosengren, G. F., 1968, "Plane Strain Deformation Near a Crack Tip in a Power-Law Hardening Material," *Journal of Mechanics and Physics of Solids*, Vol. 16, pp. 1-12.
- Riedel, H., 1989, "Creep Crack Growth," ASTM STP 1020, pp. 101-126.
- Schwartz, C. W., 1993, "Influence of Out-of-Plane Loading on Crack Tip Constraint," *Constraint Effects in Fracture*, ASTM STP 1171, pp. 318-340.
- Seshadri, R., 1991, "The Generalized Local Stress Strain (GLOSS) Analysis-Theory and Applications," *ASME Journal of Pressure Vessel Technology*, Vol. 113, pp. 219-227.
- Seshadri, R., and Fernando, C. P. D., 1992, "Limit Loads of Mechanical Components and Structures using the Gloss R-Node Method," *ASME Journal of Pressure Vessel Technology*, Vol. 114, pp. 201-208.
- Seshadri, R., and Kizhatil, R. K., 1993, "Notch Root Inelastic Strain Estimates Using GLOSS Analysis," *Advances in Multiaxial Fatigue*, ASTM STP 1191, pp. 397-411.
- Seshadri, R., and Marriott, D. L., 1993, "On Relating the Reference Stress, Limit Load and the ASME Stress Classification Concepts," *Int. J. Pres.*

Ves. & Piping **56** (1993), pp. 387-408.

Seshadri, R., and Kizhatil R. K., 1995, "Robust Approximate Methods for Estimating Inelastic Fracture Parameters," *ASME Journal of Pressure Vessel Technology*, Vol. 117, pp. 115-123.

Seshadri, R., 1996, "In Search of the Redistribution Nodes," *Proceedings of the International Conference on Pressure Vessels and Piping*, Singapore.

Shih, C. F., and Hutchinson, J. W., 1976, "Fully Plastic Solutions and Large-Scale Yielding Estimates for Plane Stress Crack Problems," *ASME Journal of Engineering Materials and Technology*, Vol. 98, No. 4, pp. 289-295.

Stowell, E. Z., 1950, "Stress and Strain Concentration at a Circular Hole in an Infinite Plate," NACA Technical Note, No.2073.

Turner, C. E., 1981, "The J -Estimation Curve and the Tearing Resistance Concepts Leading to a Proposal for a J -Based Design Curve Against Fracture," *Fitness for Purpose Validation of Welded Construction*, Welding Institute, Cambridge, Paper 10.

Turner, C. E., 1984a, Post-yield Fracture Mechanics, Latzko, D. G. H., et al Eds., Elsevier Applied Science Publishers, second edition, Chapter 5.

Turner, C. E., 1984b, "Further Developments of a J -Based Design Curve and its Relationship to Other Procedures," *Elastic-Plastic Fracture: Second Symposium, Vol. II-Fracture Resistance Curves and Engineering Applications*, ASTM STP 803, pp. II-80-II-102.

Wu, S., and Seshadri, R., 1995a, "Estimation of 3D Crack Tip Plastic Zone

Size Using the GLOSS Method,” *Proceedings of 15th Canadian Congress of Applied Mechanics*, University of Victoria, Victoria, Canada.

Wu, S., and Seshadri, R., 1995b, “*J*-Estimation for Smooth-Ended Notches Using the GLOSS Method,” *Proceedings of 15th Canadian Congress of Applied Mechanics*, University of Victoria, Victoria, Canada.

Wu, S., and Seshadri, R., 1995c, “Robust *J*-Estimation of Circular-Ended Notches,” *ASME/JSME PVP-95-DA3*, Honolulu, Hawaii, USA.

Wu, S., and Seshadri, R., 1996, “A Simplified Three-Dimensional Model for Analyzing Pressure Components with Defects,” Accepted for ASME 1996 PVP Conference, Montreal.

Appendix A

Implementation of GLOSS Analysis

A.1 GLOSS Method

This appendix describes the procedure for implementing the GLOSS method into the ANSYS (1992) finite element software. After performing a linear elastic finite element analysis, the user file GLOSS-MAC is input for performing the elastic modulus corrections. Subsequently, a second linear elastic finite element analysis is carried out. The user file GLOSS-MAC also performs the necessary post-processing for extracting the equivalent stress from the first and second linear elastic analyses, from which the constraint parameter λ can be obtained. The user file is listed in the following sections.

A.1.1 3-D Mode I Single Edge Through-Cracked Specimen

The input file consists of geometric and material data, and the loads and boundary conditions of the problem. The problem of 3-D Mode I cracked specimen is discussed in Section 4.3. The macro FRACT is used to create the SOLID95 crack tip elements from the SOLID45 elements using a weighted midside node position (quarter point location).

```
!  
!ANSYS INPUT FILE  
!3D MODE I SINGLE EDGE THROUGH-CRACKED SPECIMEN  
!  
  
*SET,YM,30e06           ! Young's Modulus  
*SET,YS,60e03          ! Yield Stress  
*SET,NU,0.3            ! Poisson's Ratio  
*SET,C,0.15            ! Geometric Parameters  
*SET,DB,6  
*SET,RB,3  
*SET,B,-1  
*SET,W,6  
*SET,H,6  
*SET,A,2  
*SET,Div1,4  
*SET,Div2,6
```

```

*SET,Div3,6
*SET,PX,          ! Load
*SET,PY,20e03
*SET,PZ,
/title, 3 D Mode I fracture model
/prep7          ! Pre-processing
shpp,off
antype,static
et,1,45        ! SOLID45 element
et,2,45
et,3,95        ! SOLID95 element
MP,ex,1,YM
MP,ex,2,YM
MP,ex,3,YM
MP,NUXY,1,NU
MP,NUXY,2,NU
MP,NUXY,3,NU
KB=RB**(1/(DB-1))  ! Geometry
SK=1
*DO,i,1,DB-1
SK=SK+KB**i
*ENDDO
mb=0
*DO,m,0,DB,1

```

```

n,1+18*m,, ,mb
n,11+18*m,, ,mb
n,12+18*m,, ,mb
n,13+18*m,, ,mb
n,14+18*m,, ,mb
n,15+18*m,, ,mb
n,16+18*m,, ,mb
n,17+18*m,, ,mb
n,18+18*m,, ,mb
n,2+18*m,-C/2,, ,mb
n,6+18*m,0,C/2,mb
n,10+18*m,C/2,, ,mb
csys,1
fill,2+18*m,6+18*m
fill,6+18*m,10+18*m
csys,0
mb=mb+B/SK*(KB**m)
*ENDDO
type,2
*DO,i,1,DB,1
cc=18*(i-1)
en,1+8*(i-1),2+cc,3+cc,11+cc,1+cc,20+cc,21+cc,29+cc,19+cc
*DO,j,1,7,1
cc1=cc+j-1

```

```

en,1+8*(i-1)+j,3+cc1,4+cc1,12+cc1,11+cc1,21+cc1,22+cc1,30+cc1,29+cc1
*ENDDO
*ENDDO
ib=0
*DO,i,0,DB,1
csys,0
k,1+6*i,-C/2,,ib
k,2+6*i,,C/2,ib
k,3+6*i,C/2,,ib
k,4+6*i,-5*C,,ib
k,5+6*i,,5*C,ib
k,6+6*i,5*C,,ib
l,2+6*i,5+6*i,5,2.5
l,1+6*i,4+6*i,5,2.5
l,3+6*i,6+6*i,5,2.5
csys,1
l,1+6*i,2+6*i,4
l,2+6*i,3+6*i,4
l,4+6*i,5+6*i,4
l,5+6*i,6+6*i,4
csys,0
ib=ib+B/SK*(KB**i)
*ENDDO
*DO,i,1,DB,1

```

```

*D0,j,0,5,1
l,1+6*(i-1)+j,7+6*(i-1)+j,1
*ENDDO
*ENDDO
ib=0
*D0,i,0,DB,1
k,1+6*(DB+1)+7*i,-A,0,ib
k,2+6*(DB+1)+7*i,-A,h,ib
k,3+6*(DB+1)+7*i,0,h,ib
k,4+6*(DB+1)+7*i,W-A,h,ib
k,5+6*(DB+1)+7*i,W-A,0,ib
k,6+6*(DB+1)+7*i,-A,2*h/7,ib
k,7+6*(DB+1)+7*i,W-A,2*h/7,ib
l,5+6*i,3+6*(DB+1)+7*i,Div2,3
l,4+6*i,1+6*(DB+1)+7*i,Div1,3
l,1+6*(DB+1)+7*i,6+6*(DB+1)+7*i,4,2
l,6+6*(DB+1)+7*i,2+6*(DB+1)+7*i,Div3,1.5
l,3+6*(DB+1)+7*i,2+6*(DB+1)+7*i,Div1,1.5
l,3+6*(DB+1)+7*i,4+6*(DB+1)+7*i,Div2,1.5
l,7+6*(DB+1)+7*i,4+6*(DB+1)+7*i,Div3,1
l,5+6*(DB+1)+7*i,7+6*(DB+1)+7*i,4,2
l,6+6*i,5+6*(DB+1)+7*i,Div2,2.5
l,5+6*i,6+6*(DB+1)+7*i,Div1,2
l,5+6*i,7+6*(DB+1)+7*i,Div2,2

```

```

ib=ib+B/SK*(KB**i)
*ENDDO
*DO,i,1,DB,1
1,1+6*(DB+1)+7*(i-1),1+6*(DB+1)+7*i,1
1,2+6*(DB+1)+7*(i-1),2+6*(DB+1)+7*i,1
1,3+6*(DB+1)+7*(i-1),3+6*(DB+1)+7*i,1
1,4+6*(DB+1)+7*(i-1),4+6*(DB+1)+7*i,1
1,5+6*(DB+1)+7*(i-1),5+6*(DB+1)+7*i,1
1,6+6*(DB+1)+7*(i-1),6+6*(DB+1)+7*i,1
1,7+6*(DB+1)+7*(i-1),7+6*(DB+1)+7*i,1
*ENDDO
type,1
*DO,i,1,DB,1
dd=6*(i-1)
dd1=6*(DB+1)+7*(i-1)
v,1+dd,2+dd,5+dd,4+dd,7+dd,8+dd,11+dd,10+dd
v,2+dd,3+dd,6+dd,5+dd,8+dd,9+dd,12+dd,11+dd
v,4+dd,5+dd,11+dd,10+dd,1+dd1,6+dd1,13+dd1,8+dd1
v,6+dd,5+dd,11+dd,12+dd,5+dd1,7+dd1,14+dd1,12+dd1
v,5+dd,3+dd1,10+dd1,11+dd,6+dd1,2+dd1,9+dd1,13+dd1
v,5+dd,3+dd1,10+dd1,11+dd,7+dd1,4+dd1,11+dd1,14+dd1
*ENDDO
vmesh,all
nummrg,node

```

```
nsel,s,loc,x,0
nsel,r,loc,y,0
cm,cracktip,node
```

```
/nerr,0
```

```
fract,2
```

```
! Macro
```

```
/nerr,defa
```

```
/output
```

```
outpr,,all
```

```
fini
```

```
/solu
```

```
! Solution
```

```
nsel,s,loc,x,0,W-a
```

```
! Boundary Conditions
```

```
nsel,r,loc,y,0
```

```
d,all,uy,0
```

```
nsel,all
```

```
nsel,s,loc,z,B
```

```
d,all,uz,0
```

```
nsel,all
```

```
nsel,s,loc,y,0
```

```
nsel,r,loc,x,0
```

```
nsel,r,loc,z,B
```

```
d,all,ux,0
```

```
nsel,all
```

Page 146

**missing from the
original book**

```

! MACRO TO CREATE 3D SOLID95 CRACK TIP ELEMENTS FROM 3D SOLID45 ELEMENTS
! MAKE A COMPONENT CONTAINING THE CRACK TIP NODES (CRACKTIP)
! THE CRACK TIP IS BETWEEN NODES K AND O
! SET ELEMENT TYPE TO POINT TO SOLID95
! SET ARG1 TO n (the type of the elements around the crack tip)
!
/NOPR
NSEL,ALL
*GET,N,NODE,,NUM,MAX ! CURRENT MAXIMUM NODE NUMBER
CMSEL,S,CRACKTIP ! SELECT THE TIP NODES
ESLN ! ANY ELEMENTS ATTACHED
*GET,ELMAX,ELEM,,NUM,MAX ! CURRENT MAXIMUM ELEMENT NUMBER
*DO,IEL,1,ELMAX ! LOOP ON MAX ELEMENT
    ELMI=IEL
    *IF,ELMI,LE,0,EXIT ! NO MORE SELECTED
    *GET,ELTYPE,ELEM,ELMI,ATTR,TYPE ! GET ELEMENT TYPE
    *IF,ELTYPE,NE,ARG1,CYCLE ! CHECK FOR OLD ST85
    N3 = NELEM(ELMI,3) ! GET NODE 3 (K)
    *IF,NSEL(N3),LE,0,CYCLE ! IT MUST BE SELECTED
    N7 = NELEM(ELMI,7) ! GET NODE 7 (L)
    *IF,NSEL(N7),LE,0,CYCLE ! IT MUST ALSO BE SELECTED
    N1 = NELEM(ELMI,1) ! GET NODE 1 (I)
    N2 = NELEM(ELMI,2) ! GET NODE 2 (J)
    N5 = NELEM(ELMI,5) ! GET NODE 5 (M)

```

```

N6 = NELEM(ELMI,6)           ! GET NODE 6 (N)

X3 = 0.75*NX(N3)             ! WEIGHTED POSITION OF N3
Y3 = 0.75*NY(N3)
Z3 = 0.75*NZ(N3)

X  = 0.25*NX(N2) + X3       ! QUARTER POINT LOCATION ( NODE (R) )
Y  = 0.25*NY(N2) + Y3
Z  = 0.25*NZ(N2) + Z3

N  = N + 1                   ! NEXT NODE

N10 = N

N,N10,X,Y,Z                  ! MIDSIDE NODE LOCATION

X  = 0.25*NX(N1) + X3
Y  = 0.25*NY(N1) + Y3
Z  = 0.25*NZ(N1) + Z3

N  = N + 1

N12= N

N,N12,X,Y,Z

X7 = 0.75*NX(N7)
Y7 = 0.75*NY(N7)
Z7 = 0.75*NZ(N7)

X  = 0.25*NX(N6) + X7
Y  = 0.25*NY(N6) + Y7
Z  = 0.25*NZ(N6) + Z7

N  = N + 1

```

```

N14 = N
N,N14,X,Y,Z
X = 0.25*NX(N5) + X7
Y = 0.25*NY(N5) + Y7
Z = 0.25*NZ(N5) + Z7
N = N + 1
N16 = N
N,N16,X,Y,Z
N4=N3
N8=N7
NSEL,ALL
TYPE,3
EN,ELMI,N1,N2,N3,N4,N5,N6,N7,N8 ! REDEFINE THE ELEMENT
EMORE,0,N10,0,N12,0,N14,0,N16
EMORE,
*ENDDO
CMSEL,U,CRACKTIP ! UNSELECT THE TIP NODES
NUMMRG,NODE ! MERGE MIDSIDE NODES
NSEL,ALL ! SELECT ALL ELEMENTS
ESEL,ALL ! SELECT ALL ELEMENTS
/GOPR
*END

```

The GLOSS-MAC file modifies the moduli of all elements above the material yield, σ_y ,

$$E_s = \left(\frac{\sigma_y}{\sigma_e} \right) E_0$$

where E_s is the modified modulus, E_0 is the original modulus, and σ_e is the centroidal equivalent stress. The file GLOSS-MAC also performs post-processing calculation. It obtains the equivalent stress in the local element after two linear elastic analyses. These values are then used to calculate the constraint parameter λ .

```
!  
!(GLOSS-MAC)  
!THIS USER FILE (GLOSS-MAC) CALCULATES MODIFIED ESEC = E0 * SIGY/SIGE  
!  
  
/post1  
SET,1  
ETABLE,SIGC,S,EQV  
  
/output,cylg1  
PRETAB,SIGC  
/output  
  
ESEL,S,ETAB,SIGC,YS,(YS*10E10)  
*SET,MN,2
```

```

*GET ,EL2 ,ELEM ,0 ,NUM ,MAX

*CFOPEN ,SUKUA

: STA

*GET ,EL1 ,ELEM ,0 ,NUM ,MIN

*GET ,STEQ ,ELEM ,EL1 ,ETAB ,SIGC

*SET ,ESEC ,(YS/STEQ)*YM

*CFWRITE ,EX ,MN ,ESEC

*SET ,MN ,MN+1

*SET ,EL1 ,EL1+1

ESEL ,R ,ELEM , ,EL1 ,EL2

*IF ,EL1 ,LE ,EL2 , : STA

*CFCLOS

ESEL ,ALL

ESEL ,S ,ETAB ,SIGC ,YS ,(YS*10E10)

*SET ,MN ,2

*GET ,EL2 ,ELEM ,0 ,NUM ,MAX

*CFOPEN ,SUKUB

: STB

*GET ,EL1 ,ELEM ,0 ,NUM ,MIN

*CFWRITE ,MAT ,MN

```

```
*CFWRITE,EMODIF,EL1
*SET,MN,MN+1
*SET,EL1,EL1+1
ESEL,R,ELEM,,EL1,EL2
*IF,EL1,LE,EL2,:STB
*CFCLOS
EALL
FINISH

/PREP7
RESUME
MODMSH,DETACH
EX,1,YM
*USE,SUKUA
*USE,SUKUB
FINISH

/SOLU
SAVE
SOLVE
FINISH

/POST1
SET,1
```

```
ETABLE,SIGC,S,EQV  
/output,cylg2  
PRETAB,SIGC  
/output  
FINISH
```

The user file GLOSS-MAC is written in a general form and can be used for any component geometry. The file is used in conjunction with the ANSYS input files for all GLOSS analysis in this thesis.

A.1.2 2-D Single-Edge Circular Notch Specimen

The ANSYS input file for the single-edge circular notch specimen discussed in Section 5.4 is listed in this section. The user file to perform GLOSS analysis is the same as for the example of 3-D Mode I cracked specimen discussed in the previous section, and this is not listed here.

```
!  
!ANSYS INPUT FILE  
!SINGLE-EDGE CIRCULAR NOTCH SPECIMEN  
!  
  
*SET,YM,2.11e5  
*SET,YS,488.43  
*SET,NU,0.3  
*SET,W,50  
*SET,H,50  
*SET,H1,12  
*SET,A,10  
*SET,R,2.5  
*SET,Div1,6  
*SET,Div2,10  
*SET,Div3,5  
*SET,Div4,5  
*SET,Div5,6  
*SET,Div6,8
```

```
*SET,Div7,6
*SET,PX,0
*SET,PY,90
*SET,kn,0
/title, 2 D notch model
/prep7
antype,static
et,1,42,0,0,kn
MP,ex,1,YM
MP,NUXY,1,NU

k,1,a
k,2,a-r,r
k,3,a+h1
k,4,a-r,r+h1
k,5,,r
k,6,,r+h1
k,7,,h
k,8,a-r,h
k,9,w,h
k,10,w

csys,1
1,1,2,Div1
```

```
1,3,4,Div1
csys,0
1,1,3,Div2,4
1,2,4,Div2,4
1,5,6,Div2,4
1,2,5,Div3,2
1,4,6,Div3,2
1,8,7,Div3
1,4,8,Div4,2
1,6,7,Div4,2
1,8,9,Div5,2
1,10,9,Div6,3
1,3,10,Div7,2

a,1,2,4,3
a,2,5,6,4
a,4,6,7,8
a,3,4,8,9,10

amesh,all
outpr,,all
fini

/solu
```

```
nsel,s,loc,x,a,w
nsel,r,loc,y,0
d,all,uy,0
nsel,r,loc,x,a
d,all,ux,0
nsel,all
nsel,s,loc,y,h
sf,all,pres,-py
nsel,all
nsel,s,loc,x,w
sf,all,pres,-px
nsel,all
nsel,s,loc,x,0
sf,all,pres,-px
nsel,all
```

```
save
```

```
solve
```

```
fini
```

```
/input,GLOSS-MAC
```

```
fini
```

A.1.3 $2\frac{1}{2}$ -D Specimen

The ANSYS input file of $2\frac{1}{2}$ -D specimen, considered in Section 6.2, is listed here.

```
!  
!ANSYS INPUT FILE  
!2 1/2-D SPECIMEN  
!  
  
*SET,YM,30e06  
*SET,YS,60e03  
*SET,NU,0.3  
*SET,C,0.0125  
*SET,DB,6  
*SET,RB,3  
*SET,B,-2  
*SET,W,6  
*SET,H,6  
*SET,A,2  
*SET,Div1,4  
*SET,Div2,5  
*SET,Div3,5  
*SET,PX,  
*SET,PY,20e03  
*SET,PZ,15e03  
  
/title, 2 1/2-D fracture model
```

```

/prep7
antype,static
et,1,45
et,2,45
et,3,95
MP,ex,1,YM
MP,ex,2,YM
MP,ex,3,YM
MP,NUXY,1,NU
MP,NUXY,2,NU
MP,NUXY,3,NU

KB=RB**(1/(DB-1))
SK=1
*DO,i,1,DB-1
SK=SK+KB**i
*ENDDO

mb=0
*DO,m,0,DB,1
n,1+26*m,, ,mb
n,15+26*m,, ,mb
n,16+26*m,, ,mb
n,17+26*m,, ,mb

```

```

n,18+26*m,, ,mb
n,19+26*m,, ,mb
n,20+26*m,, ,mb
n,21+26*m,, ,mb
n,22+26*m,, ,mb
n,23+26*m,, ,mb
n,24+26*m,, ,mb
n,25+26*m,, ,mb
n,26+26*m,, ,mb
n,2+26*m,-C, ,mb
n,8+26*m,0,C,mb
n,14+26*m,C, ,mb
csys,1
fill,2+26*m,8+26*m
fill,8+26*m,14+26*m
csys,0
mb=mb+B/SK*(KB**m)
*ENDDO
type,2
*DO,i,1,DB,1
cc=26*(i-1)
en,1+12*(i-1),2+cc,3+cc,15+cc,1+cc,28+cc,29+cc,41+cc,27+cc
*DO,j,1,11,1
cc1=cc+j-1

```

```

en,1+12*(i-1)+j,3+cc1,4+cc1,16+cc1,15+cc1,29+cc1,30+cc1,42+cc1,41+cc1
*ENDDO
*ENDDO

ib=0
*D0,i,0,DB,1
csys,0
k,1+6*i,-C,,ib
k,2+6*i,,C,ib
k,3+6*i,C,,ib
k,4+6*i,-50*C,,ib
k,5+6*i,,50*C,ib
k,6+6*i,50*C,,ib
l,2+6*i,5+6*i,12,6
l,1+6*i,4+6*i,12,6
l,3+6*i,6+6*i,12,6
csys,1
l,1+6*i,2+6*i,6
l,2+6*i,3+6*i,6
l,4+6*i,5+6*i,6
l,5+6*i,6+6*i,6
csys,0
ib=ib+B/SK*(KB**i)
*ENDDO

```

```

*DO,i,1,DB,1
*DO,j,0,5,1
l,1+6*(i-1)+j,7+6*(i-1)+j,1
*ENDDO
*ENDDO

```

```

ib=0
*DO,i,0,DB,1
k,1+6*(DB+1)+7*i,-A,0,ib
k,2+6*(DB+1)+7*i,-A,h,ib
k,3+6*(DB+1)+7*i,0,h,ib
k,4+6*(DB+1)+7*i,W-A,h,ib
k,5+6*(DB+1)+7*i,W-A,0,ib
k,6+6*(DB+1)+7*i,-A,2*h/7,ib
k,7+6*(DB+1)+7*i,W-A,2*h/7,ib
l,5+6*i,3+6*(DB+1)+7*i,Div2,3
l,4+6*i,1+6*(DB+1)+7*i,Div1,3
l,1+6*(DB+1)+7*i,6+6*(DB+1)+7*i,6,2
l,6+6*(DB+1)+7*i,2+6*(DB+1)+7*i,Div3,1.5
l,3+6*(DB+1)+7*i,2+6*(DB+1)+7*i,Div1,1.5
l,3+6*(DB+1)+7*i,4+6*(DB+1)+7*i,Div2,1.5
l,7+6*(DB+1)+7*i,4+6*(DB+1)+7*i,Div3,1
l,5+6*(DB+1)+7*i,7+6*(DB+1)+7*i,6,2
l,6+6*i,5+6*(DB+1)+7*i,Div2,2.5

```

1,5+6*i,6+6*(DB+1)+7*i,Div1,2

1,5+6*i,7+6*(DB+1)+7*i,Div2,2

ib=ib+B/SK*(KB**i)

*ENDDO

*DO,i,1,DB,1

1,1+6*(DB+1)+7*(i-1),1+6*(DB+1)+7*i,1

1,2+6*(DB+1)+7*(i-1),2+6*(DB+1)+7*i,1

1,3+6*(DB+1)+7*(i-1),3+6*(DB+1)+7*i,1

1,4+6*(DB+1)+7*(i-1),4+6*(DB+1)+7*i,1

1,5+6*(DB+1)+7*(i-1),5+6*(DB+1)+7*i,1

1,6+6*(DB+1)+7*(i-1),6+6*(DB+1)+7*i,1

1,7+6*(DB+1)+7*(i-1),7+6*(DB+1)+7*i,1

*ENDDO

type,1

*DO,i,1,DB,1

dd=6*(i-1)

dd1=6*(DB+1)+7*(i-1)

v,1+dd,2+dd,5+dd,4+dd,7+dd,8+dd,11+dd,10+dd

v,2+dd,3+dd,6+dd,5+dd,8+dd,9+dd,12+dd,11+dd

v,4+dd,5+dd,11+dd,10+dd,1+dd1,6+dd1,13+dd1,8+dd1

v,6+dd,5+dd,11+dd,12+dd,5+dd1,7+dd1,14+dd1,12+dd1

v,5+dd,3+dd1,10+dd1,11+dd,6+dd1,2+dd1,9+dd1,13+dd1

```
v,5+dd,3+dd1,10+dd1,11+dd,7+dd1,4+dd1,11+dd1,14+dd1
```

```
*ENDDO
```

```
vmesh,all
```

```
nummrg,node
```

```
nsel,s,loc,x,0
```

```
nsel,r,loc,y,0
```

```
cm,cracktip,node
```

```
/nerr,0
```

```
fract,2
```

```
/nerr,defa
```

```
/output
```

```
outpr,,all
```

```
fini
```

```
/solu
```

```
nsel,s,loc,x,0,W-a
```

```
nsel,r,loc,y,0
```

```
d,all,uy,0
```

```
nsel,all
```

```
nsel,s,loc,z,B
```

```
d,all,uz,0
```

```
nsel,all
```

```
nsel,s,loc,y,0
nsel,r,loc,x,0
nsel,r,loc,z,B
d,all,ux,0
nsel,all
nsel,s,loc,y,h
sf,all,pres,-py
nsel,all
nsel,s,loc,x,W-A
sf,all,pres,-px
nsel,all
nsel,s,loc,x,-A
sf,all,pres,-px
nsel,all
nsel,s,loc,z,0
sf,all,pres,-pz
nsel,all

save
solve
fini

/input,GLOSS-MAC
fini
```

A.2 GLOSS R-Node Method

The GLOSS R-Node method calculates the limit load of a component. A linear elastic analysis is first performed, and then the moduli of each element is modified according to

$$E_s = \left[\frac{(\sigma_e)_j}{\sigma_e} \right] E_0$$

where $(\sigma_e)_j$ is the equivalent stress in any arbitrary j th element, and σ_e is the equivalent stress in each element. This is accomplished by the user file RNODE-MAC. A post-processing is also used to process the results from the first and second linear elastic analyses.

A.2.1 Single-Edge Crack Specimen (SEC)

The ANSYS input file to the model of SEC specimen described in Section 7.5.1 is listed below. A GLOSS R-Node analysis is performed using the user file RNODE-MAC.

```
!  
!ANSYS INPUT FILE  
!SINGLE-EDGE CRACK PROBLEM- ELASTIC ANALYSIS  
!  
  
*SET,YM,2.11e5  
*SET,YS,488.43  
*SET,NU,0.3  
*SET,A,7.5  
*SET,W,50  
*SET,H,50  
*SET,PY,80  
  
/title, 2D SEC Specimen, elastic  
  
/prep7  
  
antype,static  
  
et,1,plane82,0,0,2  
  
MP,ex,1,YM  
  
MP,NUXY,1,NU  
  
K,1,0,0  
  
K,2,(W-A),0
```

```
K,3,(W-A),H
K,4,-A,H
K,5,-A,0

L,1,2
L,2,3
LESIZE,2,,4
L,3,4
LESIZE,3,,4
L,4,5
LESIZE,4,,6,.2
L,5,1
ESIZE,,5
KSCON,1,.15*A,1,8
AL,1,2,3,4,5
AMESH,1
OUTPR,ALL
FINI

/SOLU
nselect,s,loc,x,0
nselect,r,loc,y,0
D,ALL,UX,0
nselect,all
```

```
DL,1,1,SYMM
SFL,3,PRES,-PY
SAVE
SOLVE
FINI
```

```
/input,RNODE-MAC
FINI
```

The user file RNODE-MAC which modifies the moduli of all the elements is listed below.

```
!
!(RNODE-MAC)
!THIS USER FILE (RNODE-MAC) CALCULATES MODIFIED ESEC = E0 * SIGY/SIGE
!LPATH 1,2 is along crack ligament
!
```

```
/POST1
SET,1
ETABLE,SIGC,S,EQV
LPATH,1,2
PDEF,SIGC1,S,EQV
/output,cylg1
```

```
PRPATH,SIGC1
/output
ESEL,ALL

*SET,MN,2
*GET,EL2,ELEM,0,NUM,MAX

*CFOPEN,sukua
:STA
*GET,EL1,ELEM,0,NUM,MIN
*GET,STEQ,ELEM,EL1,ETAB,SIGC
*SET,ESEC,(YS/STEQ)*YM
*CFWRITE,MP,EX,MN,ESEC
*SET,MN,MN+1
*SET,EL1,EL1+1
ESEL,R,ELEM,,EL1,EL2
*IF,EL1,LE,EL2,:STA
*CFCLOS

ESEL,ALL

*SET,MN,2
*GET,EL2,ELEM,0,NUM,MAX
```

```
*CFOPEN,sukub
:STB
*GET,EL1,ELEM,0,NUM,MIN
*CFWRITE,MAT,MN
*CFWRITE,EMODIF,EL1
*SET,MN,MN+1
*SET,EL1,EL1+1
ESEL,R,ELEM,,EL1,EL2
*IF,EL1,LE,EL2,:STB
*CFCLOS
EALL
FINISH

/PREP7
RESUME

MP,EX,1,YM
*USE,sukua
*USE,sukub
FINISH

/SOLU
SAVE
SOLVE
```

FINISH

/POST1

RESUME

SET,1

ETABLE,SIGC,S,EQV

LPATH,1,2

PDEF,SIGC2,S,EQV

/output,cylg2

PRPATH,SIGC2

/output

ESEL,All

FINISH

A.2.2 Compact Tension Specimen (CT)

The ANSYS input file for compact tension specimen described in Section 7.5.2 is listed below.

```
!  
!ANSYS INPUT FILE  
!ELASTIC ANALYSIS OF A COMPACT-TENSION SPECIMEN  
!  
  
/title, CT SPECIMEN -- Elastic Analysis, Plane Strain  
/PREP7  
A=0.055  
B=0.05  
W=.100  
W1=.125  
H=.060  
R=0.0125  
E=0.0275  
S=0.003  
D1=0.080  
D2=0.075  
YM=211e09  
YS=488.43e06  
  
MP,EX,1,YM
```

MP,NUXY,1,.33

K,1,A

K,2,W

K,3,W,H

K,4,,H

K,5,(W-W1),H

K,6,(W-W1),S

K,7,,S

K,8,(W-D1),S

K,9,(W-D2)

K,10,,E

K,11,,E,E

CIRCLE,10,R,11,4,,8

L,1,2

*REPEAT,8,1,1

L,9,1

L,4,12

L,16,7

KSEL,S,LOC,X,-1E-6,1

LSLK,S,1

AL,ALL

KSEL,S,LOC,X,-1,1E-6

LSLK,S,1

AL,ALL

KSEL,ALL

LSEL,ALL

ET,1,PLANE2,,,2

ESIZE,A/4

KSCON,1,A/16,1,9

AMESH,ALL

WSORT,X

FINISH

/SOLU

ANTYPE,0

NSEL,S,LOC,Y

NSEL,R,LOC,X,A,W

D,ALL,UY,0

NSEL,R,LOC,X,A

D,ALL,UX,0

NSEL,ALL

FK,12,FY,80

SAVE

SOLVE

FINISH

/INPUT ,RNODE-MAC

FINI

A.2.3 Single Edge Notched Bend Specimen (SENB)

The ANSYS input file for single edge notched bend specimen described in Section 7.5.3 is listed below.

```
!  
!  
!ANSYS INPUT FILE  
!  
!ELASTIC ANALYSIS OF A SENB SPECIMEN  
!  
  
/title, SENB SPECIMEN -- Elastic Analysis, Plane Stress  
  
/PREP7  
  
A=0.05  
B=0.003  
W=.100  
H=.2125  
H1=.2  
S=0.003  
D1=0.080  
D2=0.075  
YM=211e09  
YS=488.43e06  
  
MP,EX,1,YM  
MP,NUXY,1,.33
```

```
K,1,A
K,2,W
K,3,W,H
K,4,,H
K,5,,H1
K,6,,S
K,7,(W-D1),S
K,8,(W-D2)
L,1,2
*REPEAT,7,1,1
L,8,1
AL,ALL

ET,1,PLANE2,,,3
R,1,B
ESIZE,A/3
KSCON,1,A/12,1,8
AMESH,ALL
WSORT,X

FINISH

/SOLU
ANTYPE,0
```

```
NSEL,S,LOC,Y
NSEL,R,LOC,X,A,W
D,ALL,UY,0
NSEL,ALL
NSEL,S,LOC,X,0
NSEL,R,LOC,Y,H1
D,ALL,UX,0
NSEL,ALL
FK,2,FX,-100
SAVE
SOLVE
FINISH

/INPUT,RNODE-MAC
FINI
```

Appendix B

ANSYS Input Files for Inelastic Analysis

B.1 Elasto-Plastic Analysis for Cracked Specimens

ANSYS input files to analyze the cracked configurations described in this thesis are listed in this appendix. An elastic-plastic analysis is performed using collapsed quadrilateral elements, and from the stress, strain and displacement fields, the elastic-plastic fracture parameter, J , is evaluated. The macro JIN1 is used to calculate J from Rice's formula which defines it to be a path-independent contour integral, however, it is not suitable for $2\frac{1}{2}$ -D model. The macro JIN1 is listed here for the sake of completeness.

```
!  
!JIN1 MACRO FILE TO CALCULATE THE J-INTEGRAL  
!
```

```
SEXP,W,SENE,VOLU,1,-1
LPATH,ARG1,ARG2,ARG3,ARG4
PDEF,W,ETAB,W
PCALC,INTG,J,W,YG
*GET,JA,PATH,0,LAST,J
PDEF,CLEAR
PVECT,NORM,NX,NY,NZ
PDEF,SX,S,X
PDEF,SY,S,Y
PDEF,SXY,S,XY
PCALC,MULT,TX,SX,NX
PCALC,MULT,C1,SXY,NY
PCALC,ADD,TX,TX,C1
PCALC,MULT,TY,SXY,NX
PCALC,MULT,C1,SY,NY
PCALC,ADD,TY,TY,C1
*GET,DX,PATH,0,LAST,S
DX=DX/100
PCALC,ADD,XG,XG,,,-DX/2
PDEF,UX1,U,X
PDEF,UY1,U,Y
PCALC,ADD,XG,XG,, ,DX
PDEF,UX2,U,X
PDEF,UY2,U,Y
```

```
PCALC,ADD,XG,XG,,, -DX/2
C=(1/DX)
PCALC,ADD,C1,UX2,UX1,C,-C
PCALC,ADD,C2,UY2,UY1,C,-C
PCALC,MULT,C1,TX,C1
PCALC,MULT,C2,TY,C2
PCALC,ADD,C1,C1,C2
PCALC,INTG,J,C1,S
*GET,JB,PATH,0,LAST,J
JINT=(2*(JA-JB))
PDEF,CLEAR
```

B.1.1 Single-Edge Crack Specimen

The ANSYS input file for SEC specimen discussed in Section 7.5.1 is listed below.

```
!  
!2D SINGLE-EDGE CRACK PROBLEM- NONLINEAR ANALYSIS  
!  
  
*SET, YM, 2.11e5  
*SET, YS, 488.43  
*SET, NU, 0.3  
*SET, A, 7.5  
*SET, W, 50  
*SET, H, 50  
/title, 2D SEC Specimen, nonlinear  
/prep7  
antype, static  
et, 1, plane82, 0, 0, 2  
MP, ex, 1, YM  
MP, NUXY, 1, NU  
TB, BKIN, 1, 1  
TBDATA, 1, YS, 0  
  
K, 1, 0, 0  
K, 2, (W-A), 0
```

```
K,3,(W-A),H
K,4,-A,H
K,5,-A,0

L,1,2
L,2,3
LESIZE,2,,4
L,3,4
LESIZE,3,,4
L,4,5
LESIZE,4,,6,.2
L,5,1
ESIZE,,5
KSCON,1,.15*A,1,8
AL,1,2,3,4,5
AMESH,1
OUTPR,ALL
FINI

/SOLU
ANTYPE,0
NROPT,1,,OFF
AUTOTS,ON
PRED,ON,,ON
```

```
NCNV,0
OUTRES,ALL,ALL
```

```
SIG=50
nselect,s,loc,x,0
nselect,r,loc,y,0
D,ALL,UX,0
nselect,all
DL,1,1,SYMM
```

```
TIME,1E-10
SFL,3,PRES,0
SAVE
SOLVE
```

```
TIME,9
NSUBST,900
SFL,3,PRES,-9*SIG
SAVE
SOLVE
FINISH
```

```
/INPUT,POST-MAC
FINISH
```

Another nonlinear analysis ANSYS input file is listed below.

```
!  
!ANOTHER ANSYS INPUT FILE  
!2D SINGLE-EDGE CRACK PROBLEM- NONLINEAR ANALYSIS  
!  
  
*SET,YM,2.11e5  
*SET,YS,488.43  
*SET,NU,0.3  
*SET,A,7.5  
*SET,W,50  
*SET,H,50  
/title, 2D SEC Specimen, nonlinear  
/prep7  
antype,static  
et,1,plane82,0,0,2  
MP,ex,1,YM  
MP,NUXY,1,NU  
TB,BKIN,1,1  
TBDATA,1,YS,0
```

```
K,1,0,0
K,2,(W-A),0
K,3,(W-A),H
K,4,-A,H
K,5,-A,0

L,1,2
L,2,3
LESIZE,2,,4
L,3,4
LESIZE,3,,4
L,4,5
LESIZE,4,,6,.2
L,5,1
ESIZE,,5
KSCON,1,.15*A,1,8
AL,1,2,3,4,5
AMESH,1
OUTPR,ALL
FINI

/solu
antype,0
nropt,full,,off
```

```
outres,all,all
```

```
ncnv,1,20
```

```
nsel,s,loc,x,0
```

```
nsel,r,loc,y,0
```

```
D,ALL,UX,0
```

```
nsel,all
```

```
DL,1,1,SYMM
```

```
*DO,i,1,80
```

```
PY=110+5*i
```

```
SFL,3,PRES,-PY
```

```
SAVE
```

```
SOLVE
```

```
*ENDDO
```

```
FINISH
```

```
/INPUT,POST-MAC
```

```
FINISH
```

The user file POST-MAC is used to calculate J values along various contours and the averaged value is viewed as elastic-plastic J .

!

!User File POST-MAC

!Node Numbers are different for different configurations

!

/POST1

SET, LOAD STEP NUMBER

ETABLE,SENE,SENE

ETABLE,VOLU,VOLU

JAVG=0

*USE,JIN1,5,199,195,64

J1=JINT

JAVG=JAVG+J1

*USE,JIN1,6,211,207,63

J2=JINT

JAVG=JAVG+J2

*USE,JIN1,6,79,76,63

J3=JINT

JAVG=JAVG+J3

*USE,JIN1,7,78,75,62

J4=JINT

JAVG=JAVG+J4

*USE,JIN1,8,214,208,62

J5=JINT

```
JAVG=JAVG+J5  
JAVG=(JAVG/5)
```

```
/output,temp
```

```
*STAT
```

```
/output
```

```
/sys,cat temp>>jin.out
```

B.1.2 Compact Tension Specimen

The ANSYS input file for CT specimen discussed in Section 7.5.2 is listed below.

```
!  
!ELASTIC-PLASTIC ANALYSIS OF A COMPACT-TENSION SPECIMEN  
!ELASTIC-PERFECTLY PLASTIC, COLLAPSED QUAD STIF 82 ELEMENTS  
!  
  
/title, CT SPECIMEN -- Nonlinear Analysis  
  
/PREP7  
  
A=0.05  
B=0.05  
W=.100  
W1=.125  
H=.060  
R=0.0125  
E=0.0275  
S=0.003  
D1=0.080  
D2=0.075  
YM=211e09  
YS=488.43e06  
  
ANTYPE,STATIC
```

MP,EX,1,YM

MP,NUXY,1,.33

TB,BKIN,1

TBDATA,1,488.43E06,0

K,1,A

K,2,W

K,3,W,H

K,4,,H

K,5,(W-W1),H

K,6,(W-W1),S

K,7,,S

K,8,(W-D1),S

K,9,(W-D2)

K,10,,E

K,11,,E,E

CIRCLE,10,R,11,4,,8

L,1,2

*REPEAT,8,1,1

L,9,1

L,4,12

L,16,7

KSEL,S,LOC,X,-1E-6,1

Page 193

**missing from the
original book**

NSEL,R,LOC,X,A,W

D,ALL,UY,0

NSEL,R,LOC,X,A

D,ALL,UX,0

NSEL,ALL

*DO,i,1,120

PFORCE=(400+70*i)*1000

FK,12,FY,PFORCE

SAVE

SOLVE

*ENDDO

FINISH

/INPUT,POST-MAC

FINISH

B.1.3 Single Edge Notched Bend Specimen

The ANSYS input file for SENB specimen discussed in Section 7.5.3 is listed below.

```
!  
!  
!ELASTIC-PLASTIC ANALYSIS OF A SENB SPECIMEN  
!  
!SINGULAR STIF 82 ELEMENTS USED AROUND CRACK TIP  
!  
  
/title, SENB SPECIMEN -- Nonlinear Analysis, Plane Stress  
/PREP7  
  
A=0.05  
B=0.003  
W=.100  
H=.2125  
H1=.2  
S=0.003  
D1=0.080  
D2=0.075  
YM=211e09  
YS=488.43e06  
  
ANTYPE,STATIC  
MP,EX,1,YM  
MP,NUXY,1,.33
```

TB,BKIN,1

TBDATA,1,488.43E06,0

K,1,A

K,2,W

K,3,W,H

K,4,,H

K,5,,H1

K,6,,S

K,7,(W-D1),S

K,8,(W-D2)

L,1,2

*REPEAT,7,1,1

L,8,1

AL,ALL

ET,1,PLANE82,,3

R,1,B

ESIZE,A/3

KSCON,1,A/12,1,8

AMESH,ALL

WSORT,X

FINISH

```
/solu
antype,0
nropt,full,,off
outres,all,all
ncnv,1,20
NSEL,S,LOC,Y
NSEL,R,LOC,X,A,W
D,ALL,UY,0
NSEL,R,LOC,X,A
D,ALL,UX,0
NSEL,ALL

*DO,i,1,100
PFORCE=1000+115*i
FK,2,FX,-PFORCE
FK,5,FX,PFORCE
SAVE
SOLVE
*ENDDO
FINISH

/INPUT,POST-MAC
FINISH
```

B.1.4 Circumferential Flaw in a Pressure Vessel

The ANSYS input file for circumferential flaw in a pressure vessel discussed in Section 6.5.3 is listed below.

```
!  
!CIRCUMFERENTIAL FLAW- NONLINEAR ANALYSIS  
!  
  
*SET,YM,2.11e5  
*SET,YS,488.43  
*SET,NU,0.3  
*SET,RI,100  
*SET,W,10  
*SET,A,2.5  
*SET,H,30  
*SET,RO,(RI+W)  
  
/title, 2D Axisymmetric Circumferential Cracked Specimen, nonlinear  
/prep7  
antype,static  
et,1,plane82,0,0,1  
MP,ex,1,YM  
MP,NUXY,1,NU  
TB,BKIN,1,1  
TBDATA,1,YS,0
```

```
K,1,(RI+A),0
K,2,RO,0
K,3,RO,H
K,4,RI,H
K,5,RI,0

L,1,2
L,2,3
LESIZE,2,,8
L,3,4
LESIZE,3,,6
L,4,5
LESIZE,4,,10,.2
L,5,1
ESIZE,,6
KSCON,1,.15*A,1,8
AL,1,2,3,4,5
AMESH,1
OUTPR,ALL
FINI

/solu
antype,0
```

nropt,full,,off

outres,all,all

ncnv,1,20

nsel,s,loc,x,0

nsel,r,loc,y,0

D,ALL,UX,0

nsel,all

DL,1,1,SYMM

nsel,s,loc,y,H

D,ALL,ROTX,0

D,ALL,ROTY,0

nsel,all

*DO,i,1,80

PI=9+1*i

SFL,3,PRES,-(PI*RI*RI/(RO*RO-RI*RI))

SAVE

SOLVE

*ENDDO

FINI

/INPUT,POST-MAC

FINI

B.1.5 Longitudinal Flaw in a Pressure Vessel

The ANSYS input file for longitudinal flaw in a pressure vessel discussed in Section 6.5.4 is listed below.

```
!  
!LONGITUDINAL FLAW- NONLINEAR ANALYSIS  
!  
  
*SET,YM,2.11e5  
*SET,YS,488.43  
*SET,NU,0.3  
*SET,RI,100  
*SET,W,10  
*SET,A,2.5  
*SET,RO,(RI+W)  
  
/title, 2D Longitudinal Cracked Specimen, nonlinear  
/prep7  
antype,static  
et,1,plane82,0,0,2  
MP,ex,1,YM  
MP,NUXY,1,NU  
MP,ALPX,1,0  
MP,ALPY,1,0
```

MP,ALPZ,1,1e-5

TB,BKIN,1,1

TBDATA,1,YS,0

K,1,RI+A,0

K,2,RO,0

K,4,-RO,0

K,5,-RI,0

K,7,RI,0

CSYS,1

K,3,RO,45

K,6,RI,45

CSYS,0

L,1,2

LESIZE,1,,,6

CSYS,1

L,2,3

LESIZE,2,,,24,3

CSYS,0

L,3,6

LESIZE,3,,,2

CSYS,1

```
L,7,6
LESIZE,4,,24,3
CSYS,0
L,7,1
ESIZE,,6
KSCON,1,.2*A,1,6
L,4,5
LESIZE,6,,2
CSYS,1
L,6,5
LESIZE,7,,18,3
L,3,4
LESIZE,8,,18,3
CSYS,0
AL,1,2,3,4,5
AL,6,7,3,8
AMESH,all
OUTPR,ALL
FINI

/solu
antype,0
nropt,full,,off
outres,all,all
```

```
ncnv,1,20

nsel,s,loc,x,RI+A
nsel,r,loc,y,0
D,ALL,UX,0
nsel,all
DL,1,1,SYMM
nsel,all
DL,6,2,SYMM
nsel,all

*DO,i,1,120
PI=10+0.5*i
SFL,4,PRES,PI
SFL,7,PRES,PI
SAVE
SOLVE
*ENDDO
FINI

/INPUT,POST-MAC
FINI
```

B.2 Elasto-Plastic Analysis for Notched Specimen

The ANSYS input file for circular-ended notch specimen discussed in Section 5.4 is listed here.

```
!  
!2D NOTCH PROBLEM- NONLINEAR ANALYSIS  
!  
  
*SET, YM, 2.11e5  
*SET, YS, 488.43  
*SET, NU, 0.3  
*SET, W, 50  
*SET, H, 50  
*SET, H1, 12  
*SET, A, 10  
*SET, R, 2.5  
*SET, Div1, 6  
*SET, Div2, 12  
*SET, Div3, 5  
*SET, Div4, 5  
*SET, Div5, 6  
*SET, Div6, 8  
*SET, Div7, 6
```

```
*SET,kn,0

/title, 2 D notch model-nonlinear analysis
/prep7
et,1,42,0,0,kn
MP,ex,1,YM
MP,NUXY,1,NU

TB,BKIN,1,1
TBDATA,1,YS,0

k,1,a
k,2,a-r,r
k,3,a+h1
k,4,a-r,r+h1
k,5,,r
k,6,,r+h1
k,7,,h
k,8,a-r,h
k,9,w,h
k,10,w

csys,1
1,1,2,Div1
```

```
1,3,4,Div1
csys,0
1,1,3,Div2,4
1,2,4,Div2,4
1,5,6,Div2,4
1,2,5,Div3,2
1,4,6,Div3,2
1,8,7,Div3
1,4,8,Div4,2
1,6,7,Div4,2
1,8,9,Div5,2
1,10,9,Div6,3
1,3,10,Div7,2
```

```
a,1,2,4,3
a,2,5,6,4
a,4,6,7,8
a,3,4,8,9,10
```

```
amesh,all
```

```
fini
```

```
/solu
```

```
antype,0
```

```
nropt,full,,off
outres,all,all
ncnv,1,20
```

```
nselect,s,loc,x,a,w
nselect,r,loc,y,0
d,all,uy,0
nselect,r,loc,x,a
d,all,ux,0
nselect,all
```

```
*DO,i,1,40
PY=76+4*i
NSEL,S,LOC,Y,H
SF,ALL,PRES,-PY
NSEL,ALL
SAVE
SOLVE
*ENDDO
FINISH
```

```
/INPUT,POST-MAC
FINI
```

Appendix C

Derivation of Equivalent Reference Stress

C.1 A Cylindrical Pressure Vessel with Circumferential Flaw

Limit Loads for a Rectangular Beam With an Axial Load and Bending Moment (Fig. C.1): The expression for the theoretical collapse load can be expressed as (Burgreen, 1968)

$$\frac{M}{M_o} = \frac{3}{2} \left[1 - \left(\frac{P}{P_o} \right)^2 \right] \quad (\text{C.1})$$

where $P_o = \sigma_y h$ and $M_o = \sigma_y h^2 / 6$. For an elastic perfectly-plastic material, while the ratio of applied bending moment (M) to applied axial load (P) is constant (e), that is, $M = P e$, the limit axial load (P_L) can be obtained as (Fig. C.1)

$$P_L = \sigma_y (\sqrt{4e^2 + h^2} - 2e). \quad (\text{C.2})$$

Based on the reference stress method, the equivalent reference stress, $(\sigma_e)_{ref}$, can be obtained as

$$(\sigma_e)_{ref} = \sigma_y \frac{P}{P_L} = \frac{P}{\sqrt{4e^2 + h^2} - 2e}. \quad (\text{C.3})$$

Cylindrical Pressure Vessel with Circumferential Flaw (Fig. C.2): In order to simplify the problem, case (a) can be approximately viewed as case (b) in Fig. C.2, that is, $P = p_a W$ and $M = P (\frac{a}{2})$ where p_a is the axial stress. Therefore, from Eq. (C.3) (when $h = W - a$ and $e = \frac{a}{2}$), the equivalent reference stress can be expressed as

$$(\sigma_e)_{ref} = \frac{p_a W}{\sqrt{a^2 + (W - a)^2} - a}. \quad (\text{C.4})$$

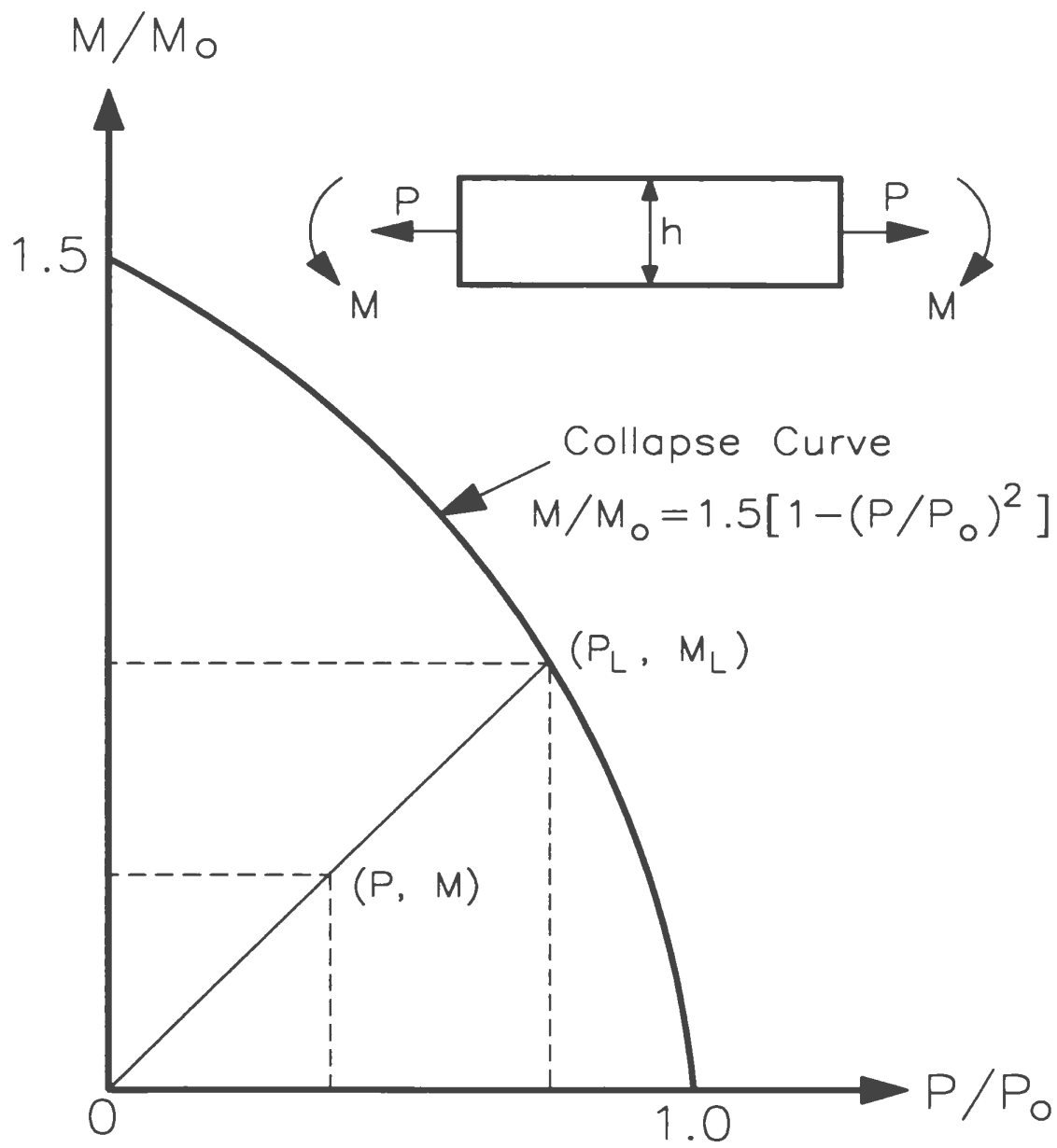


Figure C.1: Collapse Curve for a Rectangular Beam

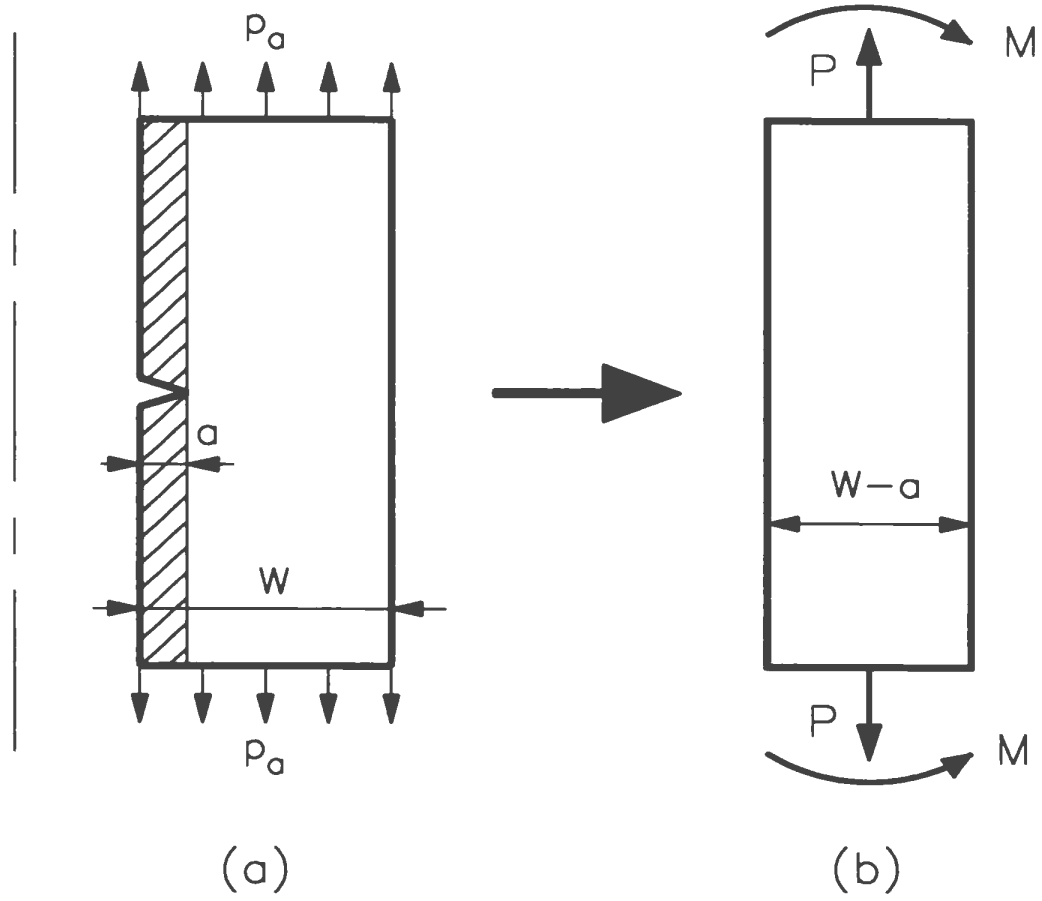


Figure C.2: Cylindrical Pressure Vessel with Circumferential Flaw

C.2 A Cylindrical Pressure Vessel with Longitudinal Flaw

Analysis of a Thick-Walled Cylinder Subjected to an Internal Pressure: The stationary creep solution for a thick-walled cylinder under internal pressure (p_i) can be expressed as (Seshadri and Fernando, 1992)

$$\begin{aligned}\sigma_\theta &= \frac{p_i}{(Y^{2/n} - 1)} \left[1 + \frac{2-n}{n} \left(\frac{R_o}{r} \right)^{2/n} \right] \\ \sigma_z &= \frac{p_i}{(Y^{2/n} - 1)} \left[1 + \frac{1-n}{n} \left(\frac{R_o}{r} \right)^{2/n} \right] \\ \sigma_r &= \frac{p_i}{(Y^{2/n} - 1)} \left[1 - \left(\frac{R_o}{r} \right)^{2/n} \right]\end{aligned}\tag{C.5}$$

where σ_θ , σ_r and σ_z are circumferential stress, radial stress and longitudinal stress respectively, and Y is the ratio of outer radius R_o to inner radius R_i . The foregoing expressions have been based on the second-stage creep relationship $\dot{\epsilon} = B\sigma^n$. The elastic stress distribution can be obtained by setting $n = 1$. The von Mises equivalent stress can be written as

$$\sigma_e = \frac{1}{\sqrt{2}} [(\sigma_\theta - \sigma_z)^2 + (\sigma_z - \sigma_r)^2 + (\sigma_r - \sigma_\theta)^2]^{1/2}.\tag{C.6}$$

Substituting Eq. (C.5) into Eq. (C.6), and simplifying

$$\sigma_e = \frac{\sqrt{3}}{n} \frac{p_i}{(Y^{2/n} - 1)} \left(\frac{R_o}{r} \right)^{2/n}. \quad (\text{C.7})$$

The value of the equivalent stress for $n \rightarrow \infty$, which corresponds to a rigid plastic material, can be expressed as

$$\sigma_e = \frac{\sqrt{3}}{2} \left[\frac{p_i}{\ln(Y)} \right] \quad (\text{C.8})$$

where, σ_e is the reference stress.

Cylindrical Pressure Vessel with Longitudinal Flaw (Fig. C.3): In order to simplify the problem, case (a) can also be approximately viewed as case (b) in Fig. C.3, that is, $Y = R_o/(R_i + a)$. From Eq. (C.8) the equivalent reference stress, $(\sigma_e)_{ref}$, can be obtained as

$$(\sigma_e)_{ref} = \frac{\sqrt{3}}{2} \left[\frac{p_i}{\ln\left(\frac{R_o}{R_i + a}\right)} \right]. \quad (\text{C.9})$$

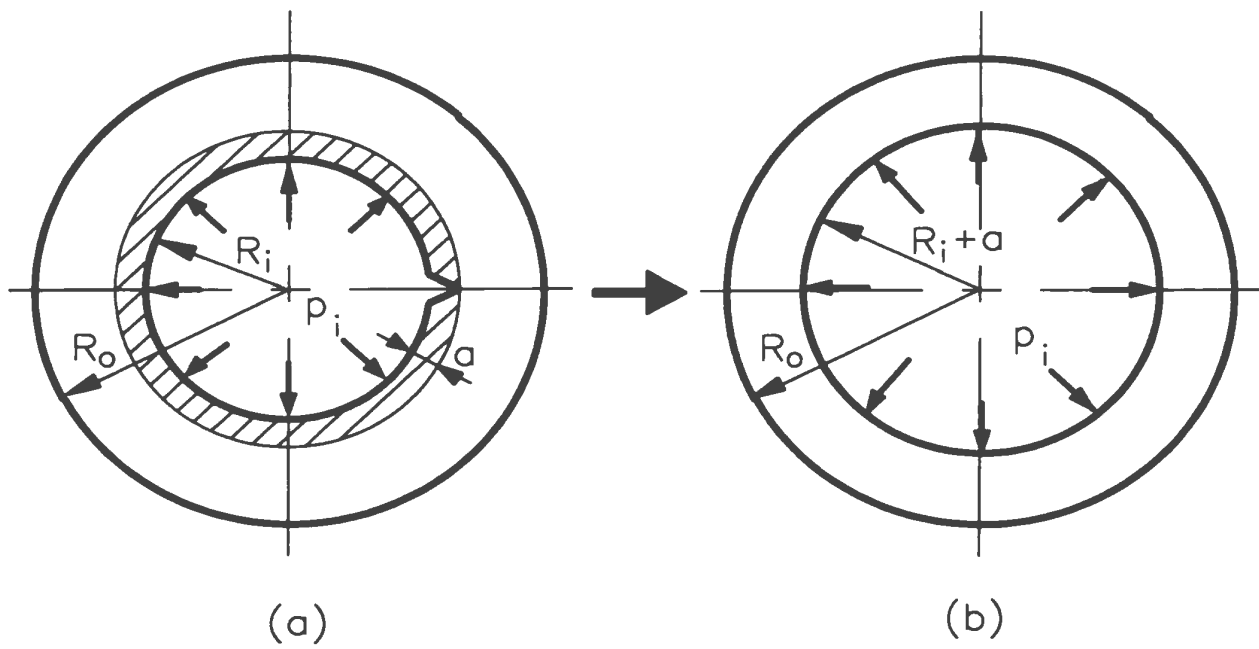


Figure C.3: Cylindrical Pressure Vessel with Longitudinal Flaw

